Design, Fabrication and Testing of Printed Monopole Antennas for Super Wideband Applications

Murli Manohar

Design, Fabrication and Testing of Printed Monopole Antennas for Super Wideband Applications

A

Thesis submitted

for the award of the degree of

Doctor of Philosophy

By

MURLI MANOHAR

Department of Electronics and Electrical Engineering

Indian Institute of Technology Guwahati

Guwahati - 781039, Assam, India

September 2014

Dedicated to

My Beloved Parents, Late Surendra Prasad Pandit and Tara Devi;

My Wife, Munmi Das Manohar;

and

My Supervisor, Dr. Rakhesh Singh Kshetrimayum and Prof. Anup Kumar Gogoi;

Certificate

This is to certify that the thesis entitled "**Design, Fabrication and Testing of Printed Monopole Antennas for Super Wideband Applications**", submitted by **Murli Manohar** (10610220), a research scholar in the *Department of Electronics and Electrical Engineering, Indian Institute of Technology Guwahati*, for the award of the degree of **Doctor of Philosophy**, is a record of an original research work carried out by him under my supervision and guidance. The thesis has fulfilled all requirements as per the regulations of the institute and in my opinion has reached the standard needed for submission. The results embodied in this thesis have not been submitted to any other University or Institute for the award of any degree or diploma.

Date:
Place: Guwahati.

Dr. Rakhesh Singh Kshetrimayum and Prof. Anup Kumar Gogoi
Associate Professor and Professor
Dept. of Electronics and Electrical Engg
Indian Institute of Technology Guwahati
Guwahati - 781039, Assam, India.

Acknowledgements

First and foremost, I feel it as a great privilege in expressing my deepest and most sincere gratitude to my supervisors Dr. Rakhesh Singh Kshetrimayum and Prof. Anup Kumar Gogoi, for their excellent guidance throughout my study. Their kindness, dedication, hard work and attention to detail have been a great inspiration to me. My heartfelt thanks to both of you sirs for the unlimited support and patience shown to me. I have no doubts that finishing my degree in a proper and timely manner was impossible without their helps, suggestions and advices.

I am also very thankful to my doctoral committee members Prof. Ratnajit Bhattacharjee, Dr. Amitabh Chatterjee, Dr. Sansam Ranbir Singh and Prof. Harshal Nemade for sparing their precious time to evaluate the progress of my work. I express my heartfelt thanks to Prof. Ratnajit Bhattacharjee for providing valuable suggestions on during the progress seminars.

I would also like to thank the Head of the Department Dr. Ratnajit Bhattacharjee and other faculty members such as Prof. Anil Mahanta for their kind help in carrying out this work. I am also grateful to all the members of the research and technical staffs of the department such as Mr. Sanjib Das and Dr. L. N. Sharma without their help I could not have completed this thesis. My special thanks to Mr. Utpal Kumar Sharma for his immense help in fabrication of antennas during the course of my Ph.D work and providing various resources useful for research work in the High Frequency lab of the department of EEE of IIT Guwahati. Apart from this, I would like to thank Mr. Dayananda Goswami for his sincere help in various measurements of antennas.

I am extremely grateful to Dr. Rajiv Kumar Panigrahi of department of Electronics and Communication Engineeering (ECE) of Indian Institute of Technology Roorkee for allowing the anechoic chamber and other allied antenna measurement facilities.

My special thanks to all my friends and well wishers in the department of Electronics and Electrical engineering, Indian Institute of Technology Guwahati such as Brijesh Kumbhani, Shivanshu Shrivastava, Deepak Joshi, Somen Bhattacharjee, Atul Kumar, Sandeep P., Mandar Maitra, Ananya Patra, Parveen Malik, Sandeep R., Resmi N.C., Madhulika Das, Vinay Kumar Pandey, Sikandar, Syed Shahanawazuddin, Shashank Dwivedi, K.T. Deepak, Rajib Jana, Syantan Hazra, Samdarshi, Himansu Jyoti Das, Basudeba Behera, Vinaya M.M., Nagendra Naik, Umesh Chaudhary, Tausif Khan N., Sonali Biswas, Mridulkanti Malakar, Kukil Khanikar, Aanand Agrawal, Santosh Kumar Yadav, and Ramesh Mishraji for their kind mental and physical support of some kind during my stay in IIT Guwahati.

Finally, to my father, Late Surendra Prasad Pandit and to my mother, Smt. Tara Devi, I owe all. No words can really describe my appreciation and gratitude to them for bearing with me for these years. I am equally indebted to my mother-in-law Smt. Deepa Das and brother-in-law Sri Joydeep Das for their constant support and love. I am ever grateful to them for their patience and keep myself on the safer side by taking all the pains on them. I really can not find words to express how much all of them mean to me.

In this short acknowledgement, I may miss the name of the people who helped who helped me to make this thesis possible. But I am equally grateful to all of them.

Murli Manohar

Abstract

In this thesis, several compact full-band and band-notched super wideband (SWB) printed monopole antennas are designed, fabricated and tested. The designed antenna provides much wider impedance bandwidth of 89.9 GHz that is 1.1 to 100 GHz (bandwidth ratio of 90.9:1). Improved designs are used for microstrip feed line, feed region of the antenna and radiating element to obtain such a super wideband (SWB) radiation characteristics. A triangular tapered microstrip feed line is used, nearly optimal taper or curve is employed in the feed region and the ground plane feed gap is optimized to get best antenna performance. Unfortunately, it is to be noted that some of the existing narrow band systems such as WiMAX (3.3−3.7 GHz), C-band (3.8−4.2 GHz), WLAN (5.15−5.85) and X-band satellite communication systems operating in 7.25−8.395 GHz (for down link: 7.25−7.745 GHz and uplink: 7.9−8.395 GHz) may cause electromagnetic interference to the SWB system. So, to mitigate this interference issue, SWB antennas with band-notched characteristics is required. Till date, most of the antennas have been designed to have notch within UWB band and occupy relatively large space. In our work, we have designed a suitable SWB antenna along with band notch characteristics in WIMAX, C-band, WLAN and X-band satellite communication systems frequency region and also supports a very large bandwidth. A parasitic element and slot have been designed for creating notches to mitigate the potential interference with the narrow band system. This band-notch SWB antenna should have good radiation characteristics with reasonable gain and compact size.

Keywords: – **Frequency band-notch function, impedance bandwidth, super wide-band (SWB) antenna, triangular tapered feedline, tapered monopole antenna**

Contents

List of Figures

List of Tables

List of Acronyms

ABW	Absolute Bandwidth
AWS	Advanced Wireless Service
BW	Bandwidth
CGP	Chamfered Ground Plane
DVD	Digital Versatile Disc
FBW	Fractional Bandwidth
FEM	Finite Element Method
EIRP	Effective Isotropic Radiation Power
Gbps	Giga bits per second
GHz	Giga Hertz
GPS	Global Positioning system
GSM	Global System for Mobile Communications
FSD	Functional Section Design
HDTV	High Definition Television
HIPERLAN	High Performance Radio Local Area Network
HFSS	High Frequency Simulation Software
IEEE	Institute of Electrical and Electronics Engineer
ISM	Industrial Scientific Medical
Mbps	Mega bits per second
MHz	Mega Hertz
MMDS	Multichannel Multidistribution Services
MMIC	Monolithic Microwave Integrate Circuit
PAN	Personal Area Network

PCB	Printed Circuit Board
PCS	Personal Communications Service
PMA	Printed Monopole Antenna
PTMA	Printed Triangular Monopole Antenna
RCFGP	Round-Corner Finite Ground Plane
RF	Radio Frequency
SWB	Super-Wideband
SMA	Sub Miniature A
SNR	Signal-to-Noise ratio
UWB	Ultra-Wideband
USB	Universal Serial Bus
VCR	Videocassette Recorder
VSWR	Voltage Standing Wave Ratio
WCS	Wireless Communication Service
WiMAX	Worldwide Inter-operability for Microwave Access
WPAN	Wireless Personal Area Network
WLAN	Wireless Local Area Network

List of Symbols

$\overrightarrow{A}$	Magnetic vector potential
(D_{max})	Maximum directivity
dz	Differential length
β	Phase constant
$I_1(x)$	Bessel function
ε_r	Dielectric constant
L_c	Height of the trapezoidal patch
$I_0 dl$	Small current carrying element
P_{rad}	Total radiated power
P_{in}	Total input power
r_c	Radius of cylindrical monopole antenna
p	Feed gap
μ_0	Permeability
R_r	radiation resistance
Γ	Reflection coefficient
f_L	Lower bandwidth edge
f_0	Resonant frequency
f_n	Notch frequency
$-20\log\|S_{11}\|$	Return loss
k	Wave number
U_0	Radiation intensity
f_H	Upper bandwidth edge
Q	Quality factor

$\overline{Z}$	Normalized impedance
$Z(z)$	Impedance function of triangular tapered feed line
Z_A	Characteristic impedance of antenna
Z_C	Characteristic impedance of transmission line
e_{rad}	Radiation efficiency
ρ	Correlation factor
τ	Delay
λ_g	Guided wavelength

1

Introduction

Contents

1.1 Brief background on super wideband (SWB)

It is worth noting that over the past decade Ultra wideband (UWB) systems have drawn a lot of attention in the modern wireless world. In February 2002, the Federal Communication Commission has suggested the authorized unlicensed use of ultra-wideband (UWB) frequency spectrum [1] in the frequency band of 3.1 to 10.6 GHz for wireless personal area network (WPAN) applications. Due to several features such as large bandwidth communications, high data rate transmission and operates at very low operational energy level, UWB technology makes an attractive option to cover short range wireless communication systems such as PC peripherals and wireless USB. Note that besides large bandwidth of this UWB (ratio bandwidth of 3.4:1) technology, current users of wireless personal area network (WPAN) are also hunger to increase more and more bandwidth (like super wideband radio technology) to cover both short range and long-range communication system. Super wideband (SWB) radio technology provide ratio bandwidth of more than 10:1 were first developed supposedly by Rumsey et al, in the late 1950s and early 1960s, which was classified as a class of frequency-independent antennas [2]. According to Shannon-Hartley's channel capacity law [3] transmission data rate can be increased by enlarging the bandwidth [4]. SWB technology has higher channels capacity and provide data, voice, and video transmission at very high data rates. It permits high resolution sensing in free space and also works in ground penetrating radar (GPR) and wall-through sensing. Existing UWB technology (3.1 to 10.6 GHz) has meets most of the features like SWB technology, except its bandwidth ratio of 3.4:1. SWB technology have all advanced features of UWB technology like higher channel capacity, higher precision and super resolution in communication, ranging and screening. Name of the technology is given as Super wideband, because of it can supports most of the communication systems, such as GPS (1.57−1.58 GHz), GSM1800 (1.71−1.88 GHz), PCS (1.85−1.99GHz), AWS-3 (2.155−2.175 GHz), WCS (2.345−2.360 GHz), ISM (2.402−2.480 GHz), MMDS (2.500−2.690 GHz), UWB (3.1−10.6 GHz) and UWB vehicle radar (22−29 GHz). Because of extremely large bandwidth SWB technology may be used for spectrum sensing in cognitive radio [5] and to achieve adequate polarization diversity [6]. SWB sensors/devices which support SWB-signaling, that could be an appropriate solution for balancing bandwidth, range and resolution.

1.2 Antenna in wireless communication system

Antenna plays an important role for any wireless communication system as it is a transducer which converts an guided wave in tranmission lines into electromagnetic waves or vice versa. According to the IEEE Standard Definitions an antenna is defined as ”a means for radiating or receiving electromagnetic waves” [7]. The existence of the electromagnetic waves in space was first predicted by James clerk Maxwell in 1873. Maxwell proposed that light is a continuously varying electromagnetic wave with time and at other wavelength, the electromagnetic radiation is also possible. After James clerk Maxwell postulated the theory of electromagnetic waves, Heinrich Rudolf Hertz proved in 1888 the physical existence of electromagnetic waves by doing some experimental arrangement to transmit and receive radio pulses.

Initially the shape of antenna was wire type radiating elements in 1940, which can be operated up to some ultra high frequency (UHF). After that drastic development was occurred in the antenna technology as the impedance bandwidth is enhanced to 40:1 or more. These wideband antennas are known as the frequency independent antennas with little or no signal attenuation, whose geometries are specified by angles [8–10] instead of linear dimensions. The important application of these frequency independent antennas includes radio and short wave sets, radar devices, navigating systems, feed for reflectors, point to point communication, etc. In the year of 1972 (but became popular starting in the 1970), microstrip antennas were invented by Bob Munson, which are used in many applications till date. Compare to earlier antenna design microstrip patch antennas are easy to fabricate and can be easily integrated with microwave integrated circuits (MICs). Due to low profile (can even be conformal) and low fabrication cost microstrip antenna has becomes a choice for many applications. Recently, a millimeter wave antenna has gone through several transformations and now-a-days these antennas can be integrated in many small handheld gadgets in which the passive and active components can be associated with the radiating elements in one component unit.

1.3 Antenna theory

According to the IEEE Standard Definitions of terms for Antennas (IEEE Std 145-1983) defines the antenna or aerial as a means for radiating or receiving radio waves. Antenna is a transducer which converts electrical quantities like voltage and current into electromagnetic waves or vice versa. In other words we can say that the antenna is used for transmitting electromagnetic energy between a guiding device, such as coaxial line or a hollow pipe (waveguide) or a microstrip to free-space. Antenna is a fundamental and important component of all wireless communication systems because in a radio link the antenna serves as the final block on the transmitter side and is the first block on the receiver side.

The main objective of this thesis is to design appropriate antennas that are suitable for the future wireless SWB communication systems. Before proceeding to the antenna design procedure, it is important to have some acquaintance with the general antenna basics and concepts. There are some important parameters that always have to be considered in antenna design. At the same time, the primary requirements for a suitable UWB and SWB antennas are discussed. Some general approaches to achieve wide operating bandwidth of antenna are presented.

1.3.1 Antenna parameters

Definitions of various parameters are required to describe the performance of an antenna.

1.3.1.1 Antenna frequency bandwidth

Frequency bandwidth (BW) of the antenna is defined as ”the range of frequencies within which the performance of the antenna, with respect to some characteristics, conforms to a specified standard”. The bandwidth can be considered to be the range of frequencies, on either side of a center frequency (usually the resonance frequency for a dipole), where the antenna characteristics (such as input impedance, pattern, beam width, polarization, side lobe level, gain, beam direction, beamwidth, radiation efficiency) are within an acceptable value of those at the center frequency. Generally, the antenna should have return loss more than +10 dB over its frequency bandwidth in wireless communications. Bandwidth is often expressed in terms either absolute bandwidth (ABW) or fractional bandwidth (FBW). If f_L and f_H are the lower ends and upper ends of the antenna bandwidth, respectively, then the ABW is defined as the difference of f_H and f_L. The FBW is defined as the percentage of the frequency difference over the center frequency, as given in equation (1.1) and (1.2), respectively.

$$ABW = (f_H - f_L) \tag{1.1}$$

$$FBW(\%) = \frac{2\,(f_H - f_L)}{(f_H + f_L)} \times 100 \tag{1.2}$$

In case of wideband antenna, the bandwidth can be expressed as the ratio of the upper ends to lower end frequencies [11] as given in equation (1.3)

$$BW = \frac{f_H}{f_L} \tag{1.3}$$

1.3.1.2 VSWR and return loss

As we know electromagnetic waves travel through different parts of the antenna system i.e., from the source to feed line, then to the antenna system and finally waves are radiated in free space. In the process, they may encounter different impedances at each interface. Depending on the impedance mismatch, portion of some energy will get reflected back to the source forming a standing wave in the feed line. The ratio of maximum to minimum voltage along the transmission line is called as standing wave ratio (SWR). Ideally SWR should be 1; then there is no reflection or return loss. But practically SWR of 1 is not possible. Voltage standing wave ratio (VSWR) of 1.5 is considered as excellent system, while values of 1.5 to 2 is considered as a good system.

The antenna input impedance can be used to determine the reflection coefficient (Γ), voltage standing wave ratio (VSWR) and return loss (RL) as a function of frequency as given by [7]

$$\Gamma = \frac{Z_A - Z_C}{Z_A + Z_C} \tag{1.4}$$

where Z_A is the characteristic impedance of the antenna and Z_C is the characteristic impedance of the transmission line.

The VSWR is defined as the ratio of the peak voltage maximum to peak voltage minimum in the standing wave pattern at an impedance discontinuity. For antenna

$$VSWR = \frac{1 + |\Gamma|}{1 - |\Gamma|} \tag{1.5}$$

where VSWR is the voltage standing wave ratio and Γ is the reflection coefficient. And the return loss is defined as

$$Return\ loss\ (RL) = -20\log|\Gamma| \tag{1.6}$$

1.3.1.3 Radiation pattern

Radiation pattern of the antenna is defined as graphical representation of the electromagnetic power distributions in free space. Also, these patterns can be considered to be representative of the relative field strengths of the field radiated by the antenna. In most cases, radiation pattern is determined in the far-field region and is represented as a function of the directional coordinates. Radiation properties include power flux density, radiation intensity, field strength, directivity, phase or polarization. Normally, the pattern describes the normalized (power) values with respect to the maximum values. The radiation property of most concern is the two- or three-dimensional spatial distribution of radiated energy as a function of the observer's position along a path or surface of constant radius. A trace of the received power at a constant radius is called the power pattern. In practice, the three-dimensional radiation pattern can be represented by multiple of two- dimensional radiation patterns. However, for most practical applications, a few plots of the pattern at certain ϕ and θ values are used to derive the required information, where ϕ and θ are the two axes in a spherical coordinate. For a linearly polarized antenna performance is generally described in terms of its principle E-plane and H-plane patterns. The E-plane is defined as the plane containing the electric field vector and the direction of maximum radiation while the H-plane is defined as the plane containing the magnetic field vector and the direction of maximum radiation. Radiation pattern of the antenna can be described using mainly three radiation patterns [12].

(a) Isotropic - Isotropic is defined as a hypothetical lossless antenna having uniform radiation in all directions. It is applicable only for an ideal antenna and practically it is not possible to realize it.

(b) Directional - Directional antenna is defined as an antenna having the property of radiating or receiving electromagnetic waves more efficient radiation in one direction than another. This is usually applicable to an antenna where its maximum directivity is significantly greater than that of a half wave dipole.

(c) Omni-directional - In case of omni-directional an antenna having an essentially non-directional pattern in a given plane and a directional pattern in any orthogonal plane. Therefore an omni-directional pattern can be considered as a special type of directional pattern.

1.3.1.4 Directivity, gain and efficiency

The directivity of an antenna is defined as the ratio of the radiation intensity U(θ,ϕ) in a given direction from the antenna to the radiation intensity averaged over all directions which are equivalent to the U_0 (radiation intensity of an isotropic antenna). For an isotropic antenna, the radiation intensity is equal to the total radiated power P_{rad} divided by 4π. Therefore mathematical expression for the directivity can be written as

$$D(\text{directivity}) = \frac{U\theta,\varphi)}{U_0} = \frac{U(\theta,\varphi)}{P_{rad}/4\pi} = \frac{4\pi U(\theta,\varphi)}{P_{rad}} \tag{1.7}$$

If the direction of an antenna is not specified, it implies the direction of maximum directivity (D_{max}) can be expressed as

$$D_{\max} = \frac{U_{\max}(\theta,\varphi)}{U_0} = \frac{4\pi U_{\max}(\theta,\varphi)}{P_{rad}} \tag{1.8}$$

Gain (G) is other important parameter of the antenna, which is defined as the ratio of the intensity in a given direction to the radiation intensity that would be obtained if the power accepted by the antenna

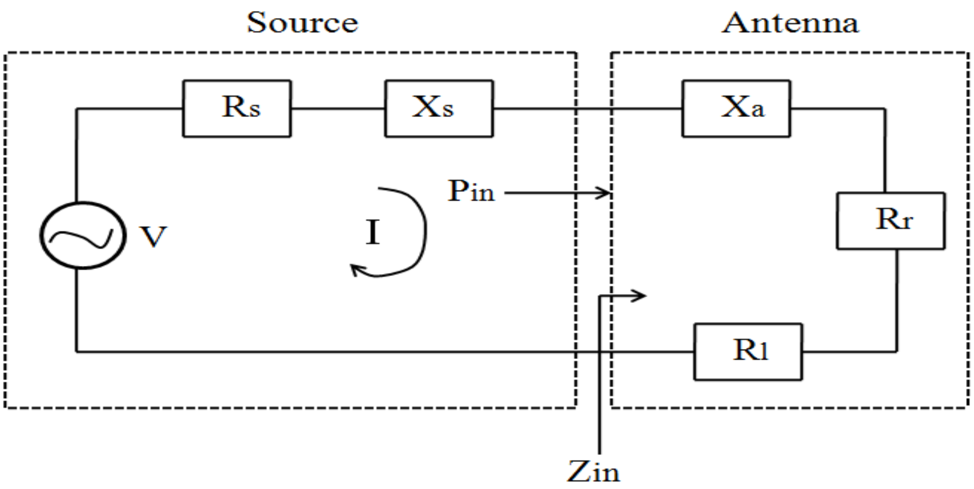

Figure 1.1: Equivalent circuit of an antenna

were radiated isotropically. Mathematical formulation of the gain G(θ,ϕ) can be expressed as

$$G\left(\theta,\varphi\right)=\frac{4\pi U(\theta,\varphi)}{\mathrm{P_{input}}} \tag{1.9}$$

Antenna gain takes into account the radiation efficiency e_{rad} as well as the directivity, as given by:

From equation (1.9)

$$G\left(\theta,\varphi\right)=\frac{4\pi U(\theta,\varphi)}{\mathrm{P_{input}}} \tag{1.10}$$

Using the equivalent circuit of the antenna as shown in Fig. 1.1 the radiation efficiency of the antenna is the ratio of power delivered to the radiation resistance R_r to the total power delivered to the total antenna resistance antenna that is $R_r + R_l$ (loss resistance). So, the radiation efficiency can be written as

$$e_{rad}=\frac{\mathrm{P_{rad}}}{\mathrm{P_{input}}} \tag{1.11}$$

$$\mathrm{P_{input}}=\mathrm{P_{rad}}+\mathrm{P_{losses}} \tag{1.12}$$

Putting the value of P_{input} in equation (1.11)

$$e_{rad}=\frac{\mathrm{P_{rad}}}{\mathrm{P_{input}}}=\frac{\mathrm{P_{rad}}}{\mathrm{P_{rad}}+\mathrm{P_{losses}}}=\frac{\frac{1}{2}R_r|I|^2}{\frac{1}{2}R_r|I|^2+\frac{1}{2}R_l|I|^2} \tag{1.13}$$

According to C. A. Balanis [13] gain does not include losses arising from impedance and polarization mismatches. It is then related to the directivity as:

$$\mathrm{G}\left(\theta,\varphi\right)=e_{rad}D\left(\theta,\varphi\right) \tag{1.14}$$

1.4 Hertzian dipole

An infinitesimally small current element whose length dl is much smaller than the wavelength i.e. $dl < \lambda$ ($dl << {}^{\lambda}\!/_{50}$) of wire is known as Hertzian dipole. It is very thin, and its radius "a" is also much smaller than the wavelength λ. An infinitesimal wire element is positioned symmetrically at the origin of the coordinate system and oriented along the z-axis as shown in Figure 1.2. Assume that the infinitesimal time varying current in Hertzian dipole is

$$I(t)=I_0e^{j\omega t}\hat{z} \tag{1.15}$$

To solve the field radiated by the infinitesimally small current carrying element, we need electromagnetic fields, It is needed to find the magnetic vector potential $\overrightarrow{A}$ by using equation (1.16)

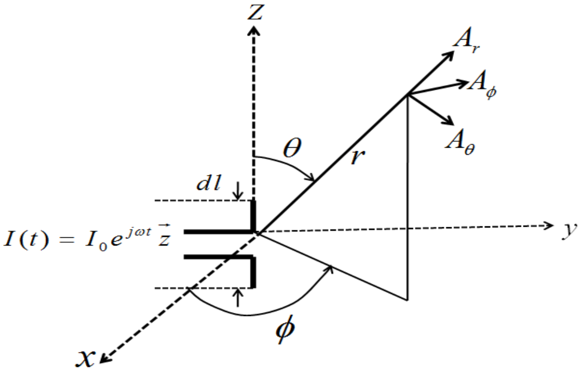

Figure 1.2: Hertzian dipole

$$\overrightarrow{A} = \frac{\mu_0 I_0 dl}{4\pi r} e^{-jkr} \hat{z} \tag{1.16}$$

where $I_0 dl$ is the small current carrying element, k is the wave number and μ_0 is the permeability of free space.

Then magnetic vector potential $\overrightarrow{A}$ is transformed into spherical coordinates as

$$A_r = A_z \cos\theta = \frac{\mu_0 I_0 dl}{4\pi r} e^{-jkr} \cos\theta \tag{1.17}$$

$$A_\theta = A_z \sin\theta = \frac{\mu_0 I_0 dl}{4\pi r} e^{-jkr} \sin\theta \tag{1.18}$$

$$A_\varphi = 0 \tag{1.19}$$

From Maxwell's equation [7], the relation between $\overrightarrow{A}$ and $\overrightarrow{H}$ can be defined as

$$\nabla \times \overrightarrow{E} = -j\omega\mu\overrightarrow{H} \tag{1.20}$$

$$\overrightarrow{H} = \frac{1}{\mu} \nabla \times \overrightarrow{A} \tag{1.21}$$

We can find E-fields and H-fields as:

$$H_r = H_\theta = 0 \tag{1.22}$$

$$H_\varphi = j\frac{kI_0 dl \sin\theta}{4\pi r}\left[1 + \frac{1}{jkr}\right] e^{-jkr} \tag{1.23}$$

$$E_r = \eta \frac{I_0 dl \cos\theta}{2\pi r^2}\left[1 + \frac{1}{jkr}\right] e^{-jkr} \tag{1.24}$$

$$E_\theta = j\eta \frac{kI_0 dl \sin\theta}{2\pi r^2}\left[1 + \frac{1}{jkr} - \frac{1}{(kr)^2}\right] e^{-jkr} \tag{1.25}$$

where $k = \frac{2\pi}{\lambda}$ is the wave number and $\eta = \sqrt{\mu/\varepsilon}$ is the intrinsic impedance in Ω. In the far field region $kr \gg 1$, the E- and H-field can be simplified by:

$$E_\varphi = 0 \tag{1.26}$$

$$E_\theta \approx j\eta \frac{kI_0 dl \sin\theta}{2\pi r^2} e^{-jkr} \tag{1.27}$$

$$H_\varphi \approx j \frac{kI_0 dl \sin\theta}{4\pi r} e^{-jkr} \tag{1.28}$$

In the far region the field distribution is essentially independent of the distance from the antenna. The E- and H-fields components are perpendicular to each other and transverse to the direction of propagation.

1.4.1 Radiation resistance

Hertizan dipole can be equivalently modeled as a radiation resistance. The real part of the input impedance for a lossless Hertizan dipole is denoted as the radiation resistance R_r. By integrating the Poynting vector over a closed surface, the total radiated power P_{rad} by the source can be found out. The radiation resistance R_r can be defined from the real part of radiated power, which is given below

$$P_{rad} = \frac{1}{2}\mathrm{Re}\int\left(\overrightarrow{E} \times \overrightarrow{H*}\right) ds = \eta\left(\frac{\pi}{3}\right)\left|\frac{I_0 dl}{\lambda}\right|^2 = \frac{1}{2}|I_0|^2 R_r \tag{1.29}$$

$$R_r = \eta\left(\frac{2\pi}{3}\right)\left|\frac{dl}{\lambda}\right|^2 = 80\pi^2\left|\frac{dl}{\lambda}\right|^2 \tag{1.30}$$

It is to be noted that from the above formula that the resistance R_r is dependent on dl and the wavelength λ

1.5 Limitations for electrically small antennas

In 1948, L. J. Chu [14] first investigated the fundamental limitations for electrically small antennas and subsequently in the year of 1960, R. F. Harrington [15] also postulated the fundamental limitations of electrically small antennas. Therefore together they are called Chu-Harrington criteria

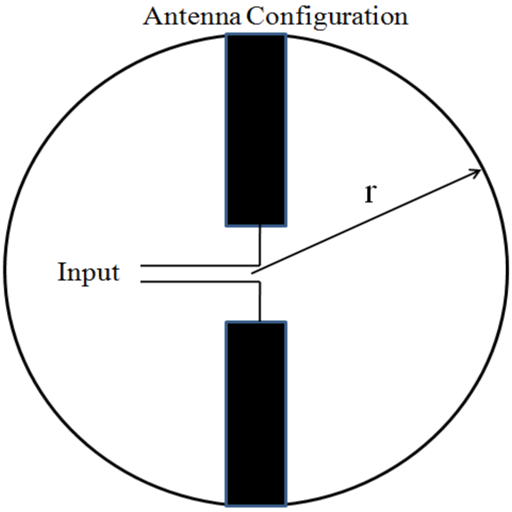

Figure 1.3: Antenna within a sphere of radius r

for electrically small antennas. In 1964, R. E. Collin and S. Rothschild evaluated the quality factor of the antenna by subtracting the energy density associated with the power flow from the total energy density. The definition of electrically small antenna reveals that the electrically small antenna is the one which fits inside a sphere of radius $r = 1/k$ where k is the wave number and equal $2\pi/\lambda$. The limitations of electrically small antennas are obtained by assuming that the whole antenna structure (with a largest linear dimension of $2r$), and its transmission line and oscillator are all enclosed within virtual a sphere of radius r [16], as shown in figure 1.3. Chu's approach uses spherical wave functions to describe the field and calculate the quality factor Q. When $kr < 1$, the quality factor Q of a small antenna can be expressed as [17]:

$$Q = \frac{1 + 2(kr)^2}{(kr)^3[1 + (kr)^2]} e_{rad} \tag{1.31}$$

where e_{rad} is the radiation efficiency of the antenna. Equation (1.31) demonstrates the relationships between the quality factor Q and the antenna size as well as the radiation efficiency. Since the Q rises rapidly as antenna size decreases, the result relates the lowest achievable Q to the maximum dimension of an electrically small antenna. Since the FBW of any antenna is inversely proportional to Q, although the increases of Q with reducing size r indeed implies a fundamental limitation on the widest achievable bandwidth FBW as shown in equation (1.32)

$$FBW = \frac{1}{Q} \tag{1.32}$$

Therefore the antenna size, quality factor, bandwidth and radiation efficiency are closely interrelated and there is absolutely no freedom to independently optimize each one. Hence there exists always tradeoff between them to obtain an optimal antenna performance.

1.6 Classification of compact antennas

Now-a-days designs of compact antennas are required for modern handheld wireless communication gadgets due to limited space available within these gadgets. Compact antenna may be classified into four categories such as microstrip antenna, dielectric resonator antenna, planar monopole antenna and printed monopole antenna.

1.6.1 Microstrip antenna

Microstrip antennas are generally composed of a thin conducting patch which is printed on one side of dielectric substrate and having a ground plane on the other side of the substrate. The radiating patch and ground plane are normally made of copper, while dielectric substrates are usually made of non-magnetic material. Dielectric constants of the substrates are usually in the range of 1 to 10. Several shapes of microstrip patch are used such as rectangular, circular, elliptical, hexagonal and triangular etc. These patch configurations can be excited by using different feeding mechanism. There are four popular feeding mechanisms viz. microstrip feed line, coaxial cable feeding, aperture coupling and proximity coupling. Effective radiation along the length of patch antenna is possible if the length of the patch would be a half of the guided wavelength. Due to fringing field creation between the periphery of the ground plane and the patch, radiation occurs from the radiating patch. To get the desired performance of the microstrip antenna such as larger bandwidth and better efficiency, low dielectric constant with thick substrate should be chosen. However as the thickness of substrate increases more surface wave and spurious radiation also increases, results in hampering the bandwidth. Microstrip antenna can be used over wide frequency range from few MHz to GHz. There are several advantages and disadvantage of microstrip antennas as given below [18].

Advantages

- Light weight, inexpensive and small size.
- Easy to integrate with the microwave integrate circuit (MMIC).
- The microstrip antenna can be easily mounted on missiles, rockets and satellite without major alteration.
- Dual frequency and dual polarization operations are possible.
- Matching element and feed line can be fabricated simultaneously with antenna structures.
- Linear and circular polarizations are possible with simple modification of radiating patch and changes in feed location.

Disadvantages

- Narrow bandwidth (typically less than 5 percent).
- Low RF power handling capability.
- Poor end fire radiation performance.
- Practical limitations on the maximum gain.
- Poor isolation between the radiating elements and feed network.

1.6.2 Planar monopole antenna

With entrance of many new services in new millennium, there is a tremendous increase in the use of planar monopole antennas, particularly owing to its low cost, small size, ease of fabrication, wideband radiation characteristics and omni-directional radiation pattern. To cater different services such as GPS, GSM 1800, Bluetooth, WLAN (2.5 or 5−6 GHz), UWB system (3.1−10.6 GHZ) and satellite communication systems by the same devices, planar monopole antennas are becoming more popular in the recent years.

The monopole antenna was first invented by Guglielmo Marconi in the year of 1895. The shape of this antenna was a straight wire monopole antenna, which was installed vertically above a perfectly conducting ground plane with simple configuration but vertical polarization as well as horizontal omni-directional radiation pattern. The impedance bandwidth of such monopole antenna can be enhanced by optimizing their structure, such as increasing the thickness of wire elements or loading the typical structures like skeletal conical monopole, helical monopole, cage monopole etc. [19–22]. Compared to thin-wire monopoles, the skeletal conical or cage monopoles are more expensive and bulky. To broaden the impedance bandwidth planar elements (less cost and simple structure) have been used to replace the wire elements of the monopoles [23–27]. By using planar radiators impedance bandwidth of monopole antennas can be broadened up to 75 percentage. Generally, the wideband antennas design for example planar fractal monopoles [28] is much simpler than multiband antenna design of narrowband applications. The replacement of planar radiating element of different shapes in place of the cylindrical wire element increases the radiating surface of the monopoles, imparts huge effect on the bandwidth of the monopole antenna. As a result, the bandwidth of the planar monopole antenna increases considerably. According to [25] mathematical expression for lower edge frequency of planar elliptical monopole antenna (as shown in Figure 1.4) can be

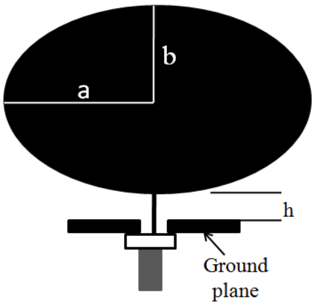

Figure 1.4: Example of planar elliptical monopole antennas

$$f_L = \frac{c}{\lambda} = \frac{7.2}{L + r + h}\text{GHz} \tag{1.33}$$

where, L is the length of the equivalent cylindrical monopole (which is equal to 2b of planar elliptical monopole height), r is the effective radius of an equivalent cylindrical monopole antenna (which is given by $2\pi rL = 2ab$) and h is the gap between the ground plane and elliptical patch antenna. The ground plane of the planar monopole antenna is also a part of the radiating configuration and the ground plane affects the characteristics of the antenna such as bandwidth enhancement and radiation characteristics. Therefore planar monopole antennas are becoming more attractive to optimistic

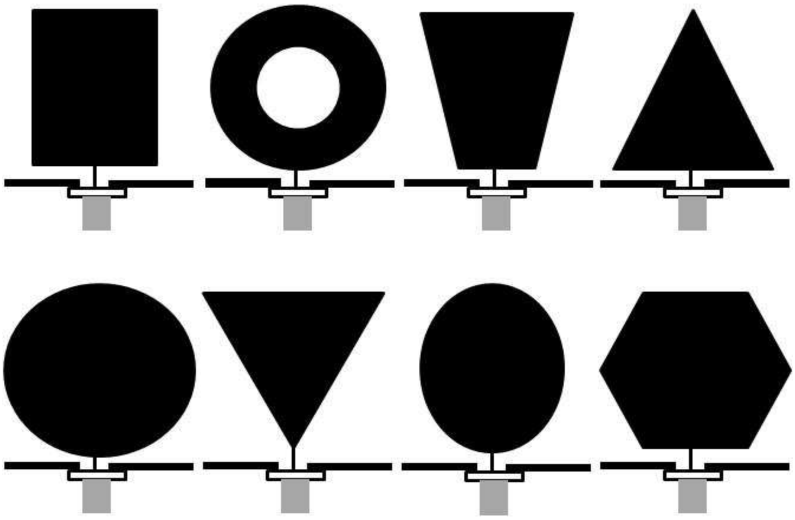

Figure 1.5: Various shapes of planar monopoles

developments such as wireless communication systems, software-defined radio systems and ultra-wideband (UWB) systems. Various of shapes of planar monopole is shown in Figure 1.5 [29].

1.6.3 Printed monopole antenna (PMA)

As discussed earlier in case of planar monopole antennas, the radiating element is perpendicular to the ground plane and hence they are not suitable for integration with printed circuit boards (PCB) or microwave monolithic integrated circuits (MMIC). Planar monopole antenna offers large bandwidth but limited application for modern hand-held wireless communication devices.

Printed monopole antennas are the versatile antenna which has generated a large attention to researchers across globe in recent year. It is because of printed monopole antenna (PMA) can offer very wide bandwidth and widely used for wireless communication applications. Here feeding structure and the radiating element are printed on the front side of the substrate and it is suitable for integration into circuit board as terminal antennas. The back side of the antenna is a partial ground plane and covers only some portion of the microstrip feed line. The function of the partial ground plane is to provide a mirror effect and impedance bandwidth enhancement. Performance of the antenna significantly varies for infinite ground plane to finite ground plane (partial ground plane) transition. Generally, structure of feeding element of the printed monopole antenna can be mainly classified into two categories. First is the microstrip line feeding structure [30–33] and second is coplanar waveguide feeding structure [34–37]. Printed monopole antenna can be used for several communication systems such as GPS, GSM1800, ISM, WLAN, HIPERLAN, UWB and UWB vehicular radar. Printed monopole antennas are also provides stable radiation-pattern characteristics and reasonable gain over the entire frequency range. The various structures of the printed monopole antennas are depicted in Fig. 1.6.

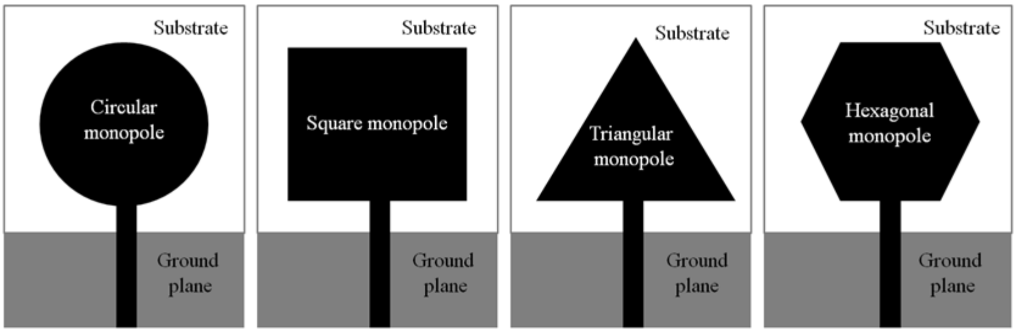

Figure 1.6: Various configurations of printed monopole antenna

1.7 Motivation

Over the past few decades, wireless communication systems have been developed substantially. Along with rapid growth in the number of wireless communication users and applications, the demand for different types of wireless communication systems such as GPS, GSM 1800, Bluetooth, WLAN, UWB and UWB vehicular radar are also increasing rapidly. To accommodate all these wireless communication systems in a single device, modern hand held gadgets are required. A SWB printed monopole antenna can cover many wireless communication services. Due to several features such as extremely large bandwidth, small size, low cost and suitable for integrating with monolithic microwave integrated circuits (MMIC) printed monopole has becomes attractive for super wideband applications.

One important challenge in the SWB communication systems is the design of an antenna to accommodate in the limited space provided by hand held gadgets and which can also offer extremely large bandwidth over entire frequency band. SWB printed monopole antenna with microstrip feeding structure are more popular for broadband application. Because of the partial ground plane on the back side of the substrate, which provides a mirror effect and hence large impedance bandwidth can be enhanced. To enhance the large impedance bandwidth, a triangularly tapered microstrip feedline is chosen for feeding the SWB band antenna. Along with tapered feed region and tapered radiating patch are also employed to get the best performance. SWB radio antenna have all the advanced features of UWB antenna like higher channel capacity, higher precision and super resolution in communication, ranging etc.. The frequency range of our SWB antenna is 1.1−100 GHz, with ratio bandwidth of 90.9:1, which is obtained by dividing the highest frequency by lowest frequency. Size miniaturization is a major challenge for the design of the SWB antenna. Because of the antenna size is directly related to the size of the devices. One important issue to be noted for SWB antenna is that, it may cause electromagnetic interference to the existing narrow band such as Worldwide Interoperability for Microwave Access (WiMAX) operating at the band of 3.3−3.7 GHz, Wireless Local Area Networks (WLAN) operating at the band of (5.15−5.825 GHz) and X- band satellite communication systems (for down link: 7.25−7.745 GHz and uplink: 7.9−8.395 GHz). These narrow bands lie within the SWB band specification. To have no or marginal effect at these bands, radiation of the SWB antenna is to be suppressed at these bands. To mitigate this interference issue, SWB antennas with band-notched characteristics have been proposed. Till date most of the antennas have been designed to have notch within UWB band.

To meet these challenges stated above, a suitable SWB antenna along with band notch characteristics in WIMAX, WLAN and X-band satellite communication systems frequency region and also that supports a very large bandwidth should be designed. To obtain such a wide frequency range, bandwidth enhancement techniques should be used. A parasitic element and slot should be designed for creating notches to mitigate the potential interference with the narrow band system. This band-notch SWB antenna should have good radiation characteristics with reasonable gain and compact size.

1.8 Contribution of the thesis

In this section, contribution of the thesis is summarized as follows:

(a) A compact printed triangular monopole antenna (PTMA) has been proposed for UWB application. This compact antenna uses a triangular radiating patch, a microstrip transition (near the front end of the radiating patch), a 50 Ω microstrip feed line and a round-cornered ground plane that provides a measured bandwidth from 1.8 GHz to 15.0 GHz. The proposed antenna structure has wide bandwidth and small size compared to the conventional antenna [38–43].

(b) Proposed a design methodology for super wideband (SWB) printed monopole antenna. This SWB monopole antenna has been composed of three parts: feed region, feed line and radiating patch. Each part of the antenna has been optimized to get best antenna performance and extremely large bandwidth (2.8−100 GHz) has been obtained.

(c) Proposed a new printed monopole antenna for super wideband applications. The simulated result shows that it is a super wideband antenna applicable for frequencies from 2.5 GHz to 80 GHz, while measured results have been shown upto 25 GHz (due to limitation of the available vector network analyzer) and can cover most of the communication systems as compared to [44–46].

(d) Proposed a new structure for realization of super-wideband radiation characteristics (.9−100 GHz) along with notch capability. By introducing U-shaped and C-shaped parasitic element single band-notch functionality has been introduced in the frequency band of 5−6 GHz for WLAN. Proposed antenna has been designed to notch within SWB region, however till date most of the antennas have been designed to notch within UWB [47–49] region.

(e) In this section a compact dual band-notched monopole antenna is proposed for super wideband (SWB) applications. Here two different antennas have been examined using two different substrates. First antenna has been designed by FR4 substrate and second antenna has been designed by RT/Duroid substrate. Dual band-notched functionality has been realized by inverted U-shaped slot, open-circuited stub (for WLAN) and U-shaped parasitic element. Proposed antenna has small size and large bandwidth with dual band-notched characteristic as compared to conventional antenna [50–53].

1.9 Organization of the thesis

This thesis is divided into six chapters. The organization of this thesis is as follows:

Chapter-1:

This chapter introduces the brief background on Super wideband (SWB) technology and the printed monopole antenna. Apart from this, chapter one also covered basic antenna theory and its parameter. The motivation and the thesis contribution are presented thereafter.

Chapter-2:

This chapter provides a brief description of design of printed triangular monopole antenna for UWB application. It also includes the simulated and experimental results of the fabricated prototype of the UWB triangular printed monopole antenna. In addition, a time domain characteristic of the antenna has been also analyzed.

Chapter-3:

Chapter 3 illustrates about the design aspect of super wideband printed monopole antenna. A triangular tapering and Raicu's optimal taper have been employed to enhance the bandwidth. The antenna is designed theoretically, simulated, fabricated and measured.

Chapter-4:

A new printed monopole antenna has been designed for super wideband applications in this chapter. A triangular tapered feed line has been used for feeding the exponentially tapered feed region and patch of the proposed antenna. All simulated and measured results are included in this chapter. Also time domain characteristics are evaluated experimentally.

Chapter-5:

This chapter includes the realization of super wideband antenna along with notch capability. To mitigate the interference issue, SWB antennas with band-notched characteristics have been proposed. Apart from that two different band-notched SWB monopole antennas structure have been designed and fabricated with two different substrates, one with FR4 substrate and another with RT/Duroid 5870 substrate. Both antenna has been designed, fabricated and tested successfully.

Chapter-6:

Chapter six provides a super-wideband antenna along with dual notch functionality. To avoid the interference problem from the existing narrow band system, it is necessary for SWB antennas to have dual band-notched characteristics. Two similar antenna structures have been realized on different substrates, one with FR4 substrate and another with RT/Duroid 5870 substrate. All simulated and measured results of the both antennas are reasonably matched.

Chapter-7:

Conclusion from thesis research work and scope for future research work are discussed in chapter seven.

2

Triangular printed monopole antenna for ultra-wideband application

Contents

2.1 Introduction

Over the past decade years usage of internet, messaging, e-mail and mobile phones are growing rapidly. Many devices are using wireless instead of wire for transmitting and receiving data. The rapid growth in technology and the successful commercial deployment of wireless communication systems are significantly changing the daily lives. Nowadays users can access data, voice and streamed multimedia across the globe from anywhere and any time and at a high data rate. It is due to the transforming of analog cellular communication to digital domain, the fast development of 3G and 4G radio systems. Since users required faster service, higher capacity and more secure communication, new technologies like ZigBee, Wi-Fi (802.11a, b, g) and Bluetooth (wireless) have to find place in this overcrowded and scarce radio frequency (RF) spectrum. All radio technology occupies specific part of spectrum to avoid interference. For instance, signals for TV, radio, mobile phones are sent at different frequencies.

Ultra-wideband communication is basically different from other communication techniques because it uses extremely narrow RF pulses to communicate between transmitters and receivers. These narrow pulses give large bandwidth in frequency domain and offer many advantages such as large throughput, covertness, robustness to jamming, and coexistence with current radio services. Typically spectrum of narrow band and ultra-wideband system are shown in fig. 2.1. It shows that the power used for ultra-wideband systems over the whole band is much lower than the power used by narrowband systems. UWB technology has large bandwidth compared to the conventional narrow band technology. Instead of transmitting over different frequencies bands, here we transmit information over a large bandwidth with very low power. Earlier, UWB technology had been used only for the military purposes. But, currently it has been used for various commercial applications due to its huge bandwidth, very low transmission power level and high data rate [54]. Applications of UWB, such as wireless universal serial bus (USB) and wireless personal area network (WPAN) with hundreds of Mega bits per second (Mbps) to some Giga bits per second (Gbps) with distances covering from 1 to 4 meters would be possible in the near future. UWB systems can replace cables connecting camcorders and VCRs, as well as other consumer electronics applications, such as laptops, DVDs, digital cameras, and portable HDTV monitors. Since UWB system operates in a wide

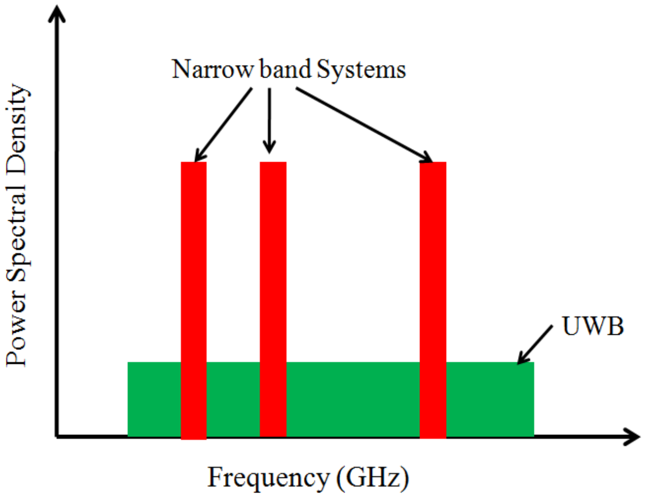

Figure 2.1: Spectrum of Narrow band and Ultrawideband systems.

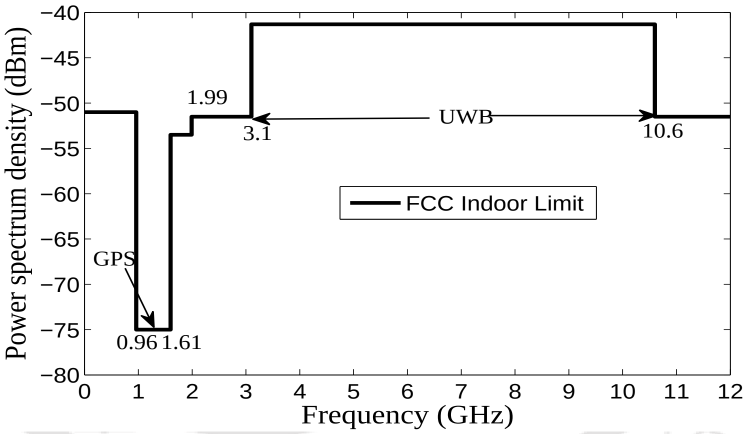

Figure 2.2: Spectral mask and bandwidth for indoor UWB communication system.

bandwidth (7.5 GHz) and hence, it is necessary to share the spectrum with other existing communication systems for commercial usage and consequently, interference may occur. To overcome this problem, Federal Communications Commission (FCC) specified spectral masks for ultra-wideband communication systems [55]. In February 2002, FCC has suggested the unlicense use of UWB in the frequency range between 3.1 to 10.6 GHz with a transmit power of -41.3 dBm/MHz for short-range indoor wireless communication. UWB pulses are extremely short pulses with fast rise and fall time [56]. So they have a very broad spectrum with low energy content. These short pulses can avoid the effects of multipaths. Fig. 2.2 shows the spectral mask and bandwidth for indoor UWB communication system as approved by the FCC. According to FCC regulations the spectrum was di-

Table 2.1: Emission limits for various UWB applications in each operational band

Application	ERIP in dBm at various operating bands(GHz)					
	0.96-1.61	1.61-1.99	1.99-3.1	3.1-10.6	10.6-22.0	22.0-29.0
Indoor Communication	-75.3	-53.3	-51.3	-41.3	-51.3	-51.3
Outdoor Communication	-51.3	-63.3	-61.3	-41.3	-61.3	-61.3
Imaging	-53.3	-51.3	-41.3	-41.3	-41.3	-51.3
Vehicular Radar	-75.3	-63.3	-63.3	-63.3	-41.3	-41.3

vided into 3 major categories such as communications, imaging, and vehicular radar. For indoor and outdoor UWB communications devices category, different emission limits are allotted. Between 1.61 GHz and 3.1 GHz, the spectral mask for outdoor devices is 10 dB lower than that for indoor devices. For imaging devices, their operation is restricted to law enforcement and protection teams. The table 2.1 [57] shows the emission limits for the three categories. UWB has several advantages, which can be summarized as follows [58].

(i) Immune to multipath effect.

(ii) Secure wireless communication.

(iii) High data rate transmission.

(iv) High penetration.

(v) Capability to share the frequency spectrum.

Multipath is caused when signals get reflected from various objects like wall, ceiling, vehicles and trees. It is a major problem for narrow band signals. But UWB signals are immune to multipath fading due to short duration of pulses and low duty cycle. Fading of UWB signals is also less because these signals are used in indoor applications within a range of 10 m [59].

Since UWB systems operate below the acceptable noise floor level, they are inherently covert and extremely difficult for unintended users to detect and hence it provides high secure and reliable communication [60].

According to channel capacity of Shannon's theorem, capacity of a channel can be enhanced by either widening the bandwidth or increasing the signal-to-noise ratio (SNR). Widening the bandwidth offers high-data-rate transmissions at low SNR. Similarly, by increasing the signal-to-noise ratio (SNR) capacity of a channel can also be enhanced [61].

UWB signals have good penetration capability through different materials. This helps UWB technology in ground penetrating radars and to communicate through walls and objects. The penetrating property works only when the signals occupy lower frequency portion of the RF spectrum.

Since the power limit of UWB system is -41.3 dBm/MHz, so the systems are allowed to be present below the noise floor of a narrow band receiver and allows the UWB signals to coexist with other narrow band receivers with minimum interference [62].

As a precursor to SWB antennas, we will discuss UWB antennas in this chapter. UWB antennas have a bandwidth ratio of (3.4:1) unlike SWB antennas which has bandwidth ratio of at least 10:1 [2].

(i) Firstly, a large frequency bandwidth is the main parameter for UWB antenna which distinguishes a UWB antenna from other antennas. In 2002 FCC had announced an absolute bandwidth of the UWB antenna should be greater than 500 MHz or a fractional bandwidth of atleast 20% [55].

(ii) Secondly, UWB antenna performance should be consistent over entire frequency band from 3.1 to 10.6 GHz. All characteristics like impedance bandwidth, radiation pattern and gain of this UWB antenna should be stable across entire operational bandwidth.

(iii) Thirdly, UWB antenna may have directional or omni-directional radiation properties for practical applications. Omni-directional radiation patterns are generally preferred in mobile communications and hand-held gadgets. Directional antenna characteristics are normally preferred for radar, imaging and other directional systems where high gain is needed.

(iv) Fourthly, UWB antenna should have small size and should be easily accommodated in the limited space provided by hand held gadgets. Also UWB antenna should be low cost, low profile and suitable for integration with printed circuit board (PCB).

(v) Finally, time domain characteristics of the UWB antenna should be acceptable. The performance of the antenna should be approximately same over entire bandwidth. Basic antenna parameters such as reflection coefficient and gain have little variation across the operating frequency for narrow band systems. In contrast, very short pulses are used for data transmission in UWB and a huge bandwidth is occupied by UWB system. Therefore, the UWB antenna cannot be treated as a ”spot filter” any more but a ”band-pass filter”. In this case, the UWB antenna provides more significant effect on the input signal. As a result, the primary aim for the UWB antenna is the minimum pulse distortion [63] because the signal is the carrier of useful information. Therefore, it is indispensable and important to study the antenna’s characteristics in time domain.

Currently, there is a great attention paid for ultrawideband (UWB) systems since Federal Communication Commission (FCC) has announced in 2002 the unlicensed use of the 3.1-10.6 GHz band with effective isotropic radiation power (EIRP) less than -41.3 dBm/MHz for commercial UWB communication applications [55]. Due to numerous features, such as high speed data rate, low power consumption, small emission power and low cost, UWB system has gained much attraction in the recent years. Some applications of UWB systems are personal area network (PAN), radar imaging systems, ground-penetrating radar and biomedical imaging, respectively [64, 65].

Printed monopole antennas are currently under consideration for use in emerging UWB application as they exhibit very attractive merits such as broadband impedance matching, compact size, and omnidirectional radiation pattern. Many techniques have been examined to improve the antenna bandwidth in the past few years. Low *et al.* [66] described enhancement of impedance bandwidth of the planar monopole by suspended plate antenna. Ammann [67] discussed control of the impedance bandwidth of wideband planar monopole antennas using a beveling technique. Jung *et al.* [68] discussed a compact and low profile wideband antenna with an L-shaped notch. Wi *et al.*. [69] achieved wideband characteristics using U-shaped microstrip parasitic elements. Oraizi and Hedayati [70] carried out a combination of Giusepe Peano and Sierpinski Carpet fractals shape for wideband impedance matching. As is well known, UWB antennas with various shapes such as cone-shaped [38], triangular-shaped [39], circular-shaped [40], fork-shaped [41], elliptical-shaped [42] and inverted-F shaped [43]

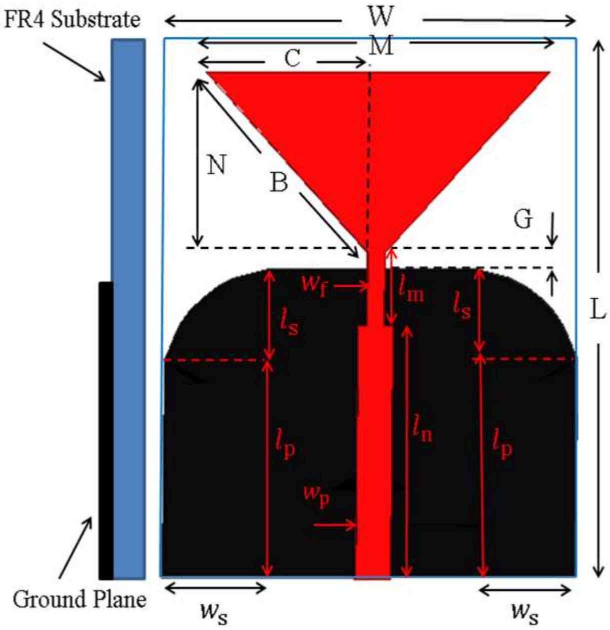

Figure 2.3: Geometry of the proposed triangular monopole antenna.

were reported in literature. However small size and wide bandwidth is essentially required for UWB applications. Size miniaturizing as well as ultrawide bandwidth of UWB monopole antenna is a challenging task for modern multipurpose handheld devices. A novel printed triangular monopole antenna (PTMA) with increased bandwidth is proposed for UWB applications. The proposed antenna structure has wide bandwidth and small in size compared to the antenna dimensions reported in [38–43, 71]. The impedance bandwidth of the proposed triangular monopole antenna is greatly improved by introducing a transition between the microstrip feed line and the printed triangular patch with a round-cornered ground plane. The antennas were simulated using frequency domain 3D full wave electromagnetic solver (HFSS version 14).

2.2 Triangular printed monopole antenna (TPMA)

2.2.1 Antenna geometry and design

The geometry of the proposed triangular monopole antenna is shown in Figure 2.3. A novel 50 Ω microstrip transition feed line fed UWB printed triangular monopole antenna (PTMA) with a round-cornered ground plane is proposed. The proposed antenna consists of a triangular-shaped radiator on the top connected with a 50 Ω microstrip transition feed line and the round-cornered ground plane is printed on the backside of FR4 substrate as shown in Fig. 2.3. The antenna is printed on a 1.6 mm

Table 2.2: Dimensions of the proposed UWB Triangular Monopole Antenna

Parameters	L	W	W_s	W_p	W_f	l_m	l_s
Units (mm)	30	24	6	2	1	4	5
Parameters	l_n	l_p	N	B	G	M	C
Units (mm)	14	12	10	13.8	1	20	9.5

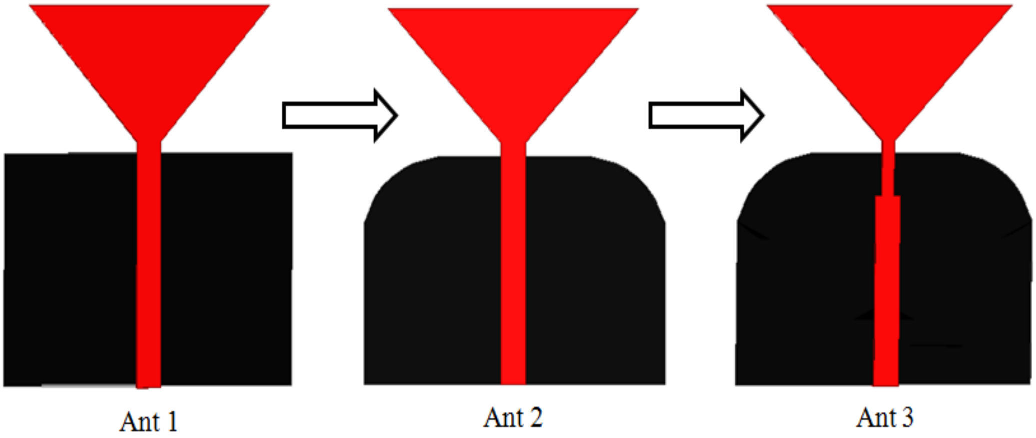

Figure 2.4: Impedance bandwidth improvement process.

thick FR4 substrate with a dielectric constant of 4.4 and a loss tangent of 0.018. The proposed antenna structure occupies overall dimension of about 24×30×1.6 mm^3. The detailed dimensions of the proposed antenna are given in Table 2.2. Fig. 2.4 shows the impedance bandwidth improvement process of the monopole antenna. Generally, a simple triangular patch antenna has a narrow band characteristics. To improve impedance bandwidth in this antenna, we shape the partially etched rectangular ground plane of the antenna 1 into round-cornered ground plane (denoted as Antenna 2). As we can see that round-cornered ground plane of the monopole antenna makes somewhat good impedance matching at high frequency region. In order to further improve the impedance matching for the entire band, a microstrip transition is introduced (near the front end of the radiating patch) between the 50 Ω microstrip feed line and the printed triangular patch (denoted as Antenna 3). Because of this transition involves stepped changes in impedance function (i.e., a single-section transformer), it increases the bandwidth of the transformer as impedance becomes closer to characteristic impedance of the microstrip feed line over a large bandwidth. The proposed antenna starts resonating from 1.8 GHz,

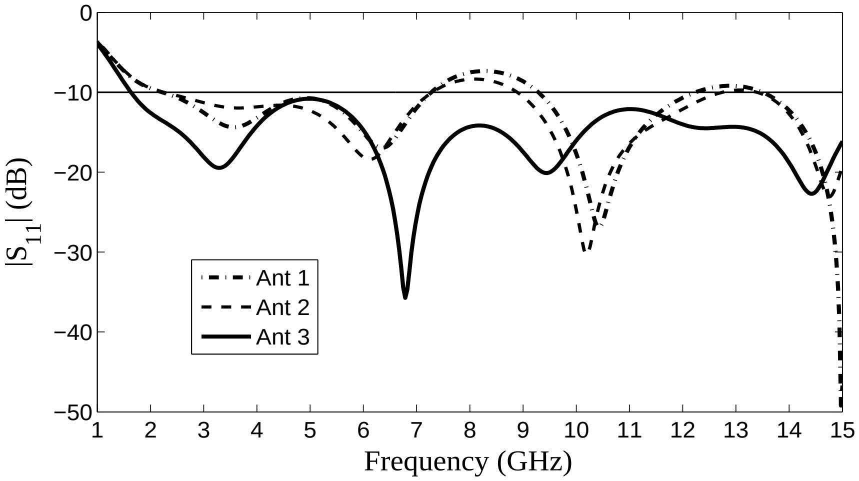

Figure 2.5: Simulated reflection coefficient of Antenna 1, Antenna 2 and Antenna 3.

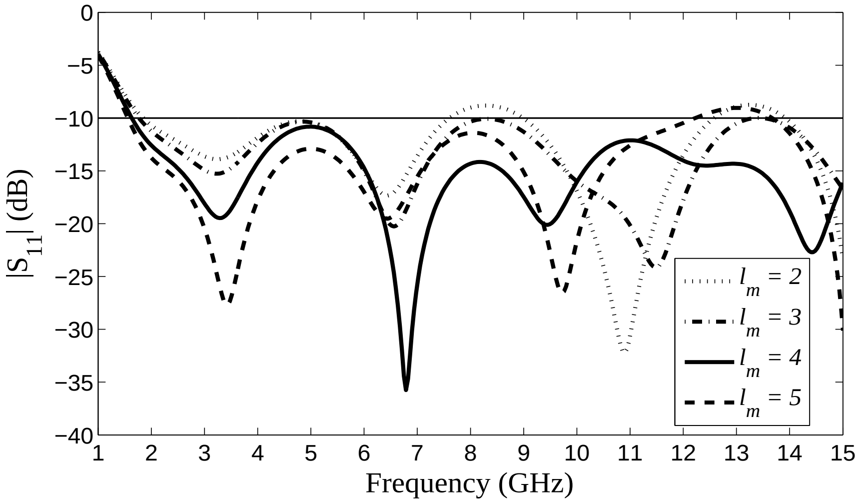

Figure 2.6: Parametric studies on the effect of different values of l_m on return loss of the proposed antenna.

due to resonant path (C+B+G) of the triangular monopole which is close to quarter-wavelength at this frequency. The lowest frequency within the bandwidth of the antenna can be calculated using three parameters C, B and G (refer to Fig. 2.3) which is given by equation 2.1

$$f_L = \frac{v_0}{4\,(C + B + G)\,\sqrt{\varepsilon_{eff}}} \tag{2.1}$$

where v_0 is the speed of light, ε_{eff} is the effective dielectric constant of the substrate.

2.2.2 Parametric study

In this section, the parametric study has been carried out by changing one parameter at a time and fixing the other. Fig. 2.5 shows comparison of the simulated reflection coefficient of Antenna

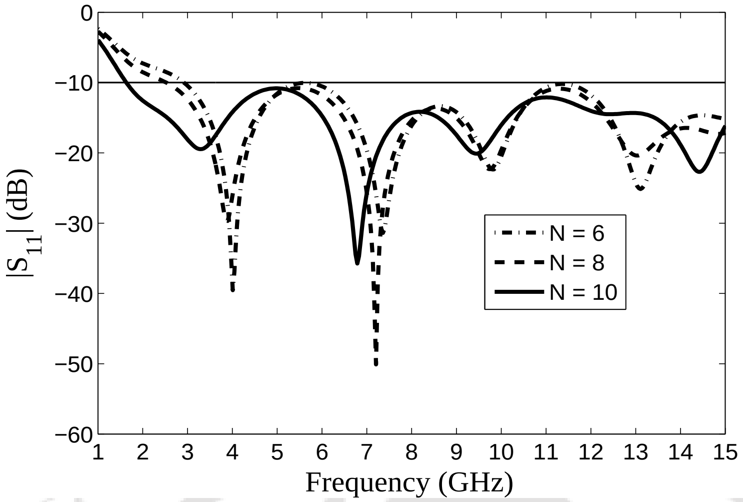

Figure 2.7: Parametric studies of effect of various patch length N on return loss of the proposed antenna.

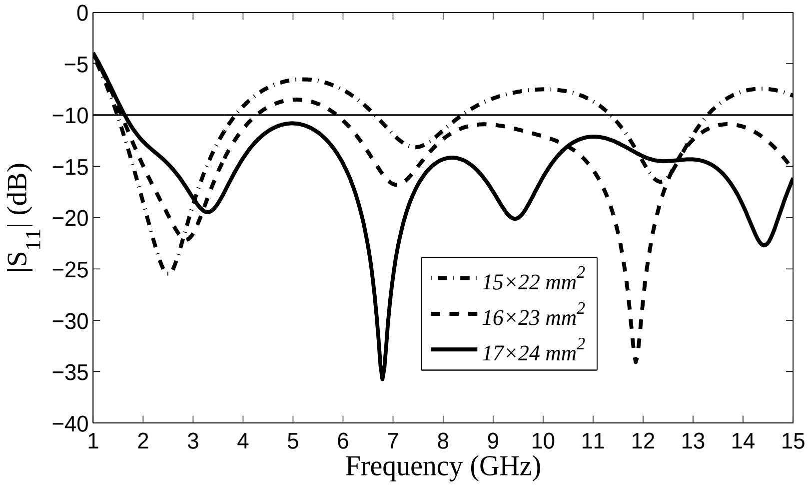

Figure 2.8: Simulated reflection coefficient curves with the different size of the overall round-cornered ground plane.

1, Antenna 2 and Antenna 3. It can be observed that by introducing an impedance step between microstrip feed line and radiating patch, the bandwidth of the proposed antenna increases from 111.1% to 157.1% for reflection coefficient < -10 dB. The simulated reflection coefficient of the UWB antenna with different values of the l_m are shown in Fig. 2.6. It is clearly seen that as l_m decreases from 4 to 2 mm, the impedance matching of the monopole antenna is gradually affected at frequencies around 8 and 13.5 GHz. However, as l_m increase from 4 to 5 mm, improvement of the impedance bandwidth within the UWB frequency region, but there is impedance mismatch for frequency band between 12 to 14 GHz. So, the optimal value of this parameter for maximum impedance bandwidth is 4 mm. Fig. 2.7 demonstrates the simulated reflection coefficient of the proposed printed triangular monopole antenna for the various patch length N. The length N of the triangular patch determines the resonant frequency. It is observed that the impedance bandwidth is the wider as the dimension of patch length N increase from 6 to 10 mm whereas by decreasing the patch length N, the lower frequency is shifted towards right, which results in decreased percentage bandwidth. At N = 10, the lowest resonant frequency moves towards lower frequency and gives wideband with minimum impedance mismatch. Thus, the impedance bandwidth of the optimized UWB monopole antenna can be enhanced by selecting the suitable value of N = 10.

Fig. 2.8 illustrates the simulated reflection coefficient curves with the different size of the overall round-cornered ground plane. As the size of the ground structure decreases from 17×24 mm^2 to 16×23 mm^2, the reflection coefficient is greater than -10 dB only at 5 GHz. Furthermore, when the size of the ground structure again decreases from 16×23 mm^2 to 15×22 mm^2, magnitude of reflection coefficient is tends to > -10 dB within the UWB frequency region. It shows that the impedance matching gradually becomes worst, when the size of the ground structure decreases. Thus, better impedance matching is achieved with a size of the ground structure of 17×24 mm^2. We can observe that antenna 3 gives broader bandwidth than Antenna 1 and Antenna 2.

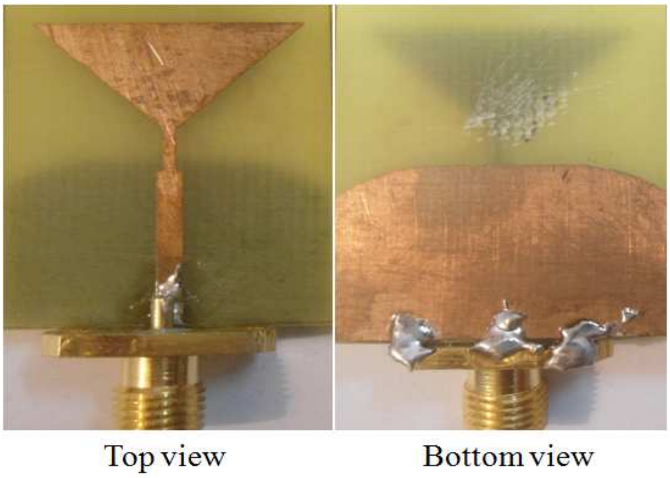
Top view Bottom view

Figure 2.9: Photograph of the fabricated printed triangular UWB monopole antenna.

2.3 Experimental results

A picture of the fabricated UWB printed triangular monopole antenna is shown in Fig. 2.9. The measurement of triangular monopole antenna was done by Rohde and Schwarz ZVA24 network an-

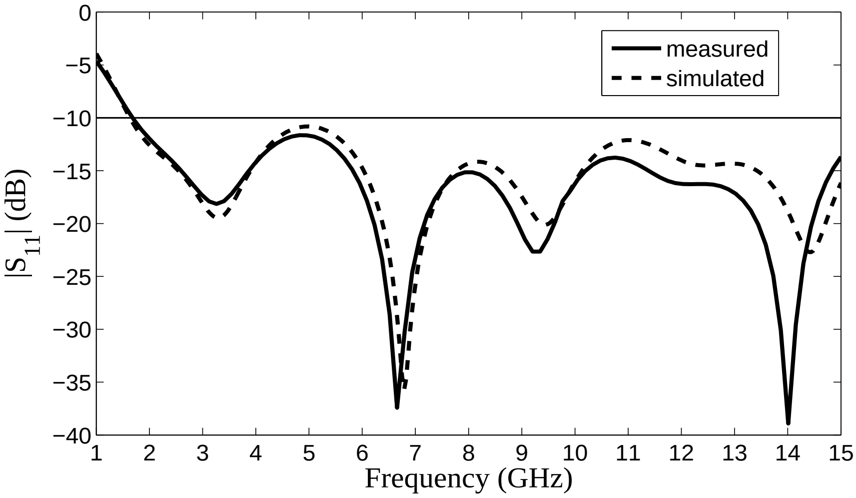

Figure 2.10: Measured and simulated return loss for the proposed triangular UWB monopole antenna.

alyzer. Fig. 2.10 plots the measured and simulated return loss as a function of frequency. There is reasonably good agreement between simulation and measurement throughout the UWB frequency region.

2.3.1 Radiation pattern

Fig. 2.11, 2.12 and 2.13 shows the measured radiation patterns in the H-planes and E-planes at frequencies 3.1, 7.0, and 10.0 GHz, respectively. The E-plane radiation pattern shows a typical figure-of-eight at frequencies of 3.1, 7.0, and 10.0 GHz, which shows that this antenna behaves like a conventional dipole or biconical antenna. A low cross polarization was observed within the FCC suggested UWB frequency region. It can be observed that the antenna has nearly omni-directional radiation pattern at frequencies of 3.1, 7.0, and 10.0 GHz in the H-Planes.

2.3.2 Gain

Fig. 2.14 plots the measured peak gain over the operating frequency from 1.8 GHz to 15.0 GHz. It can be seen that the peak gain for the triangular monopole antenna is about 3.7 dBi.

2.4 Time domain characteristics of UWB antenna

In the time domain, the UWB antenna may be represented by an impulse function and transient response $G(t,\theta,\varphi)$ of the antenna becomes more sufficient for the description of impulse systems. The antenna transient response not only dependent on time, but also depends on the angles of arrival $(\theta R_X, \varphi R_X)$, angles of departure $(\theta T_X, \varphi T_X)$ and polarization respectively [8]. Thus, the role of the an-

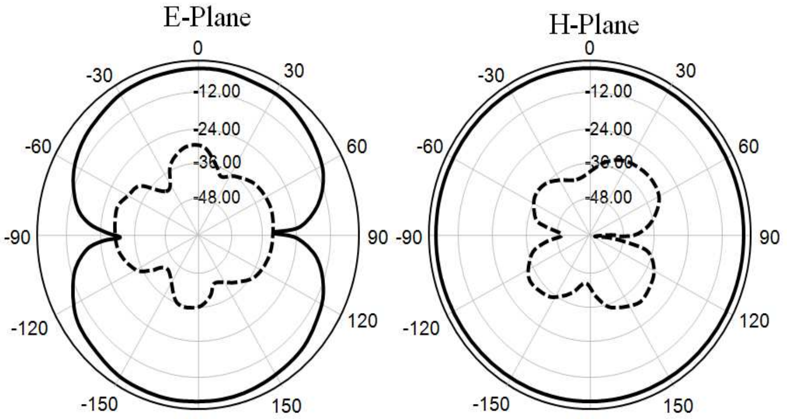

Figure 2.11: Measured radiation pattern for the proposed triangular UWB monopole antenna at 3.1 GHz. Solid line is co-polarization and dashed line is cross-polarization.

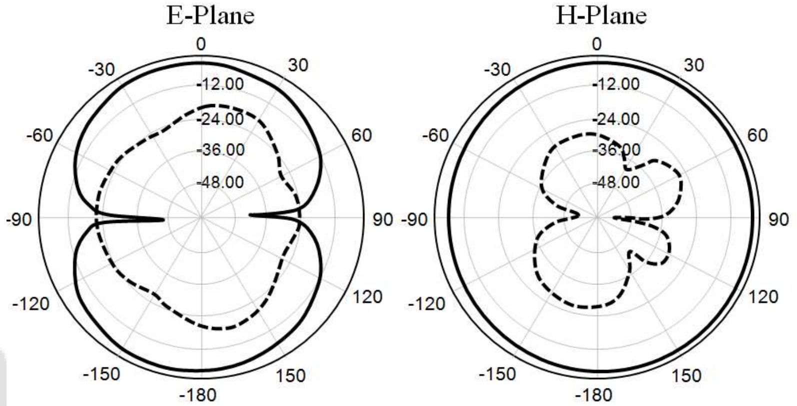

Figure 2.12: Measured radiation pattern for the proposed triangular UWB monopole antenna at 7 GHz. Solid line is co-polarization and dashed line is cross-polarization.

tenna angular behavior consideration is important in characterizing a UWB system. The transmitting antenna (T_X) and receiving antenna (R_X) link characterization in time domain is shown in Fig. 2.15 and it illustrates the input signal of the transmitting antenna passes through the system and is received by a receiving antenna. Relation between the transmitted signal and the received signal is given by equation 2.2. Using the convolution (*) property, transient response of the channel in a free-space (line of sight) can be calculated by (2.2).

$$\frac{A_{Rx}(t)}{\sqrt{Z_{CRx}}} = G_{R_X}(t,\theta_{Rx},\varphi_{Rx}) * G_{channel}(t,r_{TxRx}) * G_{Tx}(t,\theta_{Tx},\varphi_{Tx}) * \frac{A_{Tx}(t)}{\sqrt{Z_{CTx}}} \qquad (2.2)$$

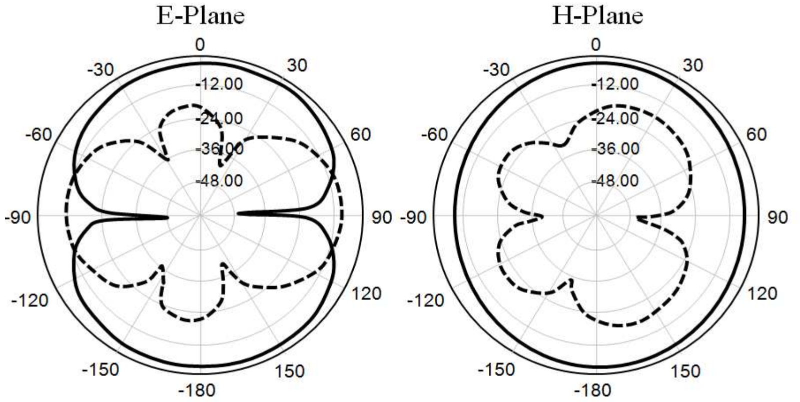

Figure 2.13: Measured radiation pattern for the proposed triangular UWB monopole antenna at 10 GHz. Solid line is co-polarization and dashed line is cross-polarization.

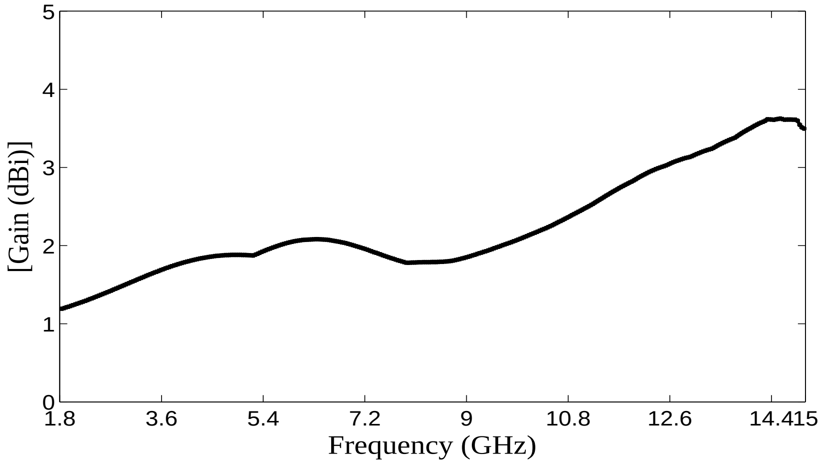

Figure 2.14: Measured gain for the proposed triangular UWB monopole antenna.

$$G_{channel}\left(t, r_{TxRx}\right) = \frac{1}{2\sqrt{\pi} r_{TxRx} C_0} \delta \left(t - \frac{r_{TxRx}}{C_0} \right) \tag{2.3}$$

where $A_{Tx}(t)$ is the amplitude of transmitted signal in [V].

$A_{Rx}(t)$ is the amplitude of received signal in [V].

$G_{Tx}\left(t, \theta_{Rx}, \varphi_{Rx}\right)$ is the impulse response of the transmit antenna in [m/ns].

$G_{Rx}\left(t, \theta_{Tx}, \varphi_{Tx}\right)$ is the impulse response of the receive antenna in [m/ns].

Z_{CTx} is the characteristic impedance of the transmit antenna in [Ω].

Z_{CRx} is the characteristic impedance of the receive antenna in [Ω].

r_{TxRx} is the distance between transmitting and receiving antennas in [m].

To analyze the signal dispersion in the UWB system, a time domain characteristic has been in-

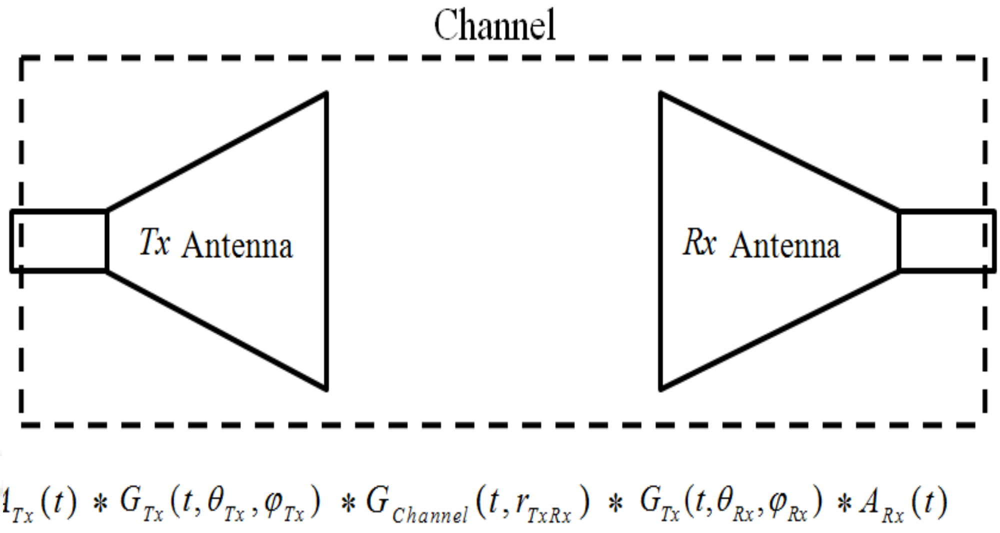

Figure 2.15: Transmitting and receiving antenna link level characteristics of UWB system in time domain.

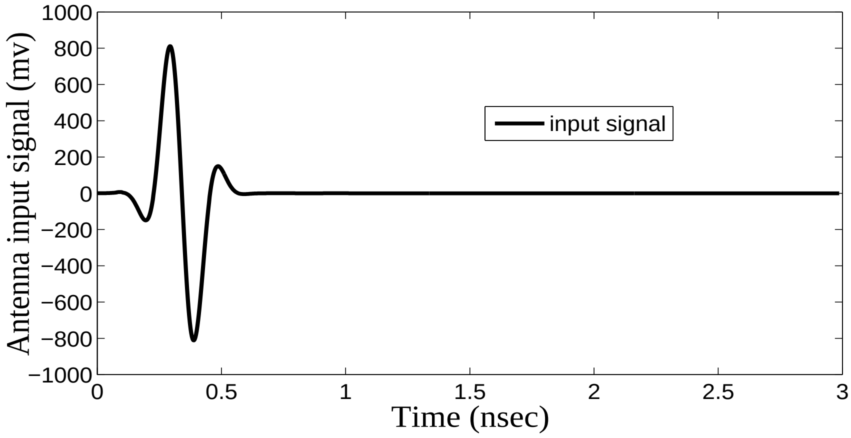

Figure 2.16: 5^{th} derivative of Gaussian pulse waveform in time domain.

vestigated. In this scheme, two identical antennas are kept at a distance of 60 cm in face-to-face and side-by-side. A 5^{th} derivative Gaussian pulse, as presented in (2.4), is used as the source signal to drive the transmitter [72].

$$G_5(t) = A\left(-\frac{t^5}{\sqrt{2\pi}\sigma^{11}} + \frac{10t^3}{\sqrt{2\pi}\sigma^9} - \frac{15t}{\sqrt{2\pi}\sigma^7}\right).\exp\left(-\frac{t^2}{2\sigma^2}\right) \tag{2.4}$$

where A is a constant chosen to meet the spectral mask set by FCC and σ has to be 51 ps to satisfy the FCC limitation. The power spectral density (dBm/MHz) of the antenna input signal (5^{th} derivative of Gaussian pulse) combined the FCC spectral mask for indoor UWB communication system is shown

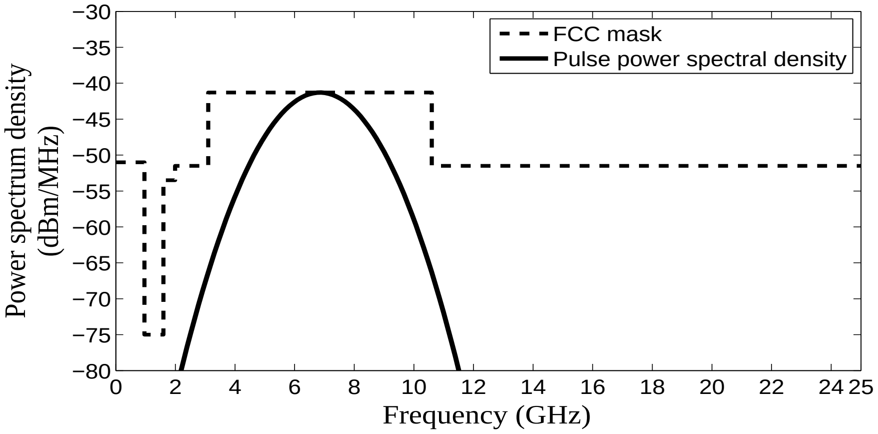

Figure 2.17: Power spectral density (dBm/MHz) of FCC spectral mask for indoor UWB communication system and power spectral density (dBm/MHz) of antenna input signal (5^{th} derivative of Gaussian pulse).

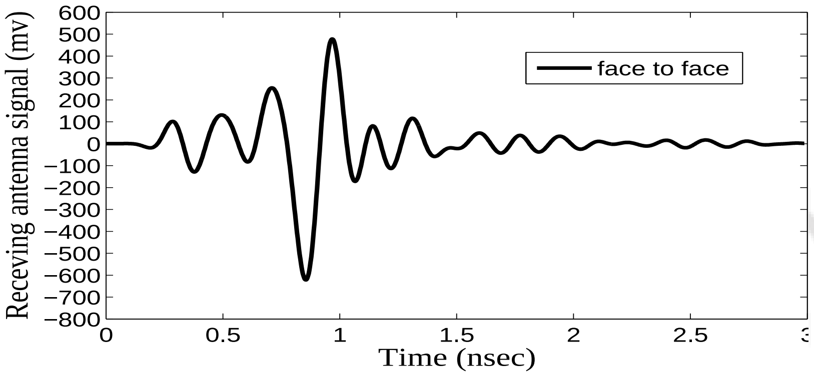

Figure 2.18: Face-to-face received pulse in time domain for a UWB system with two identical antennas.

in Fig. 2.17. The value of σ is 51 ns to ensure that the size and shape of the spectrum fit with the FCC mask. Fig. 2.16 shows the fifth-order-derivative of Gaussian pulse waveform with a width of 300ps in the time domain. The fifth order Gaussian pulse is generated in Tektronix AWG 7122B arbitrary signal generator and it is fed to the UWB antenna. At the receiver, the signal received by the UWB antenna is captured in Tektronix DPO 70804 digital phosphor oscilloscope. The received waveforms for the face-to-face and side-by-side orientations of the antenna are shown in Fig. 2.18 and Fig. 2.19 respectively. It can be observed that the there is more dispersion in side-by-side received signal as compare to face-to-face received signal. Compared with the case of the face-to-face configuration, the magnitude of the received signal is smaller when the antennas are positioned side-by-side. We have used an amplifier whose gain is about 26 dB at the receiver side, since the received signal was very weak. It could be noticed that time lag between the transmitting antennas input pulse and the

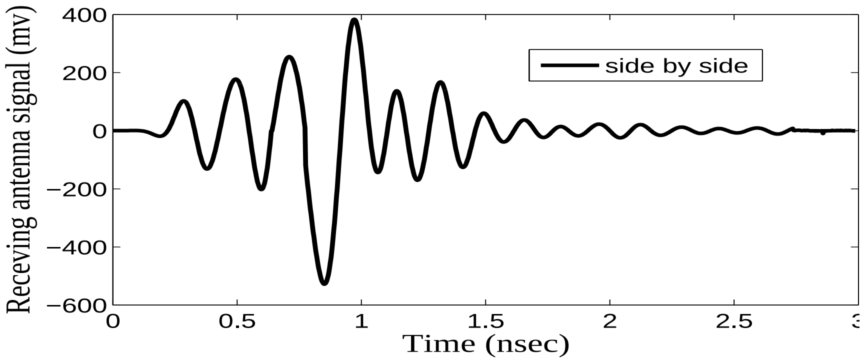

Figure 2.19: Side-by-side received pulse in time domain for a UWB system with two identical antennas.

received pulse is about 0.8 ns.

Table 2.3: Comparison of the size and bandwidth of the proposed triangular monopole antenna to conventional antennas

Antenna Structures	Dimensions (L×W×h)	Freq. range and BW
Cone shape [38]	$76.2\times76.2\times.79$ mm^3	1-10 GHz, 9 GHz
Triangular-shaped [39]	$60\times20\times1$ mm^3	4-10 GHz, 6 GHz
Circular-shaped [40]	$50\times42\times1.5$ mm^3	2.78-9.78 GHz, 7 GHz
Fork-shape [41]	$42\times24\times1.6$ mm^3	3.1-12 GHz, 8.9 GHz
Elliptical-shaped [42]	$45\times45\times1.57$ mm^3	3-14 GHz, 11 GHz
Inverted-F shaped [43]	$50\times30\times2$ mm^3	2-6 GHz, 4 GHz
Proposed triangular-shape	$30\times24\times1.6$ mm^3	1.8-15GHz, 13.2 GHz

2.5 Summary

In this chapter, a printed triangular monopole antenna fed by microstrip feed line is proposed and investigated. It gives a broad measured bandwidth from 1.8 to 15.0 GHz. To improve the impedance bandwidth, a round-corner ground plane has been employed. To further improve the impedance bandwidth for the entire band, a microstrip transition (near the antenna front end) has been introduced between the microstrip feed line and the triangular radiator. The proposed antenna structure has wide bandwidth and small size compared to the conventional antenna (refer to Table 2.3).The proposed antenna has nearly omnidirectional radiation pattern and moderate gain throughout the operating frequency region. The gain variation within the bandwidth is less than about 2.6 dBi approximately.

3

Design of super wideband (SWB) antenna

Contents

3.1 Introduction

In the last chapter, a compact UWB printed triangular monopole antenna has been investigated and proposed. This antenna structure has wide bandwidth and is small in size and can cover short range wireless communication systems. But to cover both short range and long range communication systems such a huge bandwidth is required. So to fulfill this criteria Super wideband antenna has been designed, fabricated and tested. SWB antenna supports a frequency range from 2.8 GHz to greater than 10.6 GHz (may be greater than 100 GHz). It enables high resolution sensing in free space and also works in ground penetrating radar and through wall imaging. Conventional UWB antennas of circular and elliptical shapes exist in literature [44–46]. To increase the impedance bandwidth in these antennas, techniques such as exponential tapering [73–75], Klopfenstein tapering [76] and triangular tapering [77–80] are employed. The triangular tapered monopole antenna has found wide acceptance for UWB/SWB radios due to its ease of fabrication.

In this chapter, a novel UWB/SWB antenna is proposed, whose structure is designed to meet a large bandwidth of 97.2 GHz. Functional Section Design (FSD) approach is defined as designing an object by dividing the structure into functional sections. FSD is used to design this new compact and wideband trapezoidal monopole antenna. An antenna design could be broken down into three distinct sections as shown above in Figure 3.1.

- A feedline which is used to connect an antenna to the RF front end (source signal comes and go from the feed line).
- A feed region which is used for transition between a feed line and one or more radiating elements.
- Radiating elements that serve to couple the radiation fields and the guided waves in the antenna's feedline.

In order to get the best antenna performance, we need to optimize the antenna design in each of the above three sections. Functional Section Design (FSD) approach is defined as designing an object by dividing the structure into functional sections. FSD is used to design this new compact and wideband trapezoidal monopole antenna with frequency band notched characteristic. The FSD technique follows the bottom-up strategy. It starts with the feed section - triangular tapered microstrip line is used for enhancing the impedance matching. In the next chapter, we will see that feed region also contributes in radiation.

- Feed Region - this section is intentionally kept between the feedline and the radiating element for impedance matching, its shape is chosen circular to serve the purpose of broadband impedance matching [79].
- Ground plane feed gap is optimized.
- Radiating element gives extra freedom to ease the optimization process, we have chosen trapezoidal radiating patch for our case.

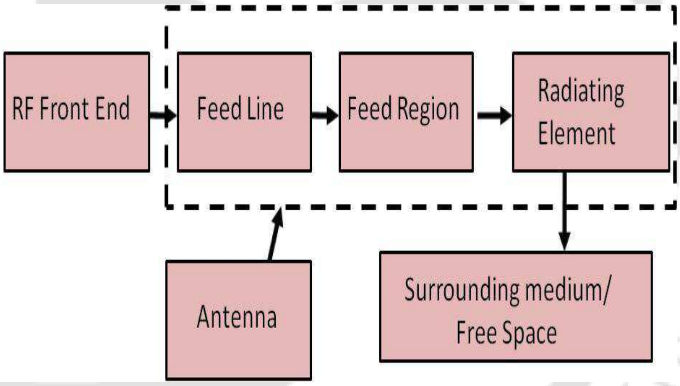

Figure 3.1: Three distinct zones of an antenna.

3.1.1 Broadband impedance matching technique of an antenna

There are two general methods to achieve a desired antenna impedance: resistive loading and geometry control. In resistive loading which is a quick and an easy way, a lossy material is introduced to an antenna structure to obtain a good match. This lossy material has extensive impact on antenna performance. Resistive loading decreases radiation efficiency in order to achieve a good match. Comparing with an unloaded antenna, a resistive loaded antenna will have a gain of at least 3 dB lower or more. There are some cases in which resistive loading are justified. For example, resistive loading can be used for an antenna with exact requirements for pattern to control side lobes and back lobes. A lossy receiver antenna however throws away the signal, resulting in low SNR and lower overall system performance.

Geometry control is found to be a preferred method to create a desired antenna impedance. Geometry control gives a good match without decreasing antenna performance in other areas which is a disadvantage in resistive loading. We have to control the antenna geometry to get a desired match. To get a good match, smooth and uniform transition of characteristic impedance from the antenna's connector through the free space is needed.

3.1.2 Tapered feed line

Two transmission lines with different characteristic impedances can be matched by a multi section quarter wave transformer, whose change in impedance level is obtained at discrete steps. A tapered transition which has a characteristic impedance that varies continuously in a smooth fashion from the impedance of one line to that of other line can also be used instead of above taper. This type of transition is called as tapered transmission line [13]. A tapered transmission line shown in Figure 3.2 is used to match a line with normalized impedance(unity) to a load with normalized impedance $\bar{Z}_L$. The tapered section has a normalized impedance $\overline{Z}$ which is a function of distance z along the taper. Figure 3.2(b) shows an approximation to the continuous taper. The taper is assumed to be made up of number of sections of line of differential length dz. The impedance changes by differential amounts $d\overline{Z}$ from section to section.

The step change $d\overline{Z}$ in impedance at z produces a differential reflection coefficient

$$d\Gamma_0 = \frac{\overline{Z} + d\overline{Z} - \overline{Z}}{\overline{Z} + d\overline{Z} + \overline{Z}} \approx \frac{d\overline{Z}}{2\overline{Z}} = \frac{1}{2} d(\ln \overline{Z}) = \frac{1}{2}\frac{d}{dz}(\ln \overline{Z})dz \tag{3.1}$$

At the input to the taper, the contribution to the input reflection coefficient from this step is

$$d\Gamma_i = e^{-j2\beta z}\frac{1}{2}\frac{d}{dz}(\ln \overline{Z})dz \tag{3.2}$$

It is assumed that total reflection coefficient can be computed by summing up all the individual contributions, as was done in approximate theory of the multi section quarter-wave transformer, the input reflection coefficient is given by

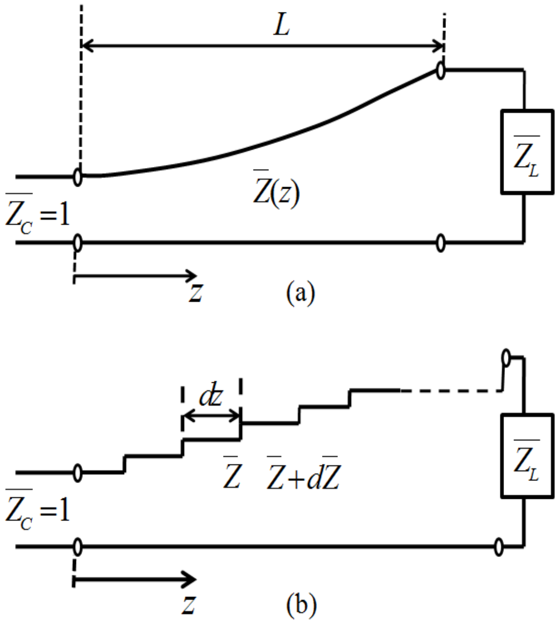

Figure 3.2: (a) Continuously tapered transmission line.,(b) Approximation to continuous taper.

$$\Gamma_i = \int_0^L e^{-j2\beta z} \frac{1}{2} \frac{d}{dz} (\ln \bar{Z}) dz \tag{3.3}$$

where L is the total taper length. If the variation in $d\bar{Z}$ with z is known, Γ_i may be readily evaluated from above equation. Alternatively, if Γ_i is specified, then $d\bar{Z}(z)$ can be found. Different kinds of taperings are discussed in this aspect like exponential, triangular and Klopfenstein tapering.

3.1.2.1 Exponential taper

The exponential tapering is the one for which $ln(\bar{Z})$ varies linearly, and hence $\bar{Z}$ varies exponentially, from unity to $ln(\bar{Z_L})$ [81].

$$\ln \bar{Z} = \frac{z}{L} \ln \bar{Z}_L \tag{3.4}$$

$$\bar{Z} = e^{(z/L) \ln \bar{Z}_L} \tag{3.5}$$

Using equation 3.3 and equation 3.5 we get

$$\begin{aligned}\Gamma_i &= \tfrac{1}{2}\int_0^L e^{-j2\beta z}\tfrac{1}{2}\tfrac{d}{dz}(\ln \overline{Z})dz \\ &= \tfrac{1}{2}e^{-j\beta z}\ln \overline{Z}_L \tfrac{\sin\beta L}{\beta L}\end{aligned} \tag{3.6}$$

At the input to the taper, the contribution to the input reflection coefficient from this step is

$$d\Gamma_i = e^{-j2\beta z}\frac{1}{2}\frac{d}{dz}(\ln \overline{Z})dz \tag{3.7}$$

It is assumed that total reflection coefficient can be computed by summing up all the individual contributions,as was done in approximate theory of the multi section quarter-wave transformer, the input reflection coefficient is given by

$$\Gamma_i = \int_0^L e^{-j2\beta z}\frac{1}{2}\frac{d}{dz}(\ln \overline{Z})dz \tag{3.8}$$

where L is the total taper length. If the variation in $d\bar{Z}$ with z is known, Γ_i may be readily evaluated from above equation. Alternatively, if Γ_i is specified, then $d\bar{Z(z)}$ can be found. Different kinds of tapering are discussed in this aspect like exponential, triangular and Klopfenstein tapering.

It is assumed that a transmission line for which $\beta = k = 2\pi/\lambda$ is taken and is not a function of z.

3.1.2.2 Triangular taper

In triangular taper $\frac{d}{dz}(\ln \overline{Z})$ is taken as a triangular function of the form

$$\frac{d}{dz}(\ln \overline{Z}) = \begin{cases} \frac{4z}{L^2}\ln \overline{Z}_L & 0 \le z \le L/2 \\ \frac{4}{L^2}(L-z)\ln \overline{Z}_L & L/2 \le z \le L \end{cases} \tag{3.9}$$

Integrating above equation gives

$$\overline{Z} = \begin{cases} e^{2(z/L)^2 \ln \overline{Z}_L} & for \quad 0 \le z \le L/2 \\ e^{(4z/L - 2z^2/L^2 - 1)\ln \overline{Z}_L} & for \quad L/2 \le z \le L \end{cases} \tag{3.10}$$

Substituting equation 3.10 in equation 3.5, and integrating we get,

$$|\Gamma_i| = \frac{\ln\left(\overline{Z}_L\right)}{2}\exp\left(-j\beta L\right)\left[\frac{\sin\left(\frac{\beta L}{2}\right)}{\frac{\beta L}{2}}\right]^2 \tag{3.11}$$

where Γ_i is the reflection coefficient and β is the phase constant.

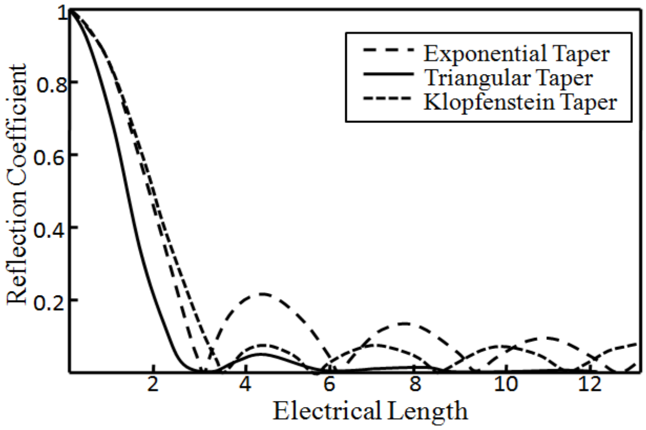

Figure 3.3: Comparison of graphs of reflection coefficient magnitudes of exponential, triangular and Klopfenstein tapers.

A plot of $\rho_i = |\Gamma_i|$ or $\frac{2|\Gamma_i|}{\ln(\overline{Z}_L)}$ versus βL is given in the Figure 3.3. For a fixed length of taper, this is a plot of ρ_i as a function of frequency since $k = 2\pi f(\mu\varepsilon)^{1/2}$. From the graph it can be seen that for exponential taper case when $L > \lambda/2$, the reflection coefficient is quite small, the first minor lobe is about 22 % of the maximum major lobe. In case of triangular taper has a first minor lobe maximum which is less than 5 % of the major lobe peak when compared to the exponential taper. However, this minimum value of reflection coefficient occurs at a taper length of about $3\lambda/2$ or for a length twice that of the exponential taper. If $\overline{Z}_L >> 1$, the triangular taper is preferred because of much smaller values of ρ_i obtained for all frequencies, such that the taper length is greater than 0.815 λ, which corresponds to the edge of the pass band as in Figure 3.3 .

3.1.2.3 Klopfenstein taper

For a given taper length, the Klopfenstein impedance has been proved to be optimum because the reflection coefficient is minimum over the pass band. Alternatively, for a maximum reflection coefficient specification in the pass band, the Klopfenstein taper yields the shortest matching section. This taper is derived from a stepped Chebyshev transformer as the number of sections increase to infinity. The logarithm of the characteristic impedance variation for the Klopfenstein taper is given by [76]

$$\ln Z(z) = \frac{1}{2}\ln Z_0 Z_L + \frac{\Gamma_0}{coshA} A^2\,\Phi(2z/L - 1, A) \qquad for\, 0 \leq z \leq L \tag{3.12}$$

where $\Phi(x, A)$ is defined as

$$\Phi(x, A) = -\Phi(-x, A) = \int_0^x \frac{I_1(A\sqrt{1-y^2})}{(A\sqrt{1-y^2})} dy \quad for\ |x| \leq 1 \tag{3.13}$$

where $I_1(x)$ is modified Bessel function. This function has a special values:

$$\Phi(0, A) = 0\Phi(x, 0) = x/2\Phi(1, A) = \frac{CoshA - 1}{A^2} \tag{3.14}$$

Using a simple and efficient method, the reflection coefficient is given by

$$\Gamma = \Gamma_0 e^{-j\beta L} \frac{\cos\sqrt{(\beta L)^2 - A^2}}{CoshA} \qquad for\, \beta L > A \tag{3.15}$$

If $\beta L < A$, the $\cos\sqrt{(\beta L)^2 - A^2}$ term becomes $\cosh\sqrt{A^2 - (\beta L)^2}$. In equation 3.13, Γ_0 is reflection coefficient at zero frequency, given by

$$\Gamma_0 = \frac{Z_L - Z_0}{Z_L + Z_0} \approx \frac{1}{2}\ln(Z_L/Z_0) \tag{3.16}$$

The maximum ripple in the pass band is at $\Gamma_m = \frac{\Gamma_0}{Cosh\,A}$. The disadvantage of this taper is that it has steps at $z = 0$and L, and so does not smoothly join the source and the load impedances. So it is rarely used.

3.2 Design of feed region

Steps in the width of microstrip lines are associated with fringing fields which results in an excess capacitance. It has to be compensated by a local change in the shape of the line. Thus a feed region [75] is designed between the transmission line and radiating element. It acts as a continuous change of impedance reducing the excess capacitance.

Apart from above impedance matching techniques, bandwidth can be increased by using log periodic antenna arrays in which the different elements are deduced from a homothetic ratio, introducing the capacitive coupling between the radiating element and the ground plane, using microstrip feed line and notching the ground plane, adding slots on either side of radiating elements, increasing the width of the antenna and by modifying the shape of the radiating element. All these techniques are based on surface current distribution to broaden antenna's impedance bandwidth.

Based on the above discussion regarding the improving of bandwidth and based on the hardware and software limitations, triangularly tapered microstrip feedline is chosen for the designing of the novel UWB or SWB band notch antenna. Klopfenstein taper is better compared to triangular taper as mentioned above, but does not join smoothly the source and load impedances and the shape is also difficult to design in the softwares.

3.3 Full band antenna

3.3.1 Antenna geometry and design

Geometry of proposed full band antenna is shown in Fig. 3.4. The proposed full band antenna have been divided into three parts. They are (A) a triangularly tapered microstrip line, (B) a curved feed region at the base of antenna patch and (C) a trapezoidal shaped radiating patch. The antennas are designed on an FR4 epoxy substrate of thickness 1.6 mm and dielectric constant 4.4. The triangular tapered microstrip line is used for optimized impedance matching between 50-Ω impedance microstrip line and the radiating element.The total size of the antenna is $30\times30\times1.6\ mm^3$. The effective dielectric constant is calculated. The proposed antenna was simulated by Ansoft HFSS (version 14) full wave simulator [82]. The fabricated prototype of the antenna is shown in Fig. 3.5. The above three parts of the antenna are discussed in the following subsections.

3.3.2 Triangularly tapered feedlines

Let Z_1 and Z_2 be the characteristic impedances and w_1 and w_2 be the widths of the microstrip line at excitation end and the antenna end. Let ε_1 and ε_2 be the effective dielectric constants at excitation end and antenna end.

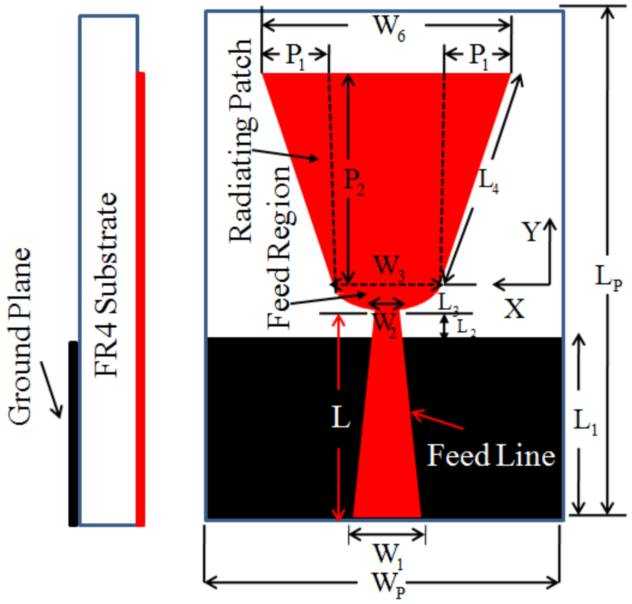

Figure 3.4: Geometry and configuration of the proposed full band antenna (antenna 1).

1. A closed form solution of the Riccati equation for triangularly tapered feed line is given by

$$|\Gamma_i| = \frac{\ln\left(\overline{Z}_L\right)}{2} \exp\left(-j\beta L\right) \left[\frac{\sin\left(\frac{\beta L}{2}\right)}{\frac{\beta L}{2}}\right]^2 \tag{3.17}$$

where $|\Gamma_i|$ is the reflection coefficient and β is the phase constant.

2. A Matlab program is written for the above formula and graph is drawn between $\frac{2|\Gamma_i|}{\ln(\overline{Z}_L)}$ and βL as shown in Fig. 3.6.

3. It should be decided how much return loss is to be achieved and accordingly, the corresponding βL is obtained from the X-axis of the graph as x_a.

4. Then using the formula $L = x_a/\beta$, we get the length of the microstrip line. If a return loss of -30 dB is required, then $|\Gamma_i|$ should be 0.03, the corresponding βL from graph shown in Fig. 3 is x_a is 2.61 [74]. 5. We know $\beta = 2\pi/\lambda_r$, where λ_r is the wavelength at resonant frequency. Since it is a band notch antenna, resonant frequency is taken as 3.1 GHz. Now L is obtained as 23.2 mm from the above formulae.

To get the widths at the two ends of the tapered lines, method reported in [74] is followed. β changes as the effective dielectric constant changes with the ratio of microstrip width W to the thick-

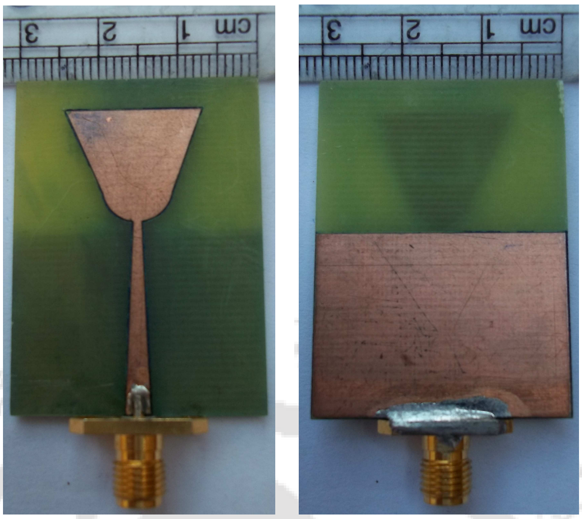

(a) (b)

Figure 3.5: Fabricated prototype of the UWB/SWB antenna (a) Top view (b) Bottom view.

ness H (H=1.6 mm in case of FR4 Epoxy substrate $\varepsilon_r = 4.4$) and is given by [83].

$$\varepsilon_{reff} = \frac{\varepsilon_r + 1}{2} + \frac{\varepsilon_r - 1}{2(1 + 10H/W)^{1/2}} \tag{3.18}$$

To find out ε_{reff} at the two ends of the line, first compute the airline impedance

$$Z_0 = Z\left(\varepsilon_{reff}\right)^{1/2} \tag{3.19}$$

where Z is the input impedance to be given in each case. For different Z, we obtain different widths. The formulae separate at W/H=1. Thus from [81]

$$Z_0 = 60\ln\left(\frac{8H}{W} + \frac{W}{4h}\right), \quad \frac{W}{H} \leq 1; \quad case \quad 1 \tag{3.20}$$

$$Z_0 = \frac{377}{\frac{W}{H} + 2.42 - \frac{0.44H}{W} + \left(1 - \frac{H}{W}\right)^6}, \quad \frac{W}{H} \geq 1; \quad case \quad 2 \tag{3.21}$$

To calculate the accurate values of widths and effective dielectric constants, Step 1 : First we keep W/H= 1 in equation 3.18 and we get $\varepsilon_{reff}(1)$

$$\varepsilon_{reff}(1) = \varepsilon_{reff}(W/H = 1) = \frac{\varepsilon_r + 1}{2} + \frac{\varepsilon_r - 1}{6.63} \tag{3.22}$$

Step 2 : Also find $Z_0(1) = Z_0(W/H = 1)$ value from equation 3.20 or equation 3.21, we get same

Table 3.1: Dimensions of the Proposed UWB/SWB Monopole Antenna 1

Parameters	Antenna 1
W_p	30
L_p	40
w_1	3
w_2	1
L	23.2
L_1	21.8
L_2	1.4
L_3	2
W_3	8.2
W_6	18
L_4	11
P_1	4.9
P_2	9.8

value as $Z_0(1) = 126.6\ \Omega$ Step 3 : With Z = 50 Ω (standard microstripline impedance, Z_1) or antenna impedance (Z_2) value and $\varepsilon_{reff}(1)$, find out Z_0 from $Z_0 = Z\{\varepsilon_{reff}(1)\}^{1/2}$. Thus we get 2 cases based on value of Z.

Case 1: If $Z_0 > Z_0$ (1), then W/H is less than or equal to 1. Then using the formula [74]

$$W/H = 2\left\{\exp(Z_0/60) - \left[\{\exp(Z_0/60)\}^2 - 8\right]^{1/2}\right\} \tag{3.23}$$

New W/H values are obtained. Substitute this value in equation 3.18, calculate new ε_{reff}(W/H), Z_0 from $Z_0 = Z\{\varepsilon_{reff}(1)\}^{1/2}$, check the condition whether Z_0(W/H)> Z_0(1) and again find new W/H from equation 3.23 iteratively until the value of W/H becomes constant. The width w_2 is found as 1 mm approximately for $Z_0 = 84\ \Omega$ since case 1 is applicable.

Case 2: $Z_0 < Z_0(1)$, then W/H is greater than 1. Then using Newtons method, an iterative equation is set up. Let = $(W/H)_{old}$, then

$$(W/H)_{new} = X - \left(\frac{X\left(X^2 + X\left\{2.42 + (1 - 1/X)^6 - 377/Z_0\right\} - 0.44\right)}{X^2 + 0.44 + 6\,(1 - 1/X)^5}\right) \tag{3.24}$$

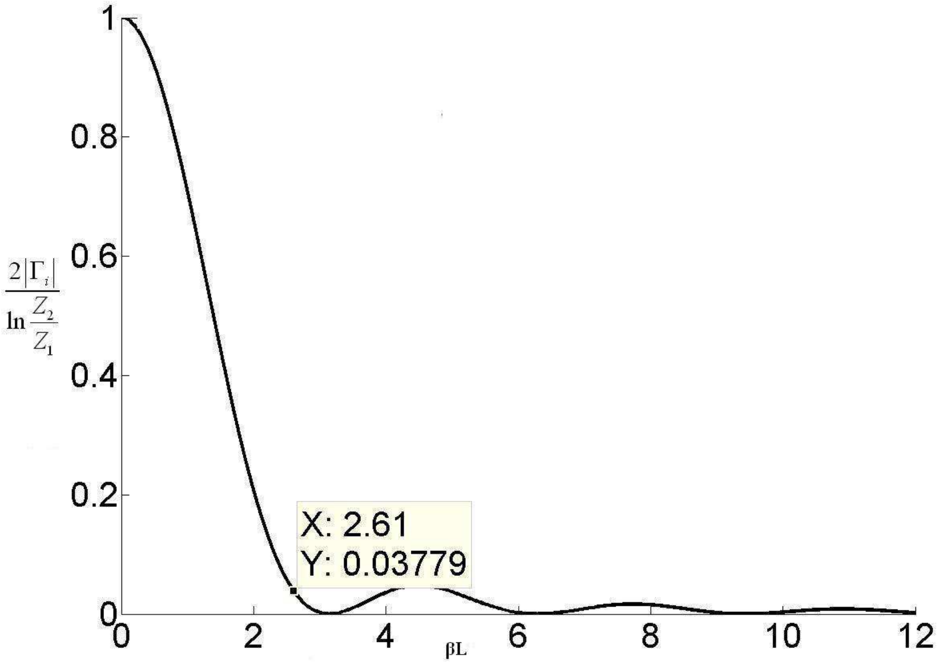

Figure 3.6: Graph between reflection coefficient vs electrical length.

New W/H values are obtained. Substitute this value in equation 3.18, calculate new ε_{reff}(W/H), Z_0 from $Z_0 = Z\{\varepsilon_{reff}(1)\}^{1/2}$ check the condition whether $Z_0(W/H) < Z_0(1)$ and again find new W/H from equation 3.24 iteratively until the value of W/H becomes constant. The width w_1 is found as 3 mm approximately for Z1 = 50-Ω since case 2 is applicable.

The effective dielectric constants ε_1 and ε_2 are 3.39 and 3.1 at excitation end and antenna end respectively. The effective dielectric constant of the tapered line is 3.245.

If $Z(z)$ is the impedance of tapered line at distance z, then from [84]

$$Z(z) = \begin{cases} Z_0 e^{2(z/L)^2} \ln(Z_L/Z_0) \quad for \ 0 \le z \le L/2 \\ Z_0 e^{\left(4z/L - 2z^2/L^2 - 1\right)} \ln(Z_L/Z_0) \quad for \ L/2 \le z \le L \end{cases} \tag{3.25}$$

3.3.3 Feed region

For increasing the bandwidth to UWB range or more, ground plane feed gap is optimized to 1.4 mm which also offers impedance matching. The radiating element is curved near the microstrip line so that all the power gets radiated and reflections reduce for frequencies greater than 2.8 GHz. Due to this curving, the bandwidth ratio is 13:1 which shows excellent matching and ultra broadband frequency range [75]. Raicu's near optimal taper design is given as

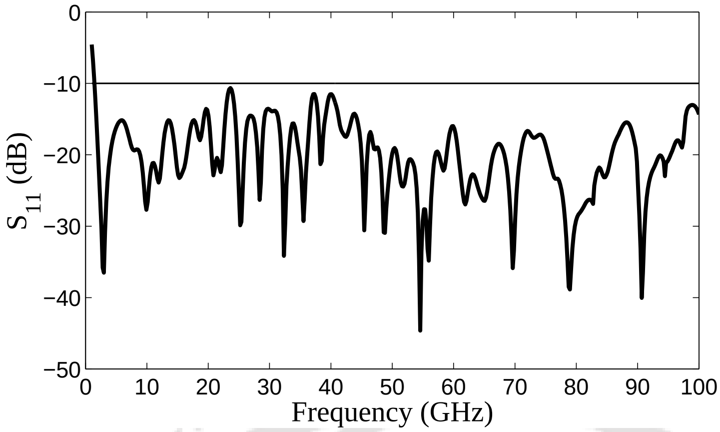

Figure 3.7: Simulated result showing return loss curve of the proposed antenna vs frequency.

$$y = \sinh^2(x) \tag{3.26}$$

where x=L_3 and y=0.5w_3 are height and width of the tapered feed region. Since it was difficult to design a $\sinh^2(x)$ curve in the software, a circular tapering is designed as an approximation for it.

3.3.4 Trapezoidal patch

A trapezoidal patch is used as radiating element whose dimensions are chosen using the formula

$$f_l = \frac{7.2}{L_c + r_c + p} \tag{3.27}$$

where L_c is the height of the trapezoid patch, r_c is the radius of the cylindrical monopole antenna, whose area is compared with that of trapezium, p is the feed gap and f_l is the first resonance frequency in the bandwidth of $|S_{11}|$ curve. f_l is 3.1 GHz, p is 1.4mm. L_c and r_c are obtained from above formula.

3.4 Results and discussion

3.4.1 Antenna return loss and VSWR

The simulated return loss (S_{11}) versus frequency curve of the proposed monopole antenna is shown in Figure 3.7. It can be seen that the bandwidth of the proposed trapezoidal printed monopole antenna spans from 2.8 GHz to 100 GHz. However, Fig. 3.8 shows the measured S_{11} curve for the proposed trapezoidal monopole antenna with frequency band of 3−25 GHz. There is some small discrepancy between the simulated result and the measured results of the S_{11} curve due to fabrication

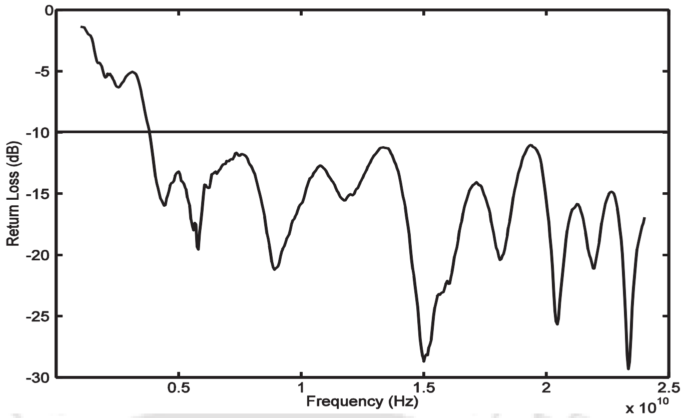

Figure 3.8: Measured result showing return loss curve of the proposed antenna vs frequency.

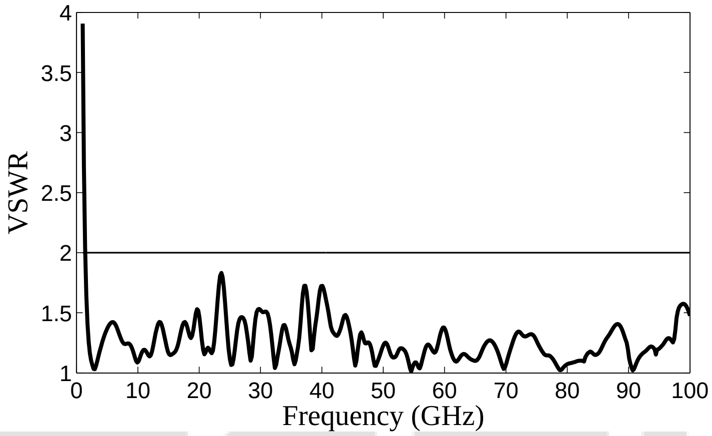

Figure 3.9: Simulated results showing antenna impedance curves of antenna vs frequency.

tolerances and SMA connector effects. But almost over the whole band the simulated and the experimental results agree well. In addition to our proposed antenna work well up to 100, we will limit measurement studies up to 25 GHz since this is the upper measurement frequency of our Rohde and Schwarz ZVA24 network analyzer. Fig. 3.9 displays the simulated VSWR curve for the proposed trapezoidal printed monopole antenna. It is found that for the entire band of frequency from 2.8 GHz to 100 GHz the VSWR ≤ 2.

In order to investigate the effects of overall dimensions of the proposed antenna, the reflection coefficient characteristics for various overall dimensions were analyzed, these are depicted in Fig. 3.10. As it is seen in Fig. 3.10, upon decreasing the overall dimensions of the proposed antenna, there is an impedance mismatch at lower frequencies as well as higher frequencies. In other words we can say that as the antenna size decreases from 30 mm × 40 mm to 25 mm × 35 mm, the overall bandwidth decreases. Since the Q rises rapidly as antenna size decreases, the result relates the lowest

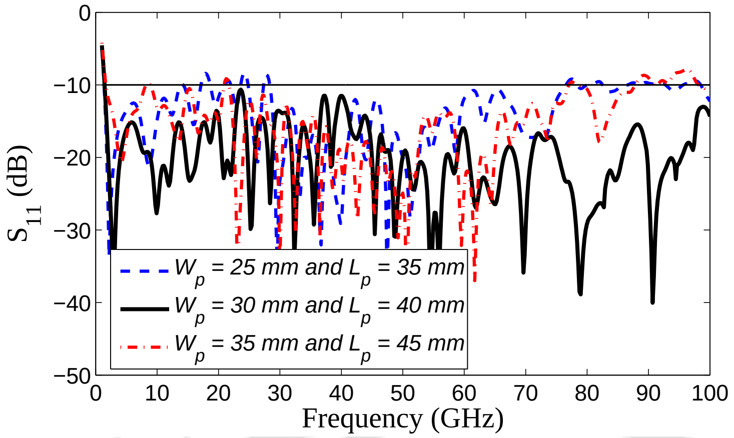

Figure 3.10: Simulated reflection coefficient characteristics curves with the different values of overall antenna dimensions.

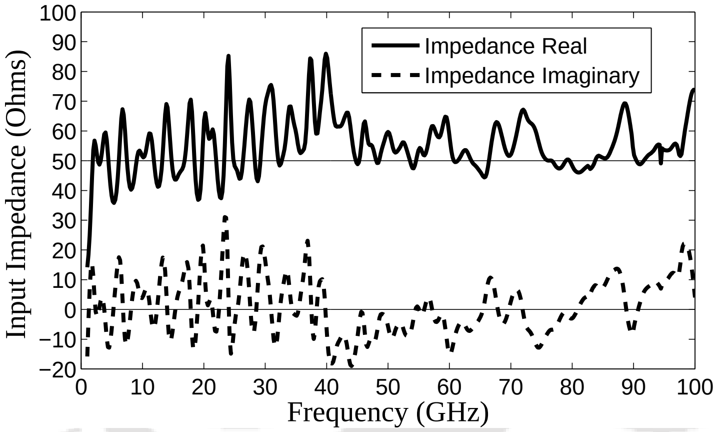

Figure 3.11: Simulated results showing antenna impedance curves vs frequency of antenna.

achievable Q to the maximum dimension of an electrically small antenna as given by equation 1.31 and equation 1.32. However as antenna size increases from 30 mm × 40 mm to 35 mm × 45 mm, there is improvement of bandwidth at lower frequencies, but there is an impedance mismatch at higher frequencies. Thus, is is decided to take 30 mm × 40 mm as the optimum value.

3.4.2 Antenna impedance

Graph is plotted between antenna impedance and frequency. The real part of the impedance of antenna at the point (frequency) where the imaginary part of impedance is zero i.e. reactance = 0 is equal to antenna impedance at the resonance frequency. Here antenna is fed with 50 Ohms characteristic impedance as shown in Figure 3.11. Microstrip line and antenna impedance is exactly 50 Ω (i.e. load impedance is matched with the source impedance).

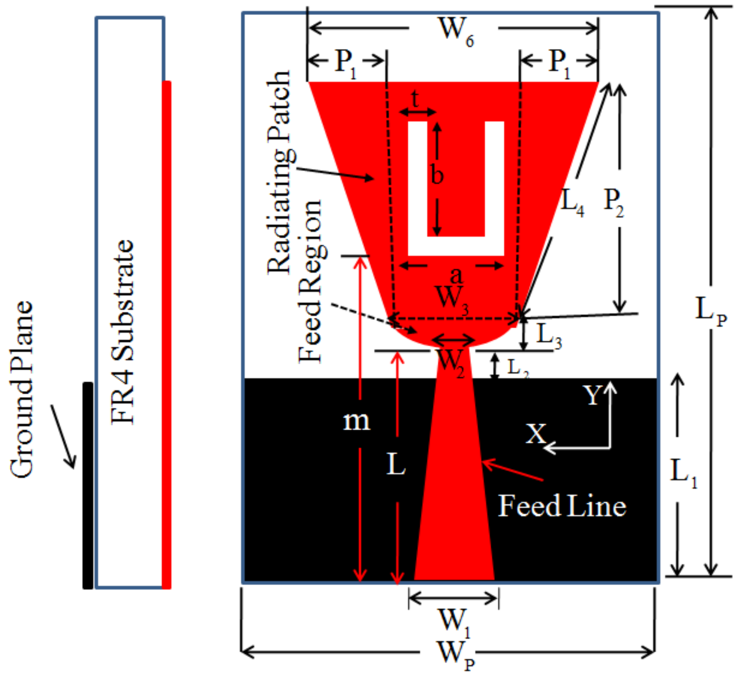

Figure 3.12: Geometry and configuration of proposed band-notched antenna (antenna 2).

3.5 Antenna with band notch function

3.5.1 Antenna geometry and design

Along with the vast operating bandwidth of the UWB (3.1-10.6GHz), there exist some narrow-band wireless services, which occupy some of the frequency bands within the UWB frequency bands. The most well-known among them is wireless local area network (WLAN) IEEE 802.11a and HIPER-LAN/2WLAN operating in 5-6 GHz band. To meet the challenges of UWB radio systems, a suitable UWB antenna with band-notch characteristics in WLAN region and also that supports a very large band width should be designed. A band-notched UWB/SWB antenna (antenna 2) configuration is shown in Fig. 3.12 and Fig. 3.13 shows its fabricated image. Detailed dimensions of the proposed band-notch antenna is shown in table 3.2. Some UWB antennas with band-notched characteristic have been reported in the literature [85]– [86]. In [87] band-notch function is achieved by using a pair of L-shaped slit in the radiating patch with impedance bandwidth of 15.94 GHz. K. Chung *et al.*. designed 5.45 GHz band-notch UWB antenna using inverted U-shaped slot [88] with impedance bandwidth of 8 GHz. Y. Zhu proposed a 3.5/5.5 GHz band notched UWB antenna using the letter

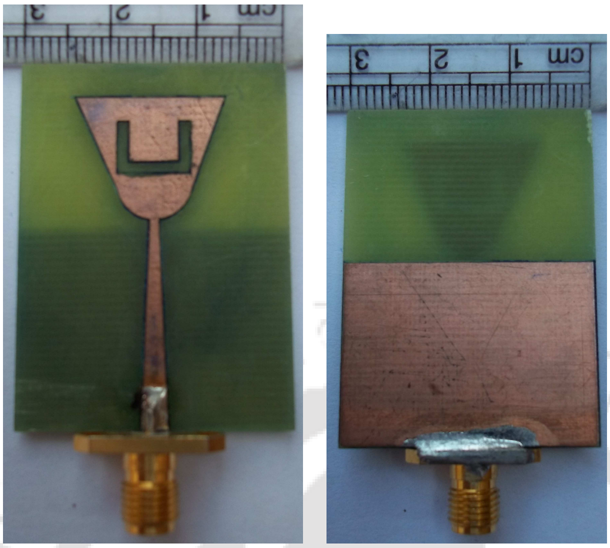

(a) (b)

Figure 3.13: **(a)** Fabricated prototype of the band-notched UWB/SWB antenna. (a) Top view (b) Bottom view.

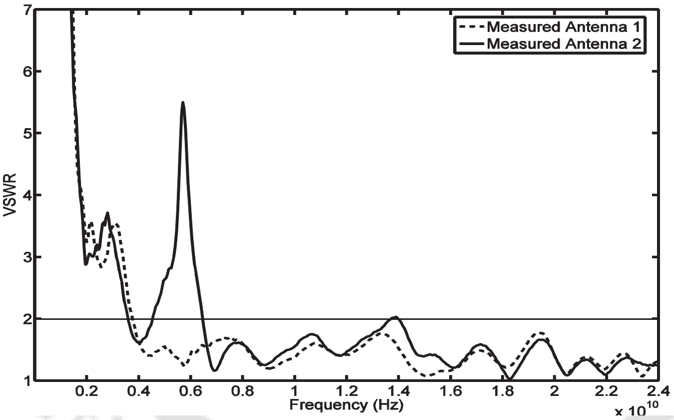

Figure 3.14: Measured results showing VSWR vs. frequency curves of full band antenna (antenna 1) and band-notch antenna (antenna 2).

C-shape slot [89].

3.5.2 U-shaped slot

Band rejection is needed from 5.150 GHz to 5.850 GHz in WLAN region to avoid interferences. For this simplicity, a U-shaped slot is preferred though there are many ways for designing the slot. A U-shaped slot is cut in the radiating element region for reflection of power [90]. The length of the slot should be approximately half the effective guided wave length.

$$L_{Slot} = a + 2b + t = 0.5\lambda_{eff} \tag{3.28}$$

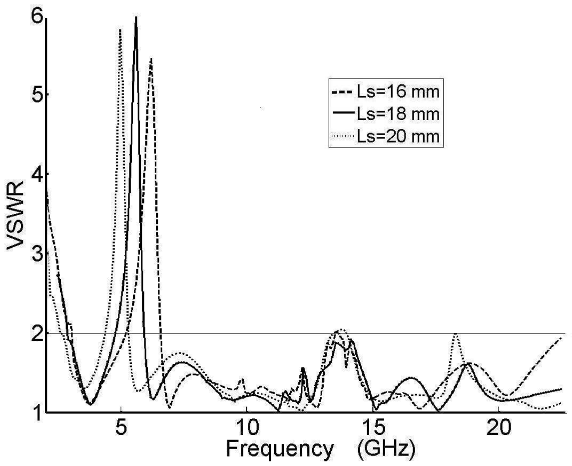

Figure 3.15: Simulated results showing effect of slot length on the notch band frequency.

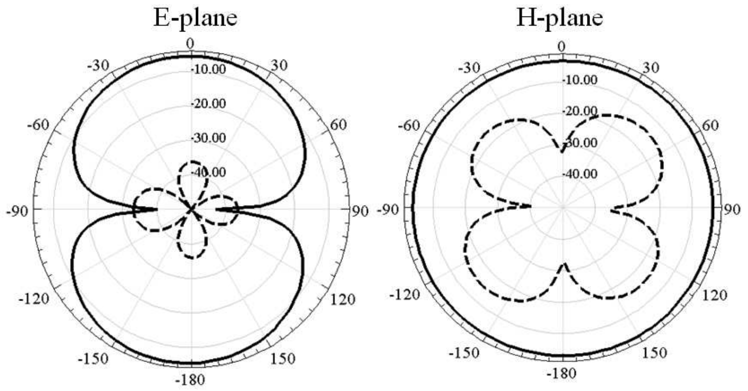

Figure 3.16: Simulated radiation pattern for the proposed UWB/SWB band-notched monopole antenna at 3.1 GHz. Solid line is co-polarization and dashed line is cross-polarization.

where

$$\lambda_{eff} = \lambda \Big/ \sqrt{\varepsilon_{eff}} \tag{3.29}$$

and

$$\varepsilon_{eff} = \frac{\varepsilon_1 + \varepsilon_2}{2} \tag{3.30}$$

By simulation, the total length of the U-shaped slot (L_{Slot}) at notch frequency(f_n) = 5.5 GHz was found to be L_{Slot}= (a+2b+t) =(8+2x4.75+1)=18.5 mm, which is (18.5/15.138)=1.22 times half of the effective wavelength(λ_{eff}/2), where λ_{eff} at 5.5 GHz was found to be 30.27 mm by using the

Table 3.2: Dimensions of the Proposed band-notched UWB/SWB Monopole Antenna 2

Parameters	Antenna 1
W_p	30
L_p	40
w_1	3
w_2	1
L	23.2
L_1	21.8
L_2	1.4
L_3	2
W_3	8.2
W_6	18
L_4	11
P_1	4.9
P_2	9.8
a	8
b	4.75
t	1
m	15.5

expression (7) and (8). Hence the simulated physical length of the U-shaped slot is almost equal to the theoretical physical length of the U-shaped slot for antenna 2.

This slot resembles a half wavelength resonator which introduces high reflections at the center frequency and acts as a band rejection filter. The height of the slot above the feed region plays an important role in band notching. Here a U-shaped slot is introduced inside the patch antenna and the results are compared for antennas with and without slot.The dimensions of the proposed antenna (antenna 2) are W_p = 30 mm, L_p = 40 mm, w_1 = 3 mm, w_2 = 1 mm, W_3 = 8.2 mm, W_6 = 18 mm, L_1 = 21.8 mm, L_2 = 1.4 mm, L_3 = 3 mm, L_4 = 11 mm, L = 23.2 mm, P_1 = 4.9 mm, P_2 = 9.8 mm, a = 8 mm, b = 4.75 mm, t = 1 mm and m = 15.5 mm.

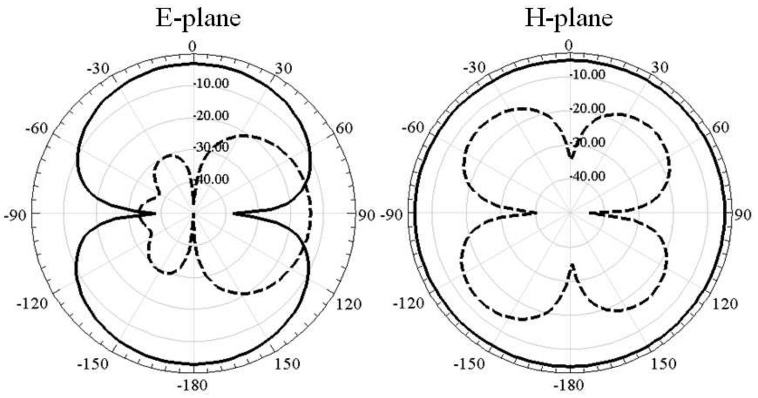

Figure 3.17: Simulated radiation pattern for the proposed UWB/SWB band-notched monopole antenna at 6.8 GHz. Solid line is co-polarization and dashed line is cross-polarization.

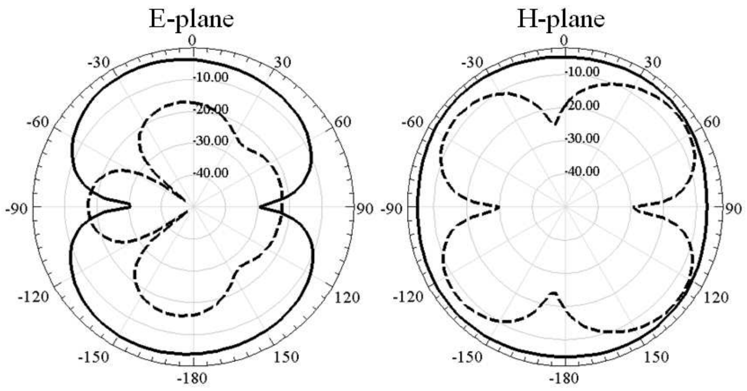

Figure 3.18: Simulated radiation pattern for the proposed UWB/SWB band-notched monopole antenna at 10.6 GHz. Solid line is co-polarization and dashed line is cross-polarization.

3.5.3 Results and discussion

3.5.3.1 Antenna VSWR

Fig. 3.14 shows the measurement VSWR curves of full band antenna (antenna 1) and band notch antenna (antenna 2). For the full band antenna (antenna 1), the bandwidth extends from 2.6 GHz to 24 GHz. Similarly, for band notch antenna (antenna 2), the bandwidth extends from 2.6 GHz to 24 GHz and it offers band rejection in 4.85 GHz - 5.85 GHz (WLAN) frequency range offering a band notch at 5.55 GHz. Hence by introducing a U-shaped slot in the full band antenna (antenna 1), a notched band is created to successfully to alleviate the WLAN interference within the entire UWB band.

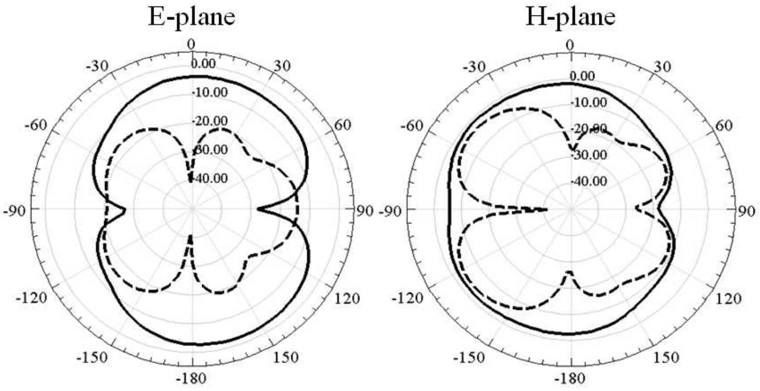

Figure 3.19: Simulated radiation pattern for the proposed UWB/SWB band-notched monopole antenna at 15.0 GHz. Solid line is co-polarization and dashed line is cross-polarization.

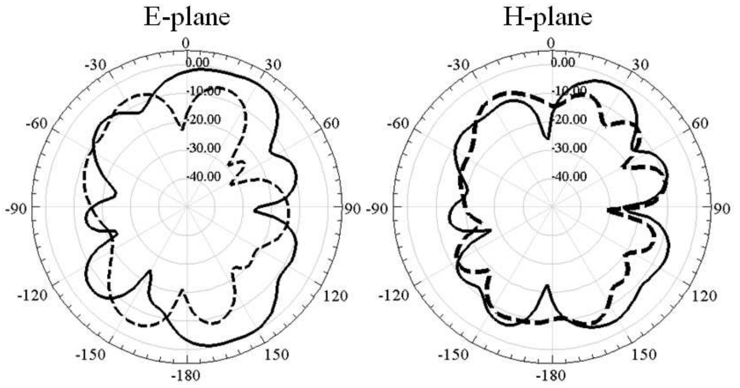

Figure 3.20: Simulated radiation pattern for the proposed UWB/SWB band-notched monopole antenna at 20 GHz. Solid line is co-polarization and dashed line is cross-polarization.

3.5.3.2 Effect of U-shaped slot length

The slot lengths are varied as 16 mm, 18 mm and 20 mm and the resultant VSWR curves are shown in Figure 3.15. This graph clearly shows that as the slot length increases, resonant frequency decreases and so the notch shifts to the left. By increasing the slot length, inductance value increases. Since inductance and resonant frequency are inversely related, so the resonant frequency decreases.

3.5.3.3 Radiation pattern

Fig. 9 shows radiation patterns of the proposed antenna in both E and H-planes, at 3.8, 6.8, 10.6, 15 and 20 GHz. The patterns show that the proposed antenna has a nearly omni-directional radiation pattern at lower frequencies in the H-plane from 3.8 to 10.6 GHz. At the frequencies 3.8, 6.8 and

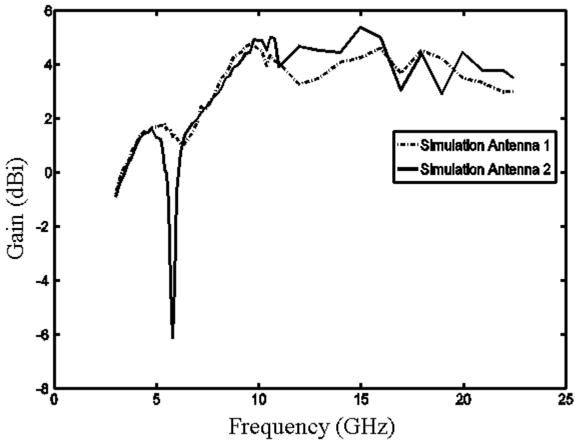

Figure 3.21: Comparison between the simulated peak gain (dBi) vs. frequency of full band antenna (antenna 1) and band-notch antenna (antenna 2).

10.6 GHz the E-plane pattern is found to be typically eight (8) shaped which shows the bidirectional patterns. The cross polarization is low at lower frequency. However, it can be seen that at higher frequencies (e.g. at 15 and 20 GHz) the cross polarization level rises.

3.5.3.4 Antenna gain

Antenna gain versus frequency curve is plotted in simulation. The simulated antenna peak gain of band-notched antenna is compared with the simulated peak gain of full band antenna in the entire super wideband is presented in the Fig. 3.21 which shows a sharp decrease in gain at 5.55 GHz. The simulated value of the antenna 2 peak gain became consistent and the peak gain was varying from -0.91 dBi to 3.48 dBi from 3 GHz to 22.5 GHz with a sharp drop in the peak gain value of -6.12 dBi at 5.55 GHz.

3.6 Summary

In this chapter UWB/SWB antenna and notch antenna are designed and fabricated. Simulated and experimental results have a good match. To mitigate the potential interference between the UWB/SWB systems and narrow band systems such as WLAN, a compact triangularly tapered trapezoidal monopole SWB antenna having circular feed region with feed gap and band rejection capability at WLAN frequencies has been proposed. The antenna is designed using FSD methodology. The dimensions of the tapered feed line, feedgap, feed region and radiating element are mathematically computed. Antenna 1 was designed, simulated, fabricated using LPKF cutting machine and experimental results are obtained using Rohde and Schwarz ZVA24 network analyzer. It gave a super wide-band of 3.1−94.7GHz (31:1 ratio and fractional bandwidth is 187.31). Later a slot is added to the UWB/SWB antenna for band rejection in WLAN frequency region. The relationship between the total dimension of the U-shaped slot and the band rejection operation has been presented. The simulated and experimental results of VSWR curves of UWB/SWB antenna and UWB/SWB notch antenna are presented. Stable radiation pattern and constant gain in the SWB frequency regions are obtained.

4

Printed monopole antenna with tapered feed line, feed region and patch for super wideband applications

Contents

4.1 Introduction

Recently, a large number of UWB antenna designs have been proposed. Sarifi *et al.* [91] proposed (2−30 GHz) bandwidth monopole disc antenna. This monopole antenna fulfils all UWB requirements, including constant group delay, $|S_{11}| < -10$ dB within the bandwidth and high gain. However, the input impedance is not well matched at lower frequencies (3−3.8 GHz). Liu *et al.* [92] proposed an elliptical monopole antenna. This antenna has a large structure and the gain is not so high at low frequencies. This antenna design exhibits wideband impedance matching. The effect of the dielectric substrate and antenna dimensions on the input impedance and the radiation beam width on tapered antennas is explicitly presented in [93]. Conventional UWB antennas in the geometry of circular [94], triangular [95] and elliptical planar monopole [96] antennas also exist. To increase the impedance bandwidth in these antennas, techniques such as exponential tapering [75, 97, 98] and triangular tapering [74, 99, 100] are used. Techniques such as feed region optimization [101] and feed gap optimization [102] have also been well investigated. Here, a novel printed monopole antenna with enhanced bandwidth is investigated. The proposed structural configurations overcome the above-mentioned limitations, including 90% size reduction compared to the designed antenna in [92], impedance matching over the whole frequency band [91] and large bandwidth (2.5−80 GHz). This antenna is capable of supporting UWB (3.1−10.6 GHz) and super wideband (SWB) radios. Two types of structures are examined: antenna 1 is fed with a triangular feed line, while antenna 2 is fed with a rectangular feed line. Here, we propose a low-cost compact printed circuit board antenna based on exponential tapered connection between the radiating patch and a triangular feed line. The ground plane is partial and is flushed with the feed line. The feed line has been tapered [103] near the antenna feeding point in order to improve the impedance matching at higher frequencies. The proposed antennas radiate an omni-directional radiation pattern. Since the vertical monopole antenna has a relatively large height ($\lambda/4$), it is not recommended when a low profile or conformal geometry is desired.

The fundamental characteristics of the proposed design, including simulated and measured return loss, computed gain and radiation patterns, over the UWB band are reported here. The proposed antenna displays good impedance matching with an acceptable radiation pattern. Simulation results have been carried out with the finite element method (FEM) based Ansoft high-frequency structure

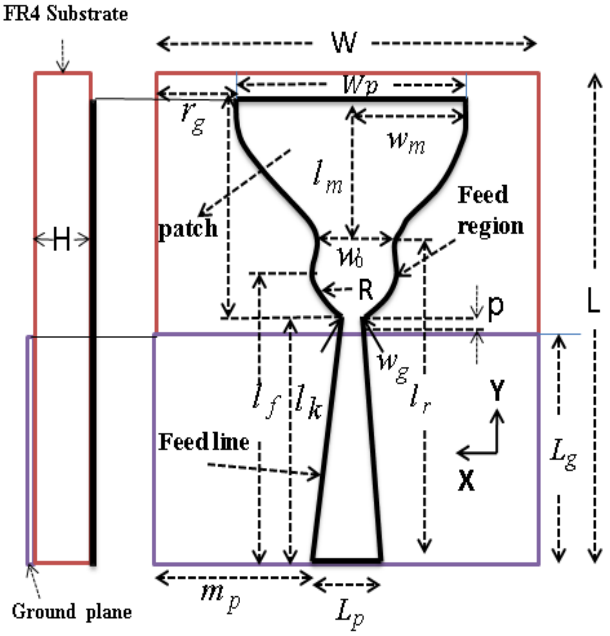

Figure 4.1: Geometry of antenna 1 with triangular tapered feed line.

simulator (HFSS) software. A detailed analysis of the proposed monopole antenna is described along with the simulation and experimental results. Finally, we have measured time domain characteristics and the correlation factor is calculated. A minor group delay variation is also observed for the UWB/SWB monopole antenna.

4.2 Antenna design

The geometrical structure and dimensions of the proposed printed monopole antennas are depicted in Fig. 4.1 and Table 4.1. The overall size of proposed antenna is 30 mm × 40 mm (ground plane size 21.7×30 mm^2) which is printed on a 1.6 mm thick FR4-epoxy substrate, with a permittivity of 4.4 and loss tangent 0.018. The antenna consists of three parts: feed region, feed line and radiating patch. A feed region connection, between the feed line and the antenna's patch, was incorporated to improve the antenna impedance matching. A tapered connection between the feed line and the main patch is applied to smooth the current's path, thus providing wider impedance bandwidth. Fig. 4.1 shows the antenna with a triangular tapered feed line, and Fig. 4.2 shows the antenna with a rectangular feed line. The structure of the newly proposed ultra-broadband printed monopole antenna is depicted in Fig. 4.1 along with the dimensions. In Fig. 4.2, we have modified the rectangular feed line instead of

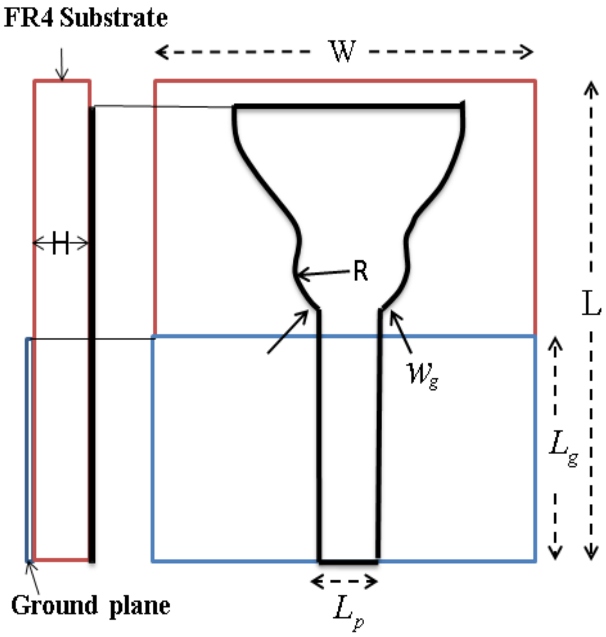

Figure 4.2: Geometry of antenna 2 with rectangular feed line.

the triangular tapered feed line. In antenna 1, a triangular tapered feed line gives broader bandwidth and the tapered feed region is optimized such that 50-Ω impedance matching is done properly to reduce the reflection of the incident waves. The tapered feed line along with the printed traveling wave antennas exhibits wideband characteristics and is capable of transmitting UWB pulses with low distortions. The photograph of the compact monopole antenna with its soldered sub-miniature version A (SMA) connector is shown in Fig. 4.3.

A tapered radiating patch is used as a radiating element whose dimensions are chosen using the formula [104]

$$f_1 = \frac{7.2}{L_c + r_c + p} GHz \tag{4.1}$$

where L_c is the height of the planar monopole antenna ($L_c = l_n$), r_c is the effective radius of the equivalent cylindrical monopole antenna, and p is the feed gap (difference between L_k and L_g) optimized to p = 1.3 mm. Unlike the planar monopole antennas, the printed configuration has a dielectric layer on one side of the monopole. This dielectric material leads to a reduction in the lower band-edge

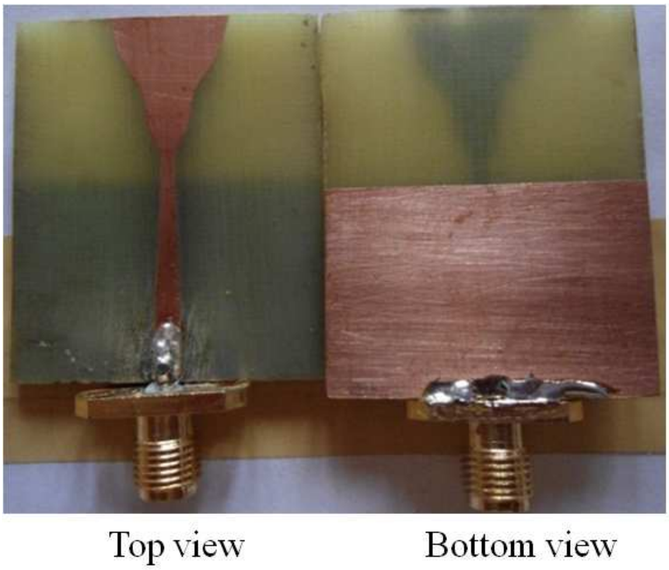

Figure 4.3: Top and bottom view of fabricated antenna 1.

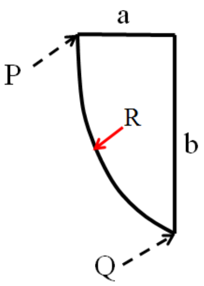

Figure 4.4: Exponential tapered feed region.

frequency. Hence, a more appropriate equation for the lower band-edge frequency is given as

$$f_1 = \frac{7.2}{(L_c + r_c + p) \times k} GHz \tag{4.2}$$

Here, the value of k = 1.18 has been chosen empirically for a dielectric layer with dielectric constant (ε_r) = 4.4. The effective radius of the cylindrical monopole antenna is given by

$$r_c = \frac{T}{2 \times \pi \times L_c} \tag{4.3}$$

where T is the area of the semi-ellipse monopole radiating patch. Owing to this curving, the bandwidth shows excellent matching over an ultra-broadband frequency range. In the triangular tapered feed line parameters, L_p and W_g do not depend on the resonant frequency and are calculated by an

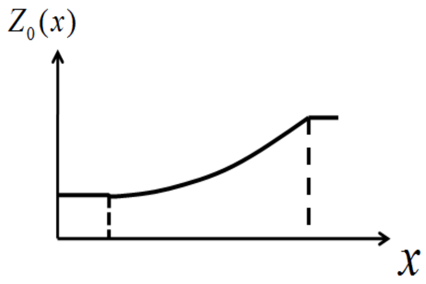

Figure 4.5: Impedance function of triangular tapered feed line.

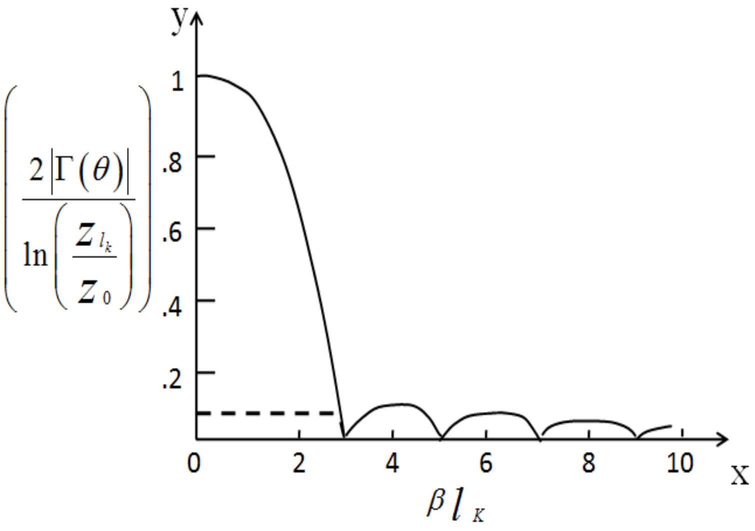

Figure 4.6: Graph of reflection coefficient against electrical length of triangular tapered feed line.

iterative method.

Fig. 4.4 indicates the exponential taper profile of tapered feed region which is defined by the R (radius of feed region) and the two points P and Q. The mathematical expression for exponential curve for feed region is given by (equation 4.4)

$$Y = \sinh^2(RX) \tag{4.4}$$

$$Y = \frac{1}{4}e^{2RX} + \frac{1}{4}e^{-2RX} - \frac{1}{2} \tag{4.5}$$

where

$$Y = 0.5b \;\; and \;\; X = a \tag{4.6}$$

Thus from the above mathematical expression, we can obtain the radius of the feed region. Let Z_L

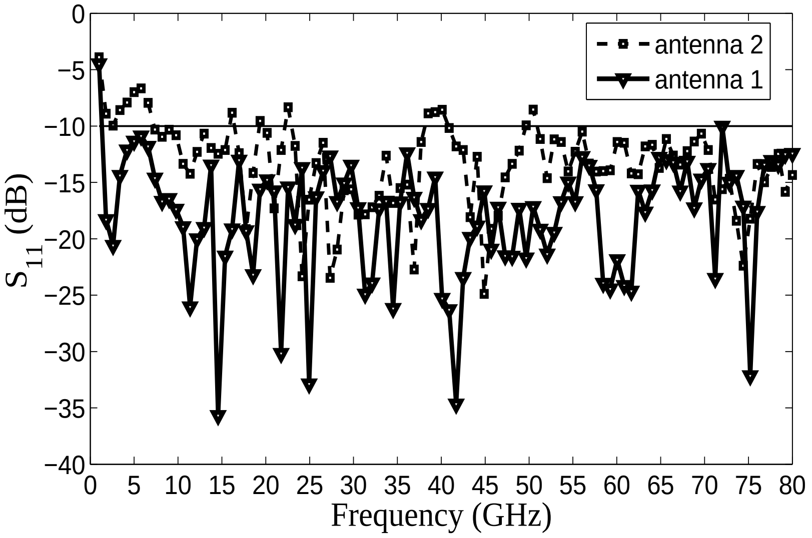

Figure 4.7: Simulated amplitude of reflection coefficient vs frequency of the both antennas.

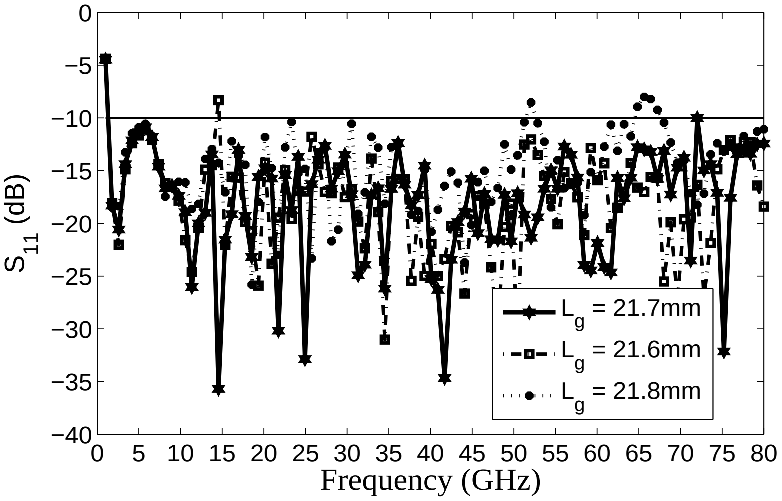

Figure 4.8: Simulated reflection coefficient vs frequency of different ground plane length of antenna 1.

and Z_0 be the antenna load impedance and characteristic impedances of the feed line. The impedance function of triangular tapered feed line in Fig. 4.5 is obtained from the equation given below [74]

$$Z(z) = f(x) = \begin{cases} {Z_0}^{2\left(Z/l_k\right)^2} \ln Z_{l_k}/Z_0, & for\ 0 < z < l_k/2 \\ Z_0 e^{\left(\frac{4z}{l_k} - \frac{2z^2}{{l_k}^2} - 1\right) \ln Z_{l_k}/Z_0}, & for\ l_k/2 < z < l_k \end{cases} \tag{4.7}$$

Relating this impedance function to the $\Gamma(\theta)$ function will result in (equation 4.8). A closed-form

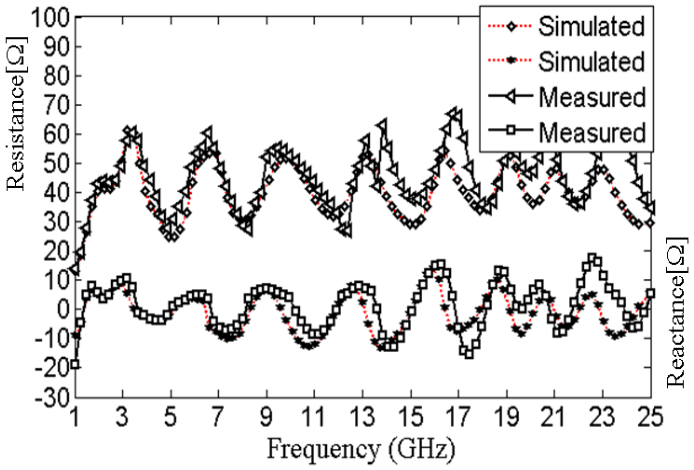

Figure 4.9: Input impedance vs frequency.

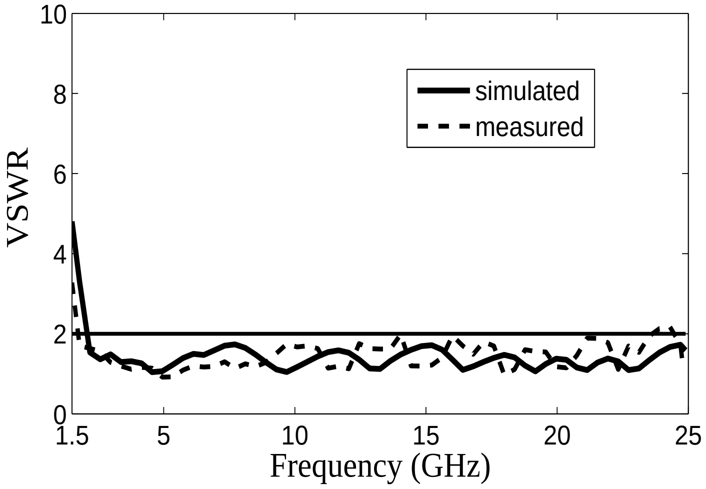

Figure 4.10: Voltage standing wave ratio vs frequency of antenna 1.

solution of the Riccati equation for triangularly tapered feed line is given in [74].

$$\Gamma(\theta) = \frac{1}{2} e^{-j\beta l_k} \ln\left(\frac{Z_{l_k}}{Z_0}\right)\left[\frac{\sin\left(\frac{\beta l_k}{2}\right)}{\frac{\beta l_k}{2}}\right]^2 \tag{4.8}$$

where $\Gamma(\theta)$ is the reflection coefficient, β is the phase constant and l_k is the triangular tapered feed line length. A matrix laboratory program is written for the above formula, and a graph is drawn between the reflection coefficient $((2|\Gamma(\theta)|)/(\ln(Z_{l_k}/Z_0)))$ and electrical length (βl_k) of the triangular tapered feed line as shown in Fig. 4.6. We should decide how much return loss is to be achieved and accordingly the corresponding βl_k is obtained from the x-axis of the graph as R_a. If a return loss of

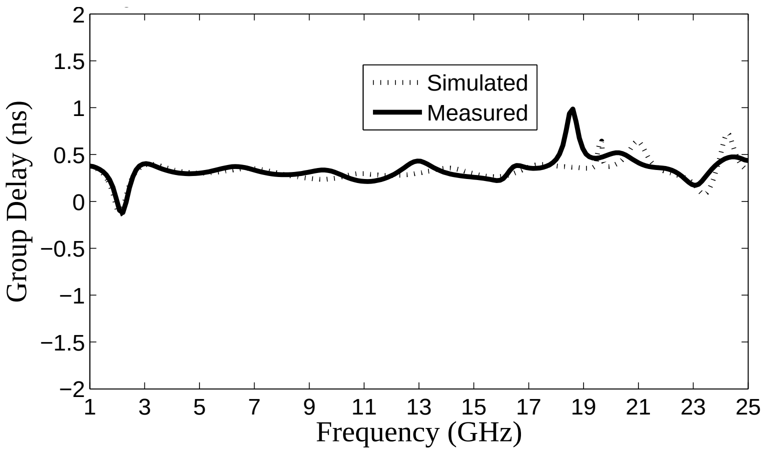

Figure 4.11: Simulated and measured group delay vs frequency of antenna 1.

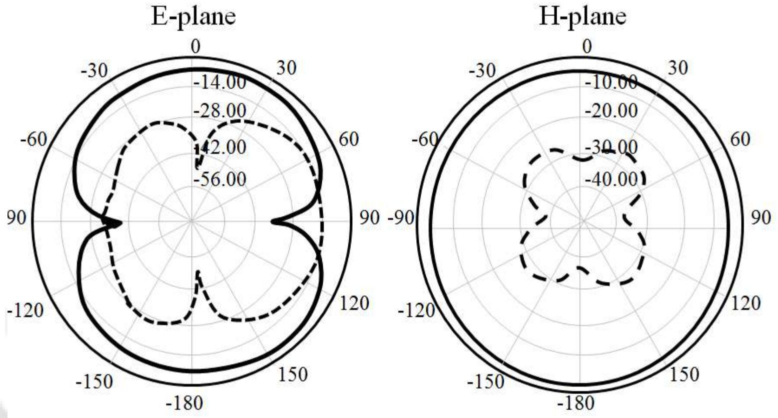

Figure 4.12: Simulated radiation pattern for the proposed SWB monopole antenna 1 at 3.1 GHz. Solid line is co-polarization and dashed line is cross-polarization.

-30 dB is required, then $\Gamma(\theta)$ should be 0.06; the corresponding βl_k from the graph shown in Fig. 4.6 is Ra = 2.86. Now l_k is obtained as 23 mm from the above formula. Owing to hardware and software limitations, a triangularly tapered microstrip feed line is chosen for the design of the novel UWB or SWB.

4.2.1 Simulation and measurement results

Fig. 4.7 shows the simulated reflection coefficients of the two types of structures (antenna 1 and antenna 2) with a triangular tapered feed line and rectangular feed line. When the feed line is altered from a triangular tapered feed line to a rectangular feed line and W_g increases from 1 to 3 mm, it can be observed that the impedance matching deteriorates for the entire frequency band. Hence, a triangular tapered feed line provides a smooth current path. Owing to this smooth current path, the impedance

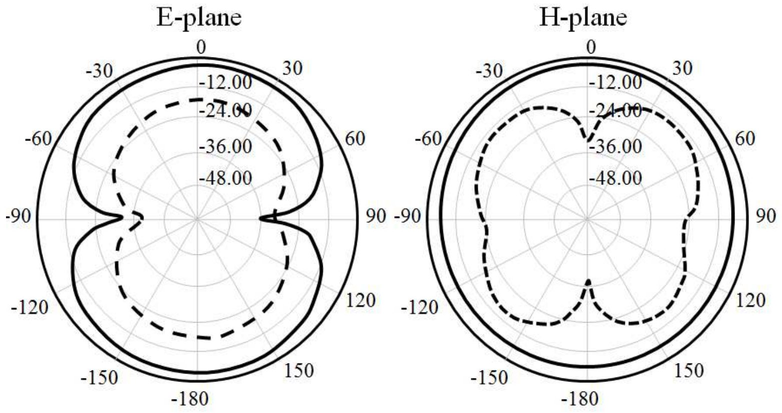

Figure 4.13: Simulated radiation pattern for the proposed SWB monopole antenna 1 at 10.6 GHz. Solid line is co-polarization and dashed line is cross-polarization.

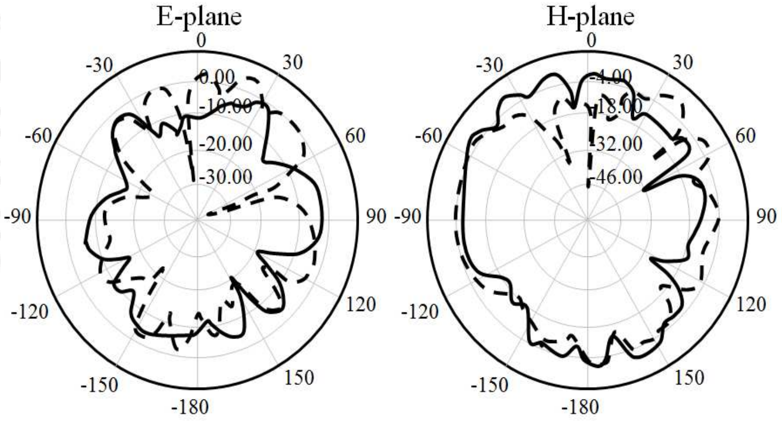

Figure 4.14: Simulated radiation pattern for the proposed SWB monopole antenna 1 at 20 GHz. Solid line is co-polarization and dashed line is cross-polarization.

matching characteristics tend to improve over the entire band, resulting in a larger bandwidth. In Fig. 4.8 we studied the ground plane size effect of the proposed monopole antenna. The area of the ground plane antenna is 21.7 mm × 30 mm. The length of the main ground plane is tailored from 21.7 mm to 21.8 mm, while the width of the antenna is kept fixed. A longer ground plane length (L_g) means a longer input microstrip feed line and higher inductance and it reduces the antenna fundamental resonant frequency and harmonic frequencies. However, if we decrease the length of the ground plane from 21.7 mm to 21.6 mm, the impedance matching is greatly influenced at 15 GHz. Therefore, the ground plane length (L_g) is chosen as 21.7 mm in our design. Although our proposed

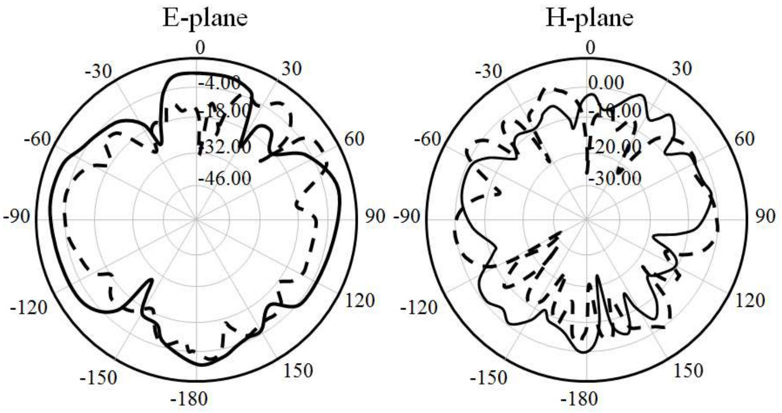

Figure 4.15: Simulated radiation pattern for the proposed SWB monopole antenna 1 at 30 GHz. Solid line is co-polarization and dashed line is cross-polarization.

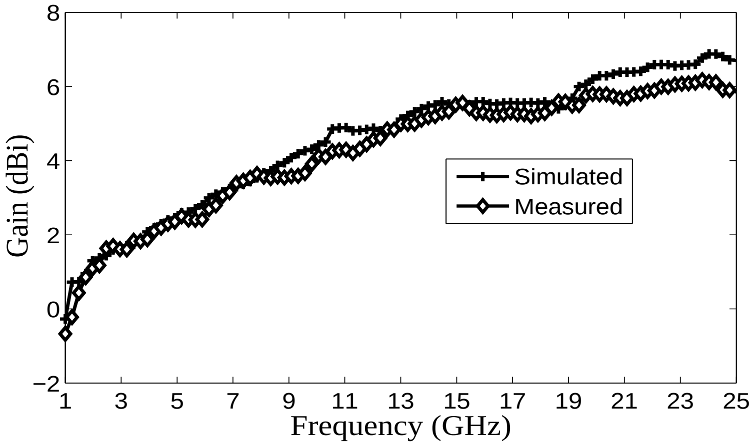

Figure 4.16: Measured and simulated gain of antenna 1.

antenna would work well up to 80 GHz, we will limit experimental studies up to 25 GHz since this is the upper measurement frequency of our vector network analyzer.

Fig. 4.9 shows the measured and simulated input impedance (Z_{in}) graph against frequency. The real part of the impedance of antenna at the frequency where the reactance is zero is equal to the antenna impedance at the resonant frequency. The antenna is fed with a line of 50 Ω characteristic impedance. When the microstrip line characteristic impedance and antenna impedance are both 50 Ω, the load impedance is matched with the line impedance. It can be observed from both measured and simulated antenna impedance that the antenna is well matched. For the simulation result at 17 GHz, one maxima occurs with an input resistance equal to 70 Ω and the measured antenna resistance at 17 GHz is 55 Ω. There is a small variation between the simulated and measured results. The

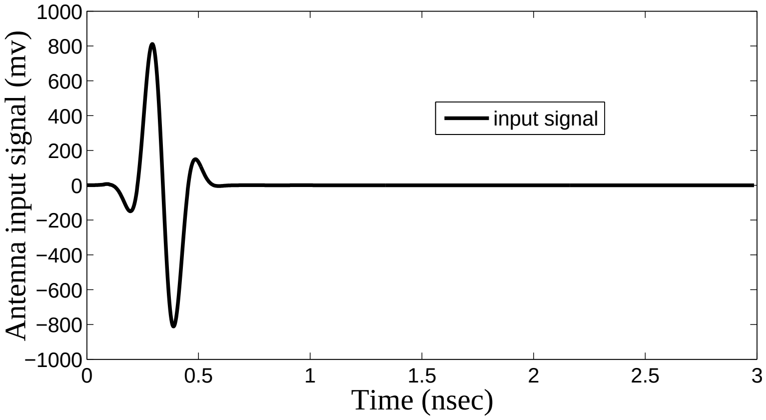

Figure 4.17: 5^{th} derivative of Gaussian pulse waveform in time domain.

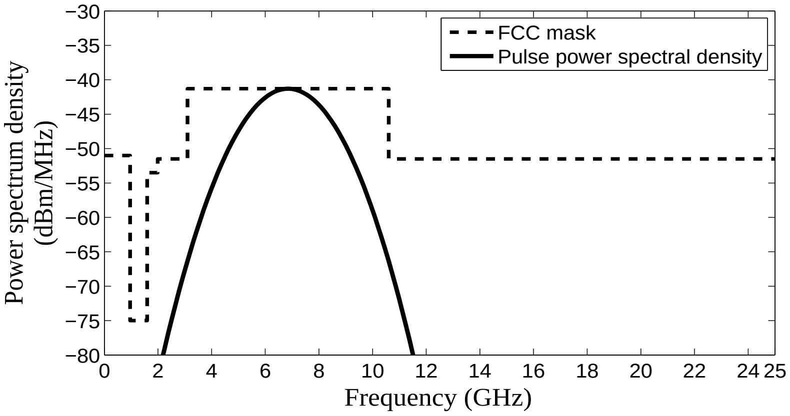

Figure 4.18: Power spectral density (dBm/MHz) of FCC spectral mask for indor UWB communication system and power spectral density (dBm/MHz) of antenna input signal (5^{th} derivative of Gaussian pulse).

simulated results are obtained using the full-wave electromagnetic field simulation software HFSS version 14 [105]. The measurement result is carried out with a Rohde and Schwarz ZVA24 vector network analyser. It shows a reasonably good agreement between the simulated and the measured results. Here measured results show broadband impedance matching performance from 2 to 25 GHz with a voltage standing wave ratio less than 2, covering the entire UWB/SWB frequency band as shown in Fig. 4.10. This shows reasonably good agreement between the simulated and the measured results. The small discrepancies may be because of the extended ground effect due to the SMA connectors which is not included in the simulation set up.

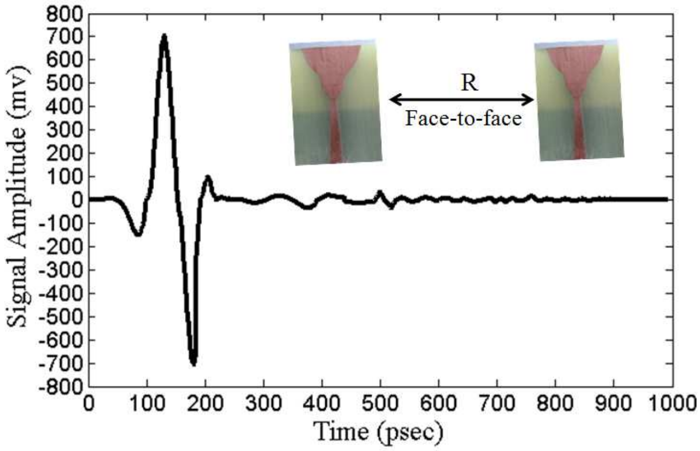

Figure 4.19: Face-to-face receiving transmitted antennas signal in time domain.

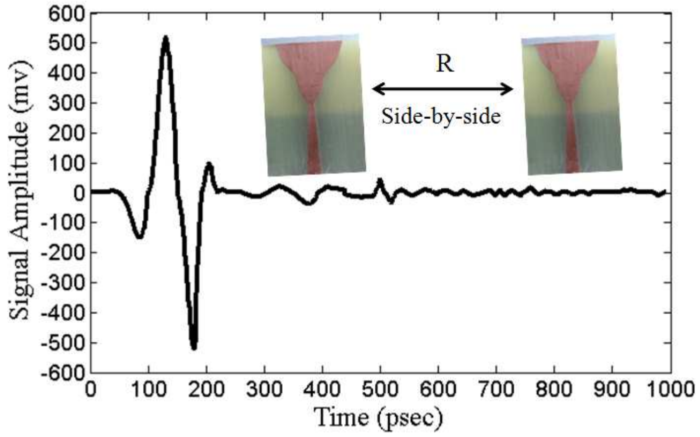

Figure 4.20: Side-by-side receiving transmitted antennas signal in time domain.

4.2.1.1 Group delay characteristics

Group delay is the measure of a signal transition time through a device. It is defined as the negative derivative of phase of the transfer function against frequency given by Wiesbeck *et al.* [106]

$$\tau_g(\omega) = -\frac{d\emptyset(\omega)}{d\omega} = -\frac{d\emptyset(\omega)}{2\pi df} \tag{4.9}$$

where ϕ is the phase response of the antenna 1 and ω is the frequency in radians per second. The phase response and group delay are related to the antenna gain response. The simulated and measured antenna group delay over the frequency from 1 to 25 GHz is presented in Fig. 4.11. From the graph,

Table 4.1: Dimensions of the Proposed UWB/SWB Monopole Antenna

Parameters	Antenna 1	Antenna 2
W	30	30
L	40	40
L_p	3	3
w_p	12	12
W_g	1	3
w_n	6	6
m_p	13.5	13.5
L_g	21.7	21.7
w_0	5	5
I_r	30	30
I_m	8	8
I_k	23	23
I_f	26	26
r_g	9	9
I_n	15	15
H	1.6	1.6
P	1.3	1.3
R	2	2

we observe that the variation in the group delay is less than 1 ns and gives a reasonably constant group delay over the UWB range (3.110.6 GHz). If the group delay variation exceeds 1 ns, the phases are no longer linear in the far-field region and a pulse distortion is caused. This can be a serious problem in UWB communication systems. Both measured and simulated group delay variation are < 0.5 ns between (3 and 18 GHz), but there is little difference between simulation and measurement ($\tau_g(\omega)$ 0.5 ns) between 18 and 19 GHz.

4.2.1.2 Radiation patterns and gain

Radiation patterns of the antenna in both the E and H-planes, at 3.1, 10.6, 20 and 30 GHz, are shown in Fig. 4.12 – Fig. 4.15. These patterns show that the antenna has a nearly omni-directional radiation pattern at lower frequencies in the H-plane from 3.1 to 10.6 GHz. At the frequencies 3.1 and

10.6 GHz the E-plane pattern is found to be eight (8) shaped which shows the bidirectional patterns. The cross-polar E-plane radiation is approximately -28 dB at 3.1 GHz and about -24 dB at 10.6 GHz. However, in the E and H-planes, it can be seen that at higher frequencies the cross-polarization level rises (e.g. at 20 and 30 GHz). Also, a few nulls are observed at higher frequencies. Fig. 4.16 shows the simulated and measured antenna gain. The peak gain of the proposed antenna is 5.9 dBi. The gain gradually increases from 1 to 18 GHz while gain decreases after 18 GHz and remains almost constant up to 25 GHz.

4.3 Time domain performance

UWB antennas are employed to transmit/receive time domain narrow pulse signals, so the time-domain characteristics of the UWB antennas [107] are very important. To investigate the time domain characteristics of the UWB antenna, two identical antennas are kept at a distance (R) of 60 cm in face-to-face and side-by-side configurations. A fifth-derivative Gaussian pulse, as presented in (10), is used as the source signal to drive the transmitter [108].

$$G_5(t) = A\left(-\frac{t^5}{\sqrt{2\pi}\sigma^{11}} + \frac{10t^3}{\sqrt{2\pi}\sigma^9} - \frac{15t}{\sqrt{2\pi}\sigma^7}\right).\exp\left(-\frac{t^2}{2\sigma^2}\right) \tag{4.10}$$

where A is the amplitude parameter, t is the time, and σ is the standard deviation. In order to satisfy the FCC mask, a shape filter can be added in the transmitter.

Fig. 4.17 and Fig. 4.18 shows the fifth-order derivative of Gaussian pulse waveform with a width of 300 ps in the time domain and its power spectral density (dBm/MHz) with reference to FCC mask. The measured results suggest that the selected fifth derivative of Gaussian pulse fits into the FCC mask reasonably well, indicating that this UWB pulse complies with the FCC mask while it is able to deliver the most possible signal power as permitted. Based on the pulse generated in a Tektronix AWG 7122B arbitrary signal generator, an optimal pulse width of 250 ps is selected for best-fitting into the FCC power mask in this design.

Figs. 4.19 and 4.20 shows the received pulse for face-to-face and side-to-side configurations. The antenna 1 acts as a received antenna. The transmit antenna is also the replica of antenna 1. That means the fifth-order derivative of the Gaussian pulse is transmitted from antenna 1 to antenna 1. Compared with the case of the face-to-face configuration, the magnitude of the received signal is smaller when the antennas are positioned side-by-side. We have used an amplifier whose gain is about 26 dB at the receiver side, since the received signal was very weak. From Figs. 4.19 and 4.20, one can see that the ringing in the tail of the received pulse is slightly more in case of side-by-side placement as compared to the ringing present in the received signal when the antenna is placed face-to-face. This is because, when the antennas are stationed face-to-face, the whole of the radiating surface is exposed to the receiving signal. This is the broadside direction of the radiation pattern. Hence the signal reception is smooth in this situation. However, when the antennas are placed side-by-side, the radiation is in the end fire direction. Overall ringing is better than the existing UWB antennas in the literature. The correlation factor between the output and input signal can be calculated with (equation 4.11)

$$\rho = \max_{\tau}\left(\frac{\int S_1(t)\,S_2(t-\tau)\,dt}{\sqrt{\int S_1^2(t)\,dt}\,\sqrt{\int S_2^2(t)dt}}\right) \tag{4.11}$$

where τ is a delay which is varied to make the numerator in (equation 4.11) maximum [109]. The correlation factor is calculated to be 0.8139 when the two antennas were positioned face-to-face, and the value becomes 0.7108 when they are fixed side-by-side. The fidelity of the case of face-to-face is better than the case of side-by-side.

4.4 Summary

A printed monopole antenna for optimal UWB/SWB performance has been proposed. A triangular tapered feed line is used for feeding the exponentially tapered feed region and patch of the proposed antenna. Tapered structures are employed so that the input signal to the antenna can radiate freely without any disturbance from the antenna. It has been observed experimentally that the antenna is well matched for a very broad frequency range. The measured group delay and gain are also within acceptable limits. Time domain characteristics of the proposed antenna have been measured and validated that the proposed antenna is suitable candidate for UWB/SWB applications. The simulated result shows that it is a super wideband antenna which is applicable for frequencies between 2.5 and 80 GHz. Such a wideband planar and compact antenna may be used for spectrum sensing in cognitive radio [110] as well.

5

Centurion bandwidth tapered monopole band-notched antenna for super wideband application

Contents

5.1 Introduction

In recent years, wireless communication devices require larger bandwidths to transmit high-data rates(>500 Mbps), operate at low power and good immunity to multipath effects. Antenna system required to accomplished this should have ultra wideband, high capacity, well matched and of high gain. The operating frequency region for ultrawideband (UWB) systems is between 3.1 to 10.6 GHz as approved by the FCC in 2002 [1]. It can be seen that bandwidth (BW) ratio of this UWB antenna is 3.4:1, which is obtained by dividing the highest frequency by lowest frequency. UWB antennas have found wide application in the area of personal area network (PAN), radar imaging systems, biomedical imaging system etc. Effort to increase the bandwidth greater than UWB is continuing. Very wideband antennas which have bandwidth ratio > 10:1 are usually called super-wideband (SWB) antenna [2]. SWB antenna covering bandwidth from 1 to 30 GHz has been reported in [111]. This antenna has bandwidth ratio of 33:1 for VSWR ≤ 2. Here the concept of fractal monopole structure has been utilized. Ke Ren Chen *et al.* [112] designed an egg-shaped super wideband monopole antenna with a bandwidth ratio greater than 12:1. In [113], Y. Dong *et al.* describe a circular monopole antenna composed of an elliptical monopole patch and a tapered feed line with bandwidth ratio greater than 25:1. This antenna has a voltage standing wave ratio (VSWR) < 2. The triangular tapered monopole antenna has found wide acceptance for UWB radios due to its ease of fabrication. One important issue to be noted for UWB antenna is that, it may cause electromagnetic interference to the existing narrow band wireless local-area network (WLAN) IEEE 802.11a and HIPERLAN/2 WLAN operating in 5.15−5.35 GHz and 5.725−5.825 GHz bands. These narrow bands lie within the UWB band specification. To have no or marginal effect at these bands, radiation of the UWB antenna is to be suppressed at these bands. To mitigate this interference issue, UWB antennas with band-notched characteristics have been proposed. In the last few years, several band-notch scheme for antennas have been investigated by researchers across the globe [114–116]. One popular design for band rejection is the cutting of slots on the radiating patch or on the ground plane. For example a letter C-shaped slot [114], inverted U-shaped slot [115], π-shaped slot [116], etc. have been used for this purpose. Parasitic elements under the radiating patch have also been used successfully for notching purpose. For example H-shaped parasitic element [47], I-shaped parasitic element [48], rod-shaped parasitic element [49], shorted parasitic element [117] and trapezoidal parasitic conductor [118] have been proposed. These antennas have been designed to have notch within UWB band.

In this thesis, we propose a new structure for realization of super-wideband radiation characteristics along with notch capability. Here we demonstrate that by employing the triangular tapered feed line and radiating patch, wider impedance bandwidth can be achieved. By using rectangular chamfered ground plane, it will further enhance the impedance bandwidth . Frequency bandwidth of 1.1 to 100 GHz of the proposed SWB antenna can be realized. Further not to effect the band from 5−6 GHz used in WLAN we introduced appropriates U-shaped parasitic element. The proposed antenna is very promising for various modern communication applications such as GSM1800 (1.71−1.88 GHz), PCS (1.85−1.99GHz), AWS-3 (2.155−2.175 GHz), WCS (2.345−2.360 GHz), ISM (2.402−2.480 GHz), MMDS (2.500−2.690 GHz) and UWB (3.1−10.6 GHz). It also exhibits band-notch characteristic from 4.75−6 GHz. The proposed antenna provides much wider impedance bandwidth of 98.3 GHz that is 1.7 to 100 GHz. The measured peak gain (1−25 GHz due to vector network analyzer limitations) varies from .5−5.4 dBi with acceptable radiation pattern across the operating band except at the notch frequency band.

5.2 Band-notched SWB antenna using FR4 substrate

Fig. 5.1 shows the configuration of the proposed SWB monopole antenna with and without band-notch characteristics. The optimal dimensions of the proposed antennas are as follows: $L = 40$ mm, $W = 30$ mm, $H = 22$ mm, $M = 22$ mm, $l_f = 7$ mm, $l_h = 8$ mm, $W_g = 7$ mm, $l_n = 12$ mm, $l_k = 5$ mm, $W_k = 8$ mm, $R_1 = 22.7$ mm, $R_2 = 3.05$ mm, $l_y = 3$ mm, $l_c = 8$ mm, $W_m = 4$ mm, $l_m = 1$ mm, $p = 1$ mm, $N = 15$ mm, $B = 3$ mm, $T = .8$ mm, $W_f = 10$ mm, $W_d = 9$ mm, $W_h = 9$ mm, $Q = 60^0$, $l_d = 10$ mm and $l_g = 4$ mm, which is fabricated on FR4-epoxy substrate with thickness of 1.6 mm, dielectric constant of 4.4 and loss tangent of 0.018. It can be seen from Fig. 1 that the proposed monopole antenna structure consists of a tapered radiating patch, tapered feed region which is fed by 50 Ω triangular tapered feed line, a defected ground structures (DGS) and a U-shape parasitic element placed under the radiating patch. The proposed antenna configuration is simulated using the FEM based Ansoft High Frequency Structure Simulator (HFSS) software, with lumped port excitation.

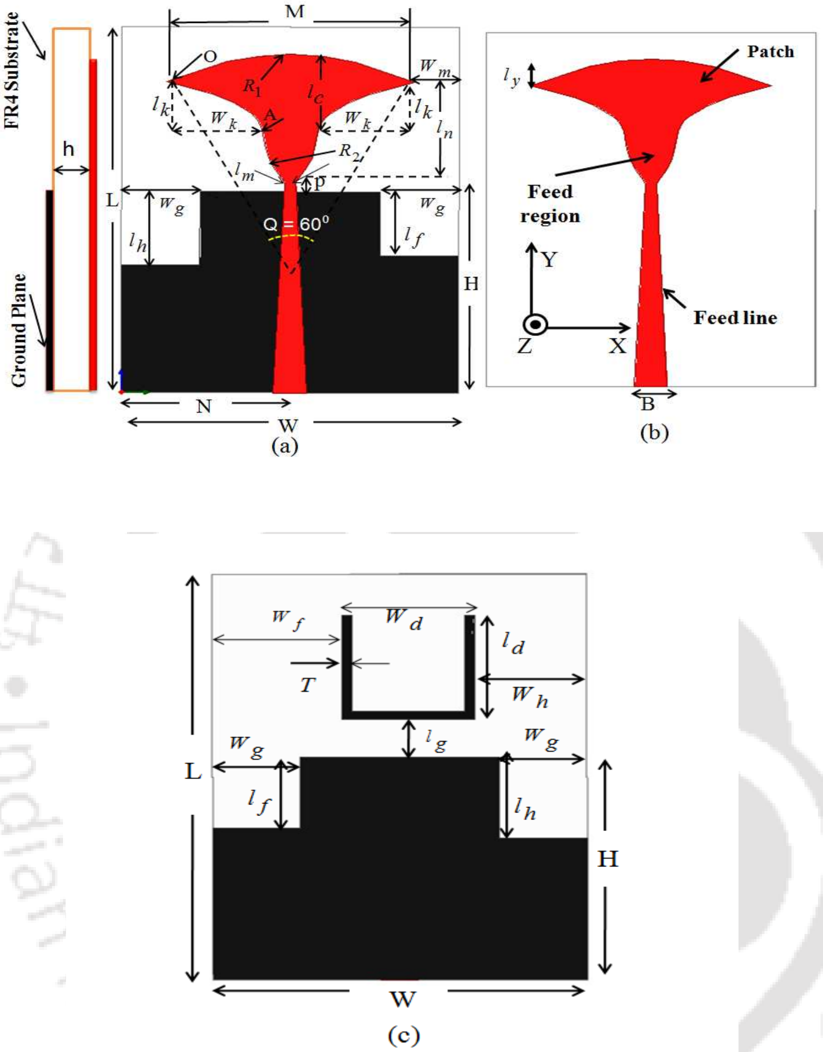

Figure 5.1: Geometry of the proposed monopole antenna: (a) Full band antenna design (b) Top view of band-notch antenna (c) Bottom view of band-notched antenna

5.2.1 SWB printed monopole antenna design

According to the present antenna configuration i.e. Fig. 5.1 (a), a feed region connection, between the feed line and the radiating patch, was brought in to improve the antenna performance. Due to optimal tapered (Raicu's universal taper) [75] connections between the feed line and the main patch, current flows on the antenna in a smooth fashion, thus providing broad band impedance bandwidth. The feed line has been triangular tapered near the antenna feeding point in order to improve the impedance matching at higher frequencies. In addition, it could be noticed that chamfered ground structures (CGS) i.e. slots integrated with ground plane are also responsible for the wider impedance

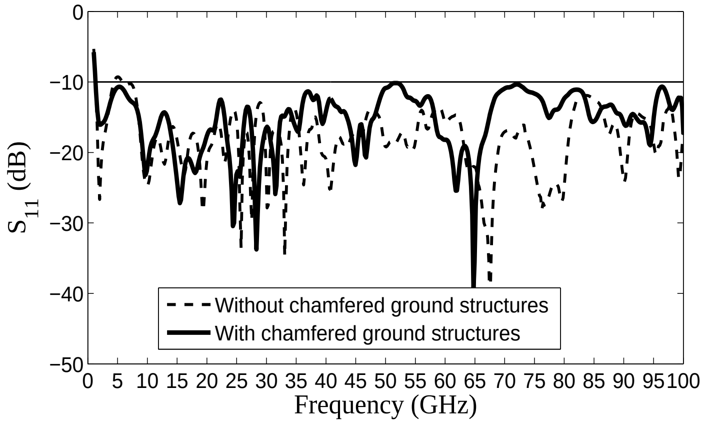

Figure 5.2: Simulated return loss vs frequency for the proposed SWB antenna with and without defected ground structures.

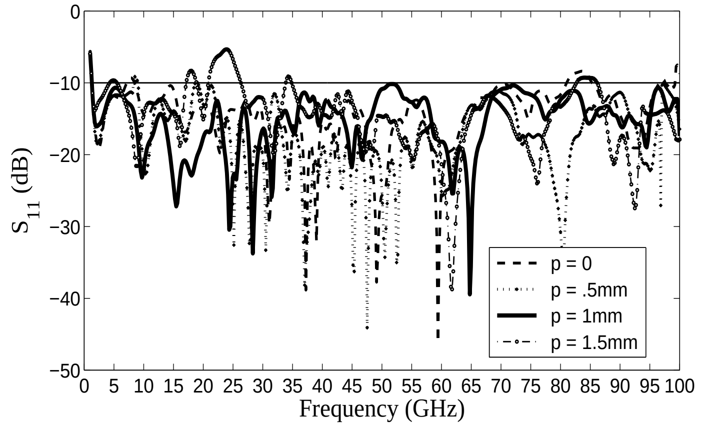

Figure 5.3: Simulated return loss vs frequency for the proposed SWB antenna with different value of feed-gap (p).

bandwidth over entire frequency band 1.1−100 GHz with ratio bandwidth of 90.9:1 except in the band of 4.75−6 GHz. Since the CGS provide an additional current path and changes characteristics of a transmission line such as line capacitance and inductance which in turn leads to change in the bandwidth. There are many parameters which have been optimized, which can affect the impedance matching and get super wideband (SWB) antenna behavior. Fig. 5.2 demonstrates the simulated return loss for the proposed monopole antenna design of Fig. 1(a) with and without CGS. It can be seen that in the absence of CGS, we observe that $|S_{11}| > -10$ dB at frequency band (3.5−6.5 GHz). By placing two slots in the ground plane it can be observed that the slots can adjust the electromagnetic coupling effects between the monopole and the ground plane and improve its impedance bandwidth [119] across the whole frequency spectrum as shown in the Fig. 5.2. Fig. 5.3 illustrates the simulated return loss for different values of feed gap p between the ground plane and main patch. The obtained

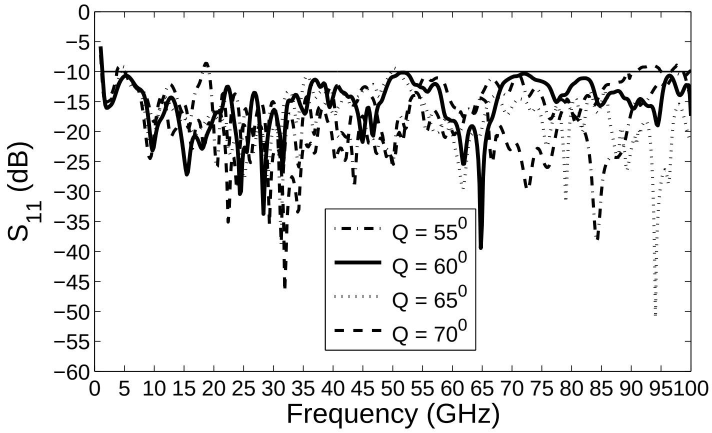

Figure 5.4: Simulated return loss vs frequency for the proposed SWB antenna with various circular arc angles (Q).

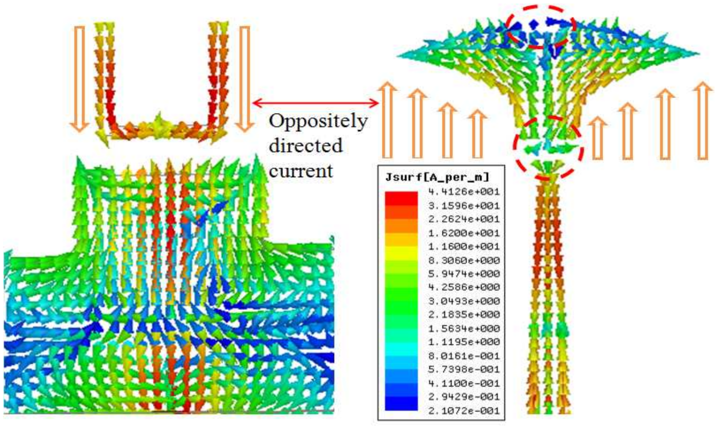

Figure 5.5: Simulated current distribution at notch frequency 5.37 GHz.

results distinctly show that the increasing the feed-gap p from 1 to 1.5 mm, the lowest resonant frequency of the proposed antenna is shifted towards left and has a great effect on the impedance matching at high frequency. When the feed-gap p decreases from 1 to .5 mm the impedance bandwidth is degraded between 6−8 GHz. In other words we can say that the impedance bandwidth significantly changes with the variation of the feed-gap. Better impedance matching is achieved with a feed-gap (p) of 1 mm. Fig. 5.4 depicts the simulated return loss for the proposed monopole antenna with various circular arc angle (Q). When the circular arc angle (Q) increases from 60^0 to 70^0, approximate wide impedance bandwidth is provided between 6−100 GHz, while impedance matching becomes worse between 4−6 GHz. As $Q = 60^0$, the super wide impedance bandwidth is achieved from 1.7 to 100 GHz. When the circular arc angle (Q) decreases from 60^0 to 55^0, $|S_{11}| > -10dB$ between (17−21

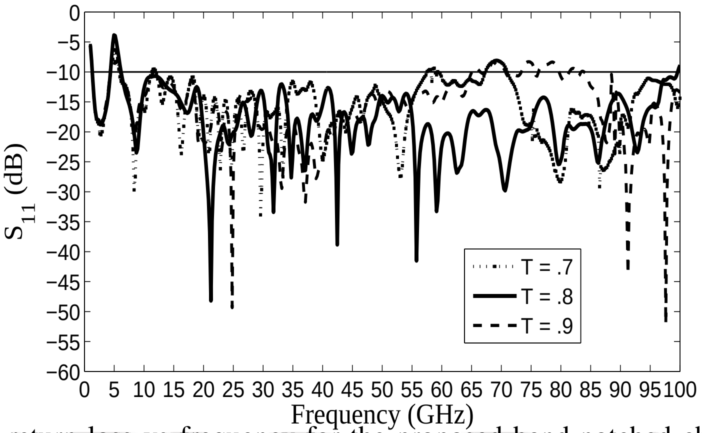

Figure 5.6: Simulated return loss vs frequency for the proposed band-notched characteristics antenna with different arm width (T)

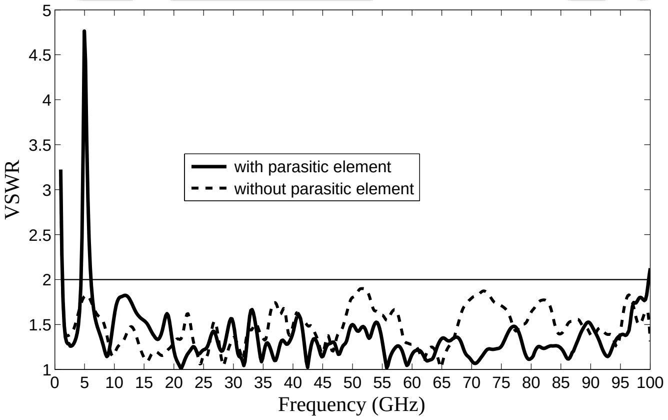

Figure 5.7: Simulated VSWR vs frequency for the proposed antenna with or without U-shape parasitic element.

GHz) band. In other words, by increasing or decreasing the circular arc angle (Q) the capacitive or inductive loading may be increased and results in impedance mismatch.

5.2.2 Study of band-notched function design

Fig. 5.1 (b) and 5.1 (c) shows that the band-suppression characteristics over the whole interference band which is realised by the U-shaped parasitic element in the back plane, which is electromagnetically coupled to the main patch. The U-shaped parasitic element acts as a half-wave resonant structure and can perturbs the current distribution at certain frequency band (4.75−6 GHz), where the band-notched characteristics of the antenna are expected. Band-notched characteristics can be achieved by tuning the parameters W_d, l_d, T and W_h. A dimension of the U-shaped parasitic elements is selected according to the following expression:

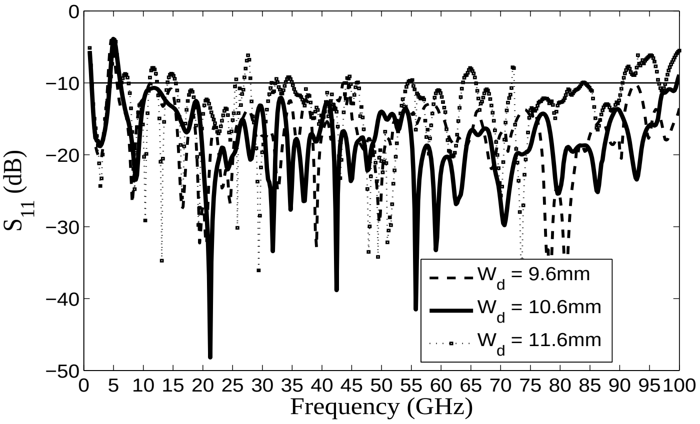

Figure 5.8: Simulated return loss vs frequency for the proposed band-notched characteristics antenna with different arm width (W_d).

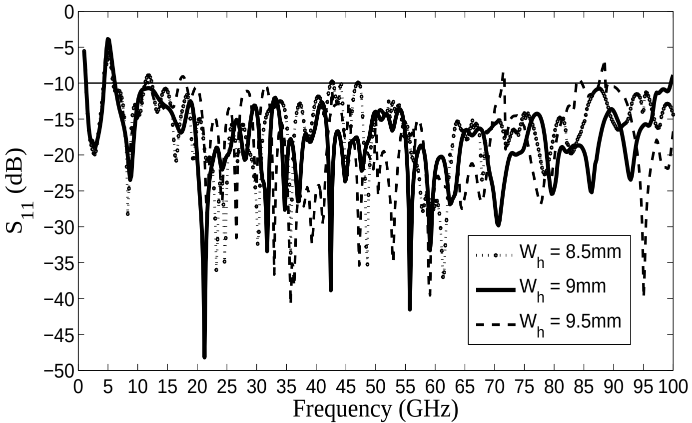

Figure 5.9: Simulated return loss vs frequency for the proposed band-notched characteristics antenna with different arm width (W_h).

$$V = .5\,\lambda_g = W_d + 2 \times l_d - T \tag{5.1}$$

where V is the physical length of an U-shaped parasitic element and λ_g is the corresponding band-notch frequency (5.37 GHz). W_d, l_d and T is the width, length and thickness of U-shaped parasitic element. Mainly, the width W_d and length l_d of the parasitic element acts as the inductance, and the distance between two arms of U-shaped parasitic element acts as the capacitance. Furthermore, the current flows on parasitic elements more egregiously around notch frequency and they are opposite in direction (out-of-phase) to the current flow on the main patch, which can easily cancels out the radiation field and offered strong attenuation near the notch frequency [115] and [120]. Fig. 5.5 indicates the simulated surface current distribution for the proposed monopole antenna at band-notch center frequency 5.37 GHz. An orange color arrow shows the direction of the surface current and

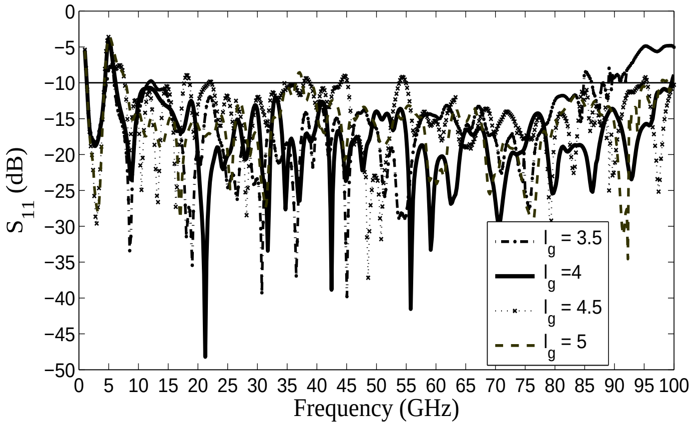

Figure 5.10: Simulated return loss vs frequency for the proposed band-notched characteristics antenna with different arm width (*Lg*).


Top view
Bottom view

Figure 5.11: Photograph of the fabricated prototype band-notched SWB antenna using FR4 substrate.

flows oppositely between the main patch and the parasitic element. Also it could be noticed that at notch frequency surface current is not distributed normally around the feed region and resulting currents cancel perfectly around the feed region leading to a null, which is indicated by dotted red color circle. However an orange color arrow indicates strong resonance occurs on the U-shaped parasitic element and makes it as a non-responsive antenna performance at notch frequency. The simulated return loss for the proposed monopole antenna with various arm width T of the U-shaped parasitic element are illustrated in Fig. 5.6. It is clearly seen from the Fig. 5.6 that the arm width T has a little effect on the rejected frequency. That is, by increasing arm width T from .8 to .9 mm weak rejection occurs at the band-notch region and when the arm width T = .8 mm, strong rejection occurs at the band-notch region. Weak rejection may occur due to decreased inductance characteristics of

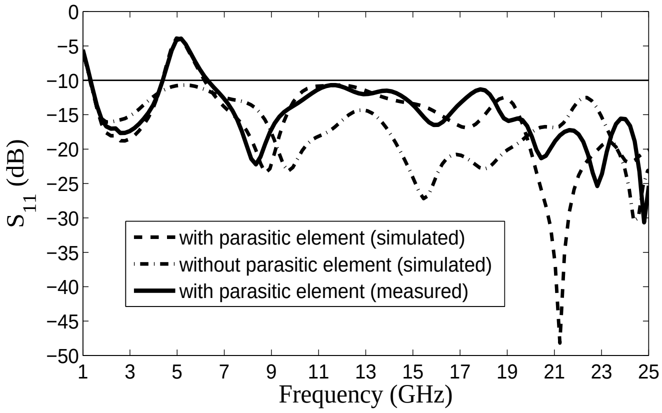

Figure 5.12: Measured and simulated return loss vs frequency for the proposed antenna.

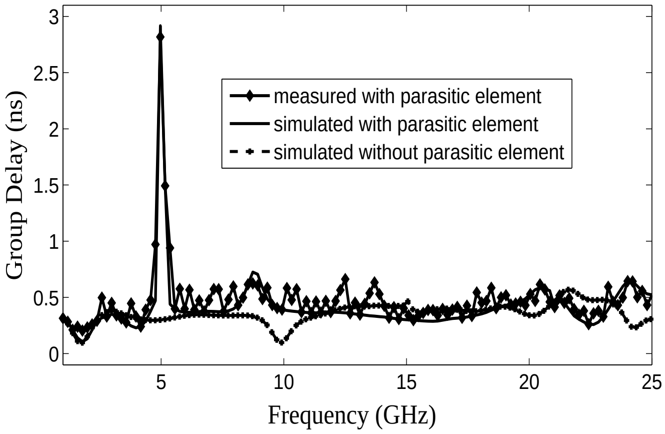

Figure 5.13: Measured and simulated group delay vs frequency for the proposed antenna.

U-shaped arm width T. Fig. 5.7 shows the voltage standing wave ratio of the proposed monopole antenna with and without band-notch function. The antenna return loss is plotted in Fig. 5.8, for different values of the difference between two arms W_d of U-shaped parasitic element. In particular, it is observed for W_d value greater than 10.5 mm notch frequency shifts 1 GHz to a higher level of the band-notch region and provide much wider notch performance i.e. 4.75−7 GHz. It indicates the coupling capacitance between two arms of U-shaped is decreased. However, it is observed that there is .2 GHz frequency shifts to a lower level of the band-notch region when W_d = 9.6 mm. So W_d has to be chosen as 10.6 mm. Fig. 5.9 exhibits the simulated return loss of various positions of the right arm W_h, and results for the position of the right arm W_h is varied from 8.5 to 9.5 mm. In this arrangement, center of the notched frequency varies from 5.37 GHz to 5.27 GHz as W_h changes from 9 mm to 9.5 mm and also high frequency bandwidth is mostly affected. When position of the right arm W_h = 8.5 mm, band-notch characteristics is less sensitive, while within the SWB region impedance matching

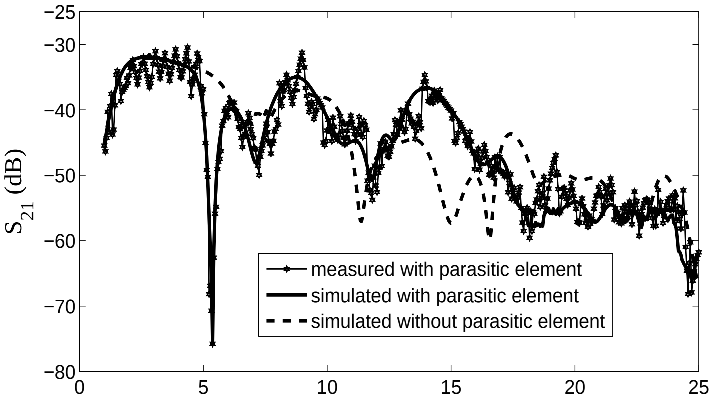

Figure 5.14: Measured and simulated magnitudes of the transfer function vs frequency for the proposed SWB antenna.

disturbs slightly. The optimised right arm W_h is chosen to be 9 mm for this case. The effect of the vertical distance between lower arm of parasitic element and ground plane L_g on the notch band is depicted in Fig. 5.10. As shown, if the dimension of L_g increases from 4 to 5 mm, higher level of the notch frequency is shifted to 2.5 GHz, which indicates that the coupling capacitance could be much decreased. With decreasing the dimension of L_g, bandwidth of the notch frequency does not effect, however the WLAN rejection is observed to be poor at the band-notch region.

5.2.3 Simulation and experimental results

The proposed SWB band-notch monopole antenna was successfully fabricated on FR4 substrate with h = 1.6 mm and $\epsilon_r = 4.4$. The photograph of the fabricated antenna is shown in Fig. 5.11. A vector network analyzer (Agilent ZVA24) was utilized to measure and verify the antenna performance. The simulation frequency range is from 1.7 GHz−100 GHz, while measurement results are performed till 25 GHz. Fig. 5.12 shows the FEM based full-wave simulated and measured return loss of the designed SWB antenna. It is to be noted that from the graph, there is good agreement between the simulated and measured results. To demonstrate the group delay and magnitude of transfer function S_{21}, two identical antennas are placed in the face-to-face orientations, with a distance of 0.3 m. Fig. 5.13 shows the measured and simulated group delay for the proposed monopole antenna. As can be seen that the group delay variation is less than 0.7 ns from the frequency range 1.7−25 GHz, except the notched frequency band 4.75−6 GHz. At notch frequency band the group delay variation approximates 3 ns, which can degrade phase linearity. Fig. 5.14 shows the measured and simulated

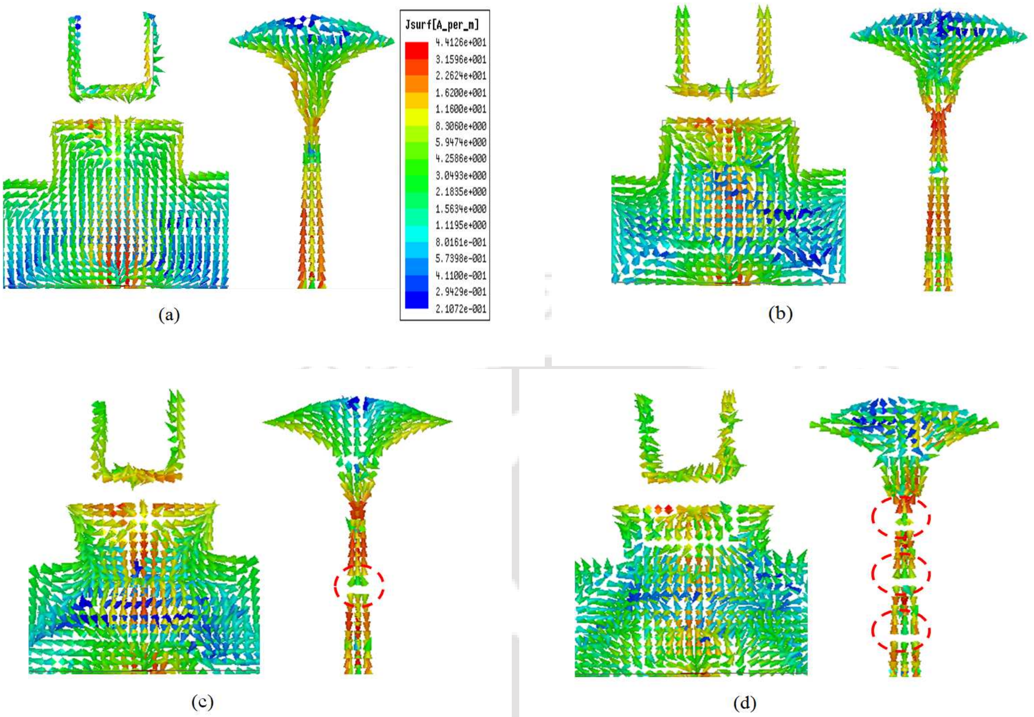

Figure 5.15: Simulated surface current current distribution for the proposed monopole antenna with a U-shape parasitic element at (a) 2.1 GHz, (b) 7 GHz, (c) 10 GHz, (d) 20 GHz.

magnitude of transfer function S_{21} for the proposed antennas. It depicts that there is little variation in the measured and simulated magnitude of transfer function except in the band-notch region. The simulated surface current distribution of the proposed antenna at frequencies 2.1, 7, 10 and 20 GHz are shown in Fig. 5.15. By inspection of Fig. 5.15 (a), (b), (c) and (d) it can observed that currents are firstly distributed around the outskirts of the monopole radiator and the triangular tapered transmission line, while considerable amount of current concentrated at the upper edge of the ground plane [121]. At frequencies 2.1 and 7GHz, surface current flows in vertical direction in monopole radiator as well as ground plane. There is small current flow at the upper edge of the ground plane leading to nearly omni directional radiation and negligible cross polarization at frequencies 2.1 and 7GHz. At frequency 10 GHz a current null occurs on the feed line (indicated by red circle) and current is sparsely distributed on the monopole radiator and the ground plane. However, at high frequency 20 GHz more null currents occurs on the feed line (indicated by red circle) and it could be noticed that X-directed current component are presents on the monopole radiator as well as ground plane also. Due to X-directed surface current component, cross-polarization becomes sturdy at high frequencies as shown

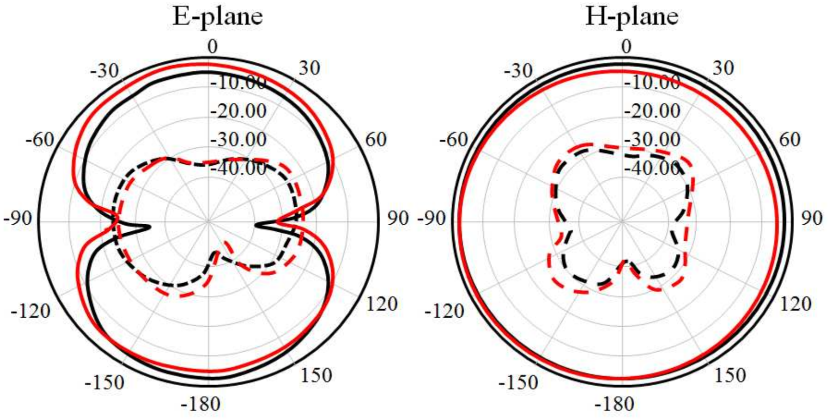

Figure 5.16: Simulated (red lines) and measured (black lines) radiation pattern for the proposed SWB monopole antenna at 2.1 GHz. Solid line is co-polarization and dashed line is cross-polarization.

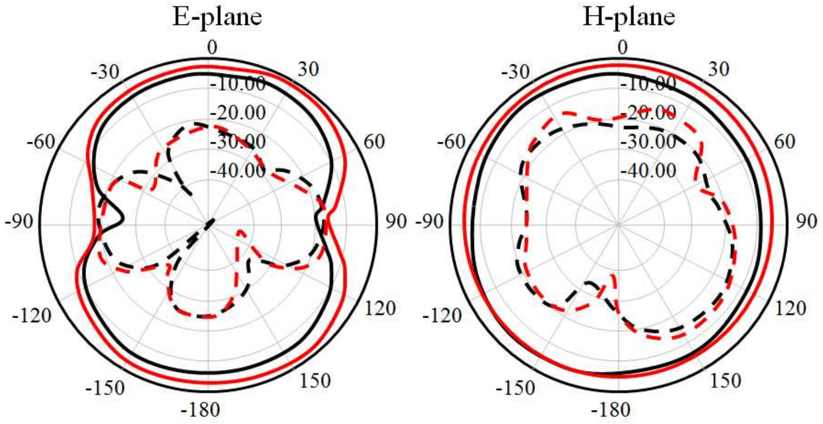

Figure 5.17: Simulated (red lines) and measured (black lines) radiation pattern for the proposed SWB monopole antenna at 5.37 GHz. Solid line is co-polarization and dashed line is cross-polarization.

in Fig. 5.16 (e). Fig. 5.16 shows far-field radiation patterns in the E-plane and H-plane at six different frequencies 2.1 GHz, 5.37, 7, 10 and 20 GHz. The proposed antenna has a nearly omni-directional and low cross polarization level in the H-plane radiation pattern at frequencies 2.1, 5.37 and 7 GHz. The E-plane radiation pattern shows a typical bidirectional (figure-of-eight) at frequencies 2.1, 5.37 and 7 GHz. Probably due to band-suppression characteristics at 5.37 GHz, the radiation in the E plane is tilted to 30^0 and 150^0. At frequency 10GHz an antenna generates null at 150^0 in the the E-plane, while multi-nulls are observed in the E-plane at frequency 20 GHz and have a lager cross-polarization at frequencies 10, and 20 GHz. Fig. 5.17 shows measured gain with parasitic element and simulated gain without parasitic element from 1.4 to 25 GHz. The measured gain was achieved by the gain

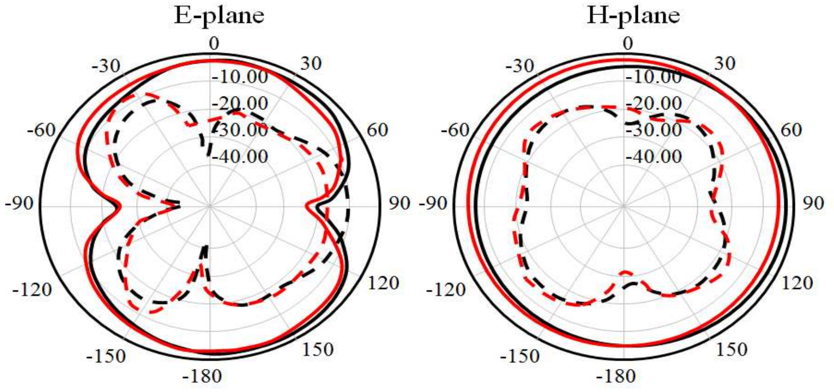

Figure 5.18: Simulated (red lines) and measured (black lines) radiation pattern for the proposed SWB monopole antenna at 7 GHz. Solid line is co-polarization and dashed line is cross-polarization.

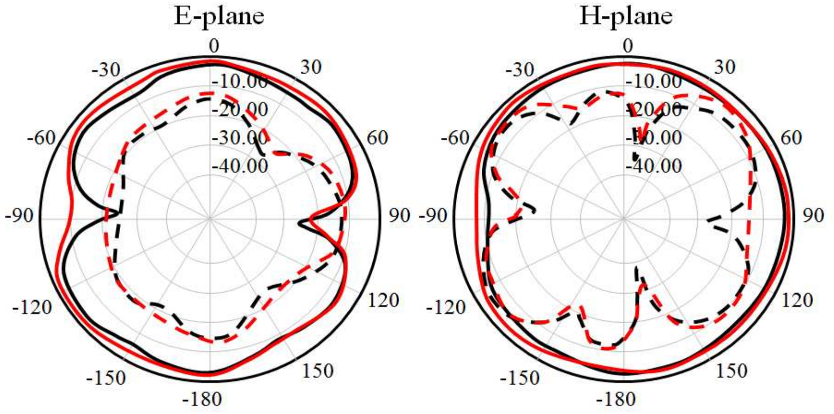

Figure 5.19: Simulated (red lines) and measured (black lines) radiation pattern for the proposed SWB monopole antenna at 10 GHz. Solid line is co-polarization and dashed line is cross-polarization.

transfer technique where a standard gain horn antenna was used as a reference. From Fig. 5.17 it can be seen that, the measured peak gain is about .5−5.4 dBi across the operating band 1.4 to 25 GHz except at the rejected bands. Around the rejection band, the gain can be as low as -7 dBi, when the parasitic elements are used.

5.3 Band-notched SWB antenna using RT/Duroid 5870 substrate

In this section we have designed SWB antenna using RT Duroid 5870 substrate. Because RT/Duroid 5870 substrate is more versatile [122] than FR4 substrate, especially for very high frequencies or millimeter wave frequencies (greater than 30 GHz).

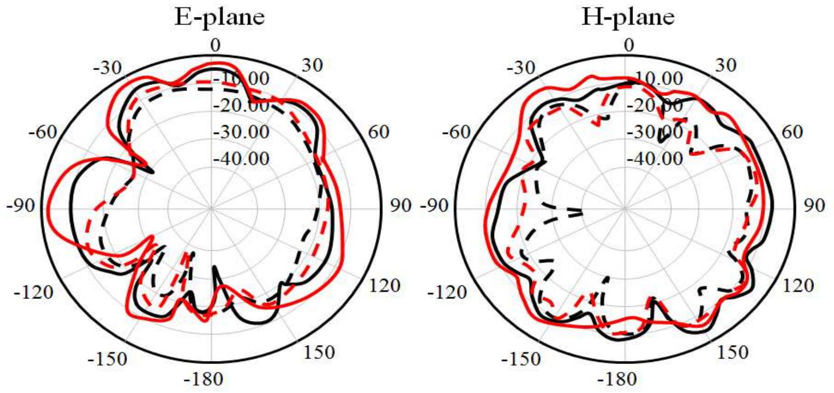

Figure 5.20: Simulated (red lines) and measured (black lines) radiation pattern for the proposed SWB monopole antenna at 20 GHz. Solid line is co-polarization and dashed line is cross-polarization.

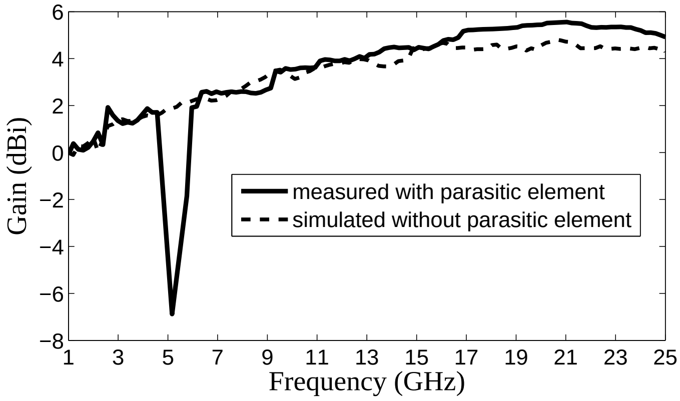

Figure 5.21: Measured and simulated gain vs frequency for the proposed antenna.

Fig. 5.22 shows the configuration of the proposed SWB monopole antenna with and without band-notch characteristics. It can be seen from Fig. 5.22 that the proposed SWB monopole antenna structure composed of a tapered radiating patch, tapered feed region which is fed by 50 Ω triangular tapered feed line, and a chamfered ground plane (CGP). To create a band-notch characteristics for WLAN a C-shape parasitic element is employed, which is electromagnetically coupled to the radiating patch. Further to improve the notching characteristics of the proposed antenna, two L-slots are placed in the chamfered ground plane (CGS). The proposed SWB antenna is designed by Rogers RT/Duroid 5870 substrate with a thickness of 0.787 mm and a dielectric constant of 2.32 and a loss tangent of 0.0012. The optimal dimensions of the proposed antennas are as follows: L = 40 mm, W = 30 mm, H = 22 mm, M = 22 mm, l_f = 7 mm, W_g = 7 mm, l_n = 11 mm, l_K = 5 mm, W_K = 8 mm, R_1 = 22.7 mm, R_2 = 3.05 mm, l_y = 3 mm, l_C = 8 mm, W_m = 4 mm, l_m = 1 mm, p = 1 mm, N = 15

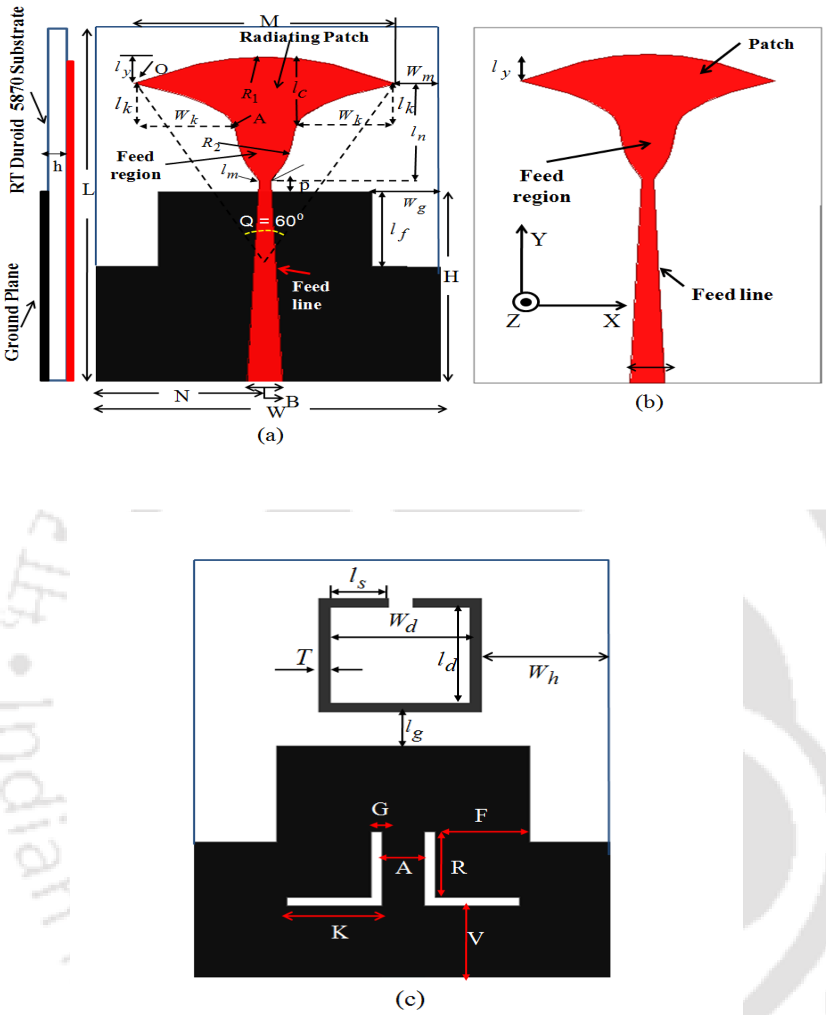

Figure 5.22: Geometry of the proposed monopole antenna: (a) Full band antenna design (b) Top view of band-notch antenna (c) Bottom view of band-notched antenna

mm, B = 3 mm, T = 0.8 mm, W_d = 10 mm, W_h = 9.5 mm, Q = 60^0, l_d = 9 mm, l_g = 4 mm, l_s = 4 mm, F = 6.7 mm, R = 6.2 mm, K = 6.8 mm, G = 0.8 mm, A = 3 mm, V = 7 mm. The proposed antenna configuration is simulated using the FEM based Ansoft High Frequency Structure Simulator (HFSS) software, with lumped port excitation.

5.3.1 SWB printed monopole antenna

According to the present antenna configuration i.e. Fig. 5.22 (a), a feed region connection, between the feed line and the radiating patch, was brought in to improve the antenna performance. Due to optimal tapered [12] (Raicu's universal taper) connections between the feed line and the main patch, current flows on the antenna in a smooth fashion, thus providing broad band impedance band-

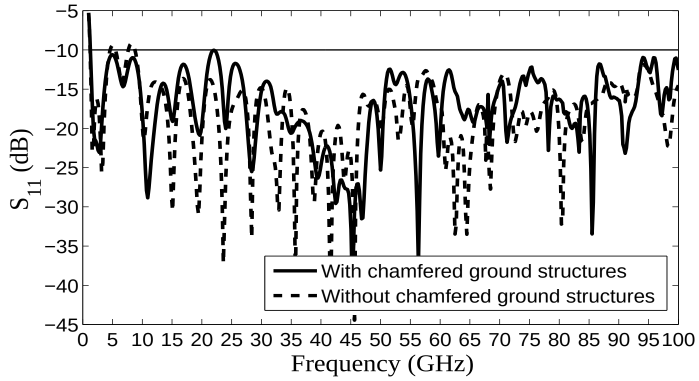

Figure 5.23: Simulated return loss vs frequency for the proposed SWB antenna with and without chamfered ground structures (CGS).

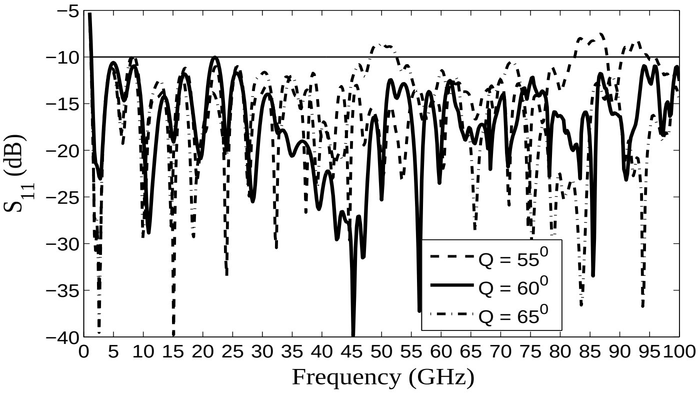

Figure 5.24: Simulated return loss vs frequency for the proposed SWB antenna with various circular arc angles (Q).

width. The feed line is triangular tapered near the antenna feeding point in order to improve the impedance matching at higher frequencies. Moreover, It could be noticed that chamfered ground structures (CGS) i.e. two rectangular slots integrated with ground plane are also responsible for the wider impedance bandwidth over entire frequency band .9−100 GHz (bandwidth ratio of 111.1:1) except in the band of 4.7−6 GHz. Since the chamfered ground structures (CGS) provide an additional current path and changes characteristics of a transmission line such as line capacitance and inductance which in turn leads to change the bandwidth. There are many parameters that have been optimized, which can affect the impedance matching and get super wideband (SWB) antenna behavior. Fig. 5.23 demonstrates the simulated return loss for the proposed monopole antenna design of Fig. 5.22(a) with and without chamfered ground structures (CGS). It can be seen that in the absence of chamfered ground structures (CGS), the behavior of $S_{11} > -10$ dB at frequency band (4−5 and

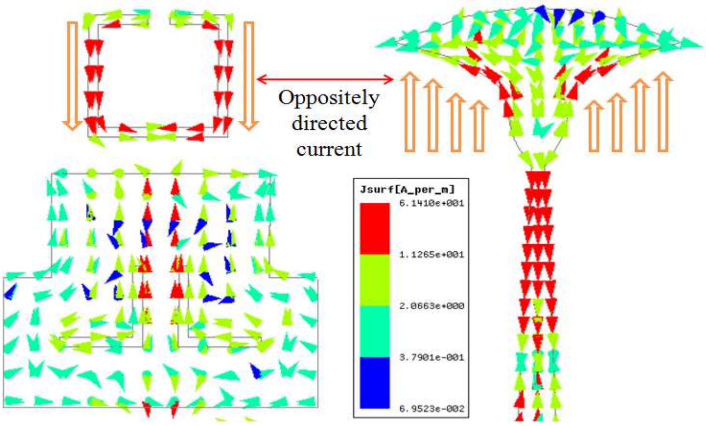

Figure 5.25: Simulated current distribution at notch frequency 5.35 GHz.

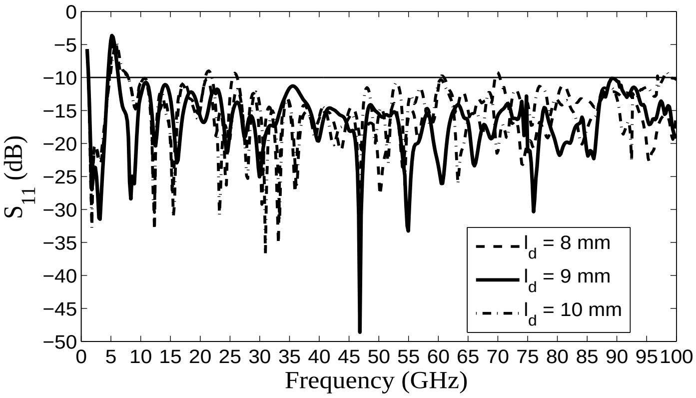

Figure 5.26: Simulated return loss vs frequency for the proposed band-notched characteristics SWB antenna with different arm length (l_d).

6−7 GHz). By placing two rectangular slots in the ground plane it can be observed that the slots can adjust the electromagnetic coupling effects between the monopole and the ground plane and improve its impedance bandwidth across the whole spectrum as shown in the Fig. 5.23. Fig. 5.24 depicts the simulated return loss for the proposed monopole antenna with various circular arc angle (Q). When the circular arc angle (Q) increases from 60^0 to 65^0, approximate wide impedance bandwidth is provided between 0.9−47 GHz, however impedance matching becomes worse between 47−53 GHz. As Q = 60^0, the super wide impedance bandwidth is achieved from 0.9 to 100 GHz. While, circular arc angle (Q) decreases from 60^0 to 55^0, $|S_{11}| > -10$ dB between (82−87 GHz and 90−95 GHz). In other words, by increasing or decreasing the circular arc angle (Q) the capacitive or inductive loading may be increased and results in impedance mismatch.

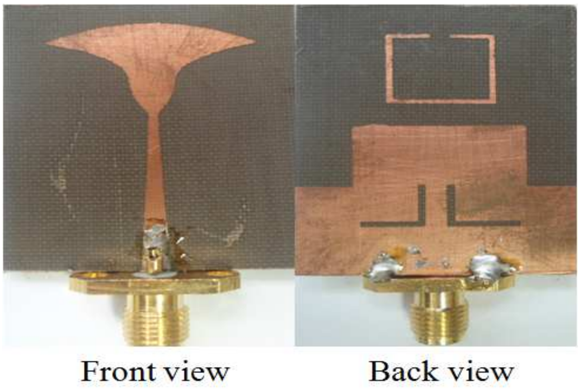

Figure 5.27: Photograph of the fabricated prototype band-notched SWB antenna using RT/Duroid substrate.

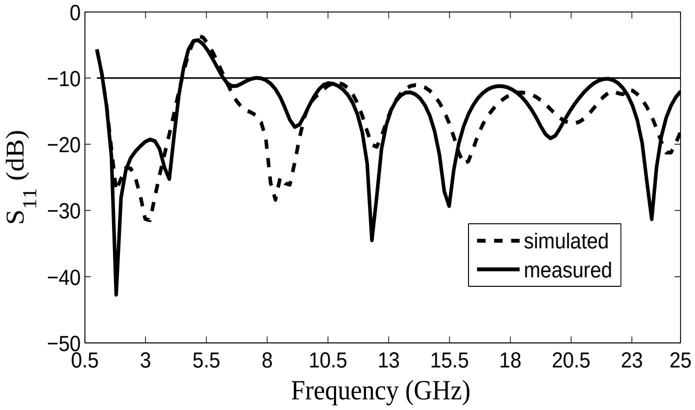

Figure 5.28: Measured and simulated return loss vs frequency for the proposed band-notched SWB monopole antenna.

5.3.2 Study of band-notched function design

Fig. 5.22 (b) and 5.22 (c) shows that the band-suppression characteristic over the whole interference band is realized by the C-shaped parasitic element in the back plane, which is electromagnetically coupled to the main patch. The C-shaped parasitic element acts as a half-wave resonant structure and can perturbs the current distribution at certain frequency band (4.7−6 GHz), where the band-notched characteristics of the antenna are expected. Further increasing the strong rejection at the band-notch region (4.7−6 GHz) two L-slots are etched with chamfered ground structure (CGS). Band-notch characteristics can be achieved by tuning the parameters W_d, l_d, T and l_s. A dimension of the C-shaped parasitic elements is selected according to the following expression

$$V \cong .5\lambda_g = W_d + 2l_d + 4\mathrm{T} + 2l_s \tag{5.2}$$

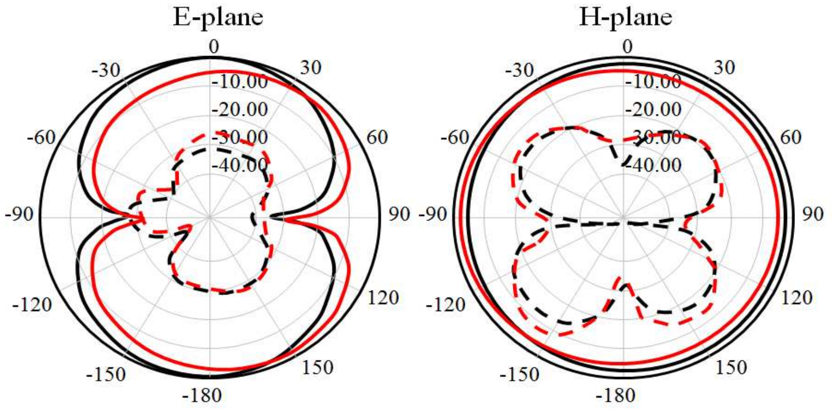

Figure 5.29: Simulated (red lines) and measured (black lines) radiation pattern for the proposed SWB monopole antenna at 3.1 GHz. Solid line is co-polarization and dashed line is cross-polarization.

where V is the physical length of a C-shaped parasitic element and λ_g is the corresponding band-notch frequency (5.35 GHz). W_d, l_d and T is the width, length and thickness of C-shaped parasitic element. Fig. 5.25 demonstrates the simulated surface current distribution for the proposed monopole antenna at band-notched center frequency of 5.35 GHz. It can be seen that current flows on the C-shape parasitic element are more egregious around notch frequency and they are opposite in direction (out-of-phase) to the current flow on the main patch, which can easily cancel out the radiation field and offered strong attenuation near the notch frequency and makes it as a non-responsive antenna performance at notch frequency 4.76 GHz. Fig. 5.26 exhibits the simulated return loss of various values of length l_d of the C-shaped parasitic element, and results for the values of l_d are varied from 8 to 10 mm. In this arrangement, center of the notched frequency varies from 5.35 GHz to 5.8 GHz as l_d changes from 9 mm to 8 mm and also its hamper the impedance matching, especially high frequency band. When position of the length l_d = 10 mm, band-notch characteristics is less sensitive, while within the SWB region impedance matching disturbs slightly. So the optimum value of l_d is 9 mm.

5.3.3 Simulation and experimental results

The photograph of the fabricated antenna is shown in Fig. 5.27. It is simulated with the 3-D electromagnetic simulation software HFSS and measured with vector network analyzer (Agilent ZVA24). Fig. 5.28 shows simulated and measured return loss of the proposed band-notch SWB antenna (using

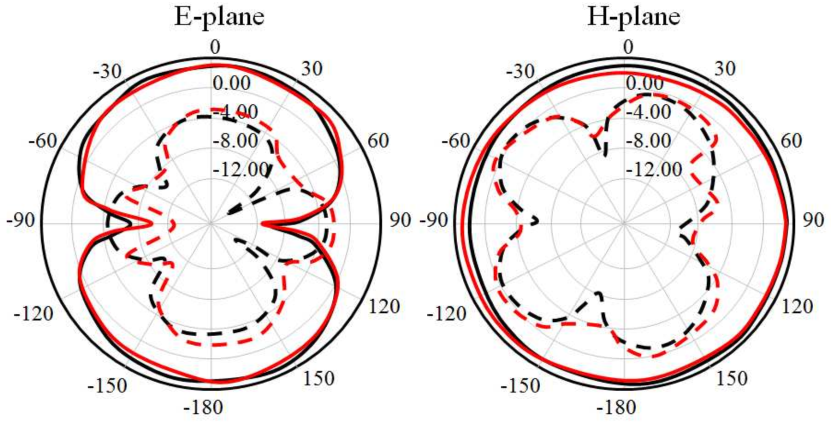

Figure 5.30: Simulated (red lines) and measured (black lines) radiation pattern for the proposed SWB monopole antenna at 10 GHz. Solid line is co-polarization and dashed line is cross-polarization.

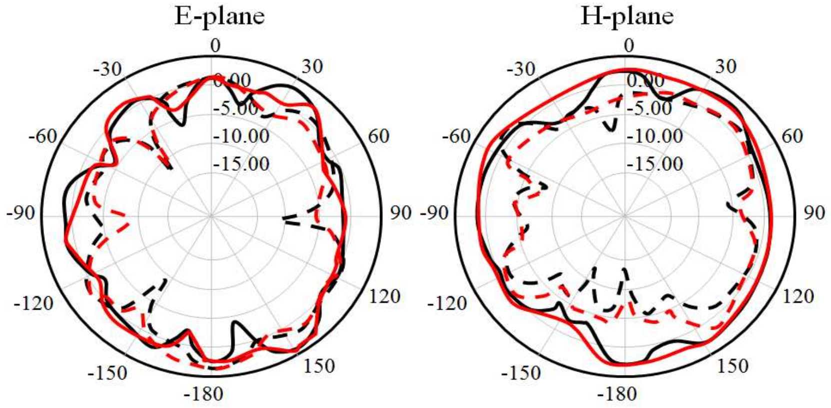

Figure 5.31: Simulated (red lines) and measured (black lines) radiation pattern for the proposed SWB monopole antenna at 20 GHz. Solid line is co-polarization and dashed line is cross-polarization.

RT/Duroid 5870 substrate). From the Fig. 5.28 it is observed that the antenna provides broadband performance (frequency band of 1 to over 25 GHz) with band-notch around 4.7−6 GHz. Fig. 5.29 to Fig. 5.31 displays far-field radiation patterns in the E-plane and H-plane at six different frequencies 3.1 GHz, 10 GHZ and 20 GHz. The proposed antenna has a nearly omni directional and low cross polarization level in the H-plane radiation pattern at frequencies 3.1 and 10GHz. Along with E-plane radiation pattern shows a typical bidirectional (figure-of-eight) at frequencies 3.1and 10 GHz. However, at frequency 20 GHz antenna generates multi-nulls in the E-plane and H-plane and also the cross polarization level increases with higher frequencies. Overall the proposed SWB monopole

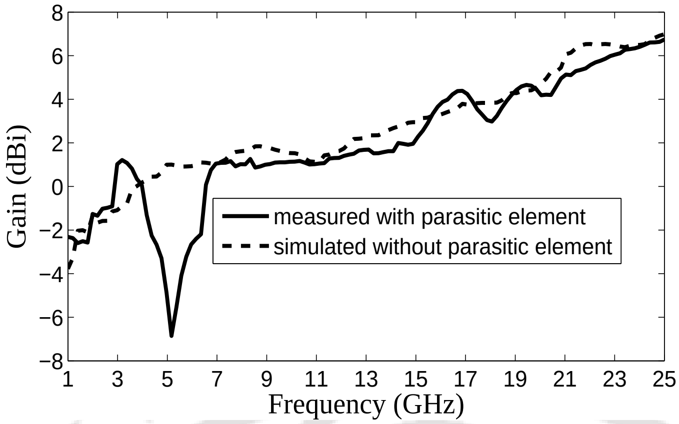

Figure 5.32: Measured and simulated gain for the proposed band-notch SWB monopole antenna.

antenna exhibits stable radiation patterns and behaves similarly to the typical planar monopole antennas. Fig. 5.32 presents the measured and simulated peak gain with and without parasitic element for the proposed band-notch SWB antenna (using RT/Duroid 5870 substrate). It is found that the measured antenna gain is about -2 dBi at 1 GHz and it increases with frequency (7 dBi at 25 GHz) except 4.7 to 6 GHz. Antenna gain decreases abruptly at the center frequency of 5.35 GHz, which shows appropriate band-notch elimination for WLAN application.

5.4 Summary

In this chapter, a band-notch super wideband monopole antennas have been proposed and extensively investigated. We have used triangular tapered feed line for broadband matching. In the tapered feed region and tapered radiating patch we have used Raicu's universal taper for best and optimal taper. Hence the signal coming to SWB antenna flows smoothly and radiates in free space. Thereby we can achieve super wideband impedance matching from 1.1−100 GHz (ratio bandwidth of 90.9:1), except in the band of 4.75−6 GHz. Two different band-notched SWB monopole antennas structure have been designed and fabricated with two different substrates, one with FR4 substrate (1.1−100) and another with RT/Duroid 5870 substrate (.9−100). With proper and simple U-shaped and C-shaped parasitic element integrated with ground plane, a band-notched performance from 4.75 to 6.0 GHz can be achieved. It has been observed that the RT/Duroid substrate is more versatile than FR4 substrate, especially when compared to return loss and gain of the both antennas. The average return loss and maximum gain of the monopole antenna with FR4 substrate is -11.5 dB and 5 dBi, however average return loss and maximum gain in case of antenna with RT/Duroid substrate is -14 dB and 6.5 dBi.

6

Design of compact dual band-notched printed monopole antenna for super-wideband (SWB) applications

Contents

6.1 Introduction

The evolution of ultrawideband (UWB) communication systems has received lot of attention due to its prominent advantages, such as high data transmission rates, large channel capacity, low power consumption, resistance to jamming, extremely low power spectral density etc. [123]. Over the past few years the research for UWB printed monopole has been continuing on full swing due to its large bandwidth, low profile, stable radiation patterns and high gain. The operating frequency region for ultra wideband (UWB) systems is between 3.1 to 10.6 GHz as approved by the FCC in 2002 [1]. It can be seen that bandwidth (BW) ratio of this UWB antenna is 3.4:1, which is obtained by dividing the highest frequency by the lowest frequency. However, it is to be noted that antenna with impedance bandwidth ratio greater than 10:1 is generally called super-wideband (SWB) antenna [2]. Due to extremely wide bandwidth, SWB antenna covers both long and short range communications. In recent years, numbers of printed monopole antennas have been reported for SWB applications [124–126]. For example an M-shaped notch at the bottom of the rectangular patch with a tapered coplanar waveguide (CPW) ground plane is proposed [124]. This antenna has bandwidth ratio of 21.9:1 for VSWR < 2. In [125], a compact elliptical monopole antenna with bandwidth ratio of 21.6:1 for VSWR < 2 was presented. K. R. Chen *et al.* [126] designed an egg-shaped super wideband monopole antenna with a bandwidth ratio greater than 12:1. Because of vast operating bandwidth it can interfere with the existing wireless communication system such as wireless local area network (WLAN) operating in 5.15-5.825 GHz) and X-band satellite communication systems operating in 7.25−8.3955 GHz (for down link: 7.25−7.745 GHz and uplink: 7.9 −8.395 GHz). To mitigate this interference issue, SWB antennas with a single and dual band-notched performance is required. Some UWB antennas with band-notched characteristic have been reported [127–130]. In [127], dual band-notched (i.e. WiMAX and WLAN bands) performance is achieved by placing L-shaped slit and E-shaped slot in the radiating patch. W. Jiang et al. [128] designed dual band-notched UWB antenna using a T-shaped stub on the radiating patch (WiMAX band) and a pair of U-shaped stubs near the feeding line (WLAN band). In [129], a triple band-notched antenna covering WiMAX, WLAN and X-bands is realized by open-ended quarter-wavelength slot and three semicircular half-wavelength slots are cut in the radiating patch. In [130], a U-slot defected ground structure (DGS) is used notching 5-6 GHz for WLAN and an H-shaped slot is etched on the radiating patch to obtain another two notched bands at 3.3-3.7 GHz for WiMAX and 7.2 GHz for some C-band satellite communication systems. All these antennas have been designed to have notch within UWB band. In this thesis, a dual band-notched printed arched monopole antenna is proposed for super wideband applications with bandwidth ratio of 16.1:1 for VSWR < 2. To increase the impedance bandwidth a triangular tapered feed line is employed with arched radiating patch and arched ground plane. By adding an open-circuited stub in the triangular tapered feed line single band-notch (5−6 GHz) performance is created. Second band-notch (7−8.4 GHz) performance can be created by cutting inverted U-shaped slot in the arched

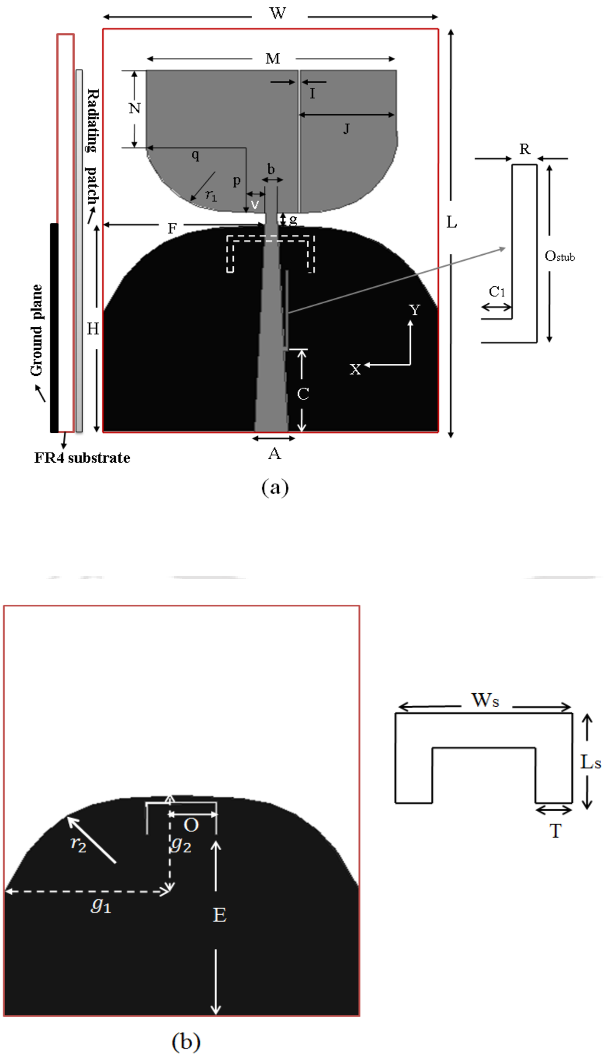

(a)

(b)

Figure 6.1: Geometry of the proposed super wideband band-notched monopole antenna (a) front view (b) bottom view.

ground plane and small strip etched on the radiating patch. The proposed antenna has a simple configuration and is easy to fabricate. The proposed antenna has been designed and simulated using of High Frequency Simulation Software (HFSS) version 14. Details of simulation and experimental results of the proposed antenna are presented.

Table 6.1: Optimized dimension of the proposed antenna

Parameters	L	W	M	N	I	v	g	E	0	H	W_s	F	L_s
Units (mm)	40	30	22	8	0.2	1	1.4	17.8	3.5	22.6	6	14.5	3.2
Parameters	R	T	0_{stub}	C_1	b	p	q	r_1	r_2	g_1	g_1	C	A
Units (mm)	0.2	0.2	8.4	0.5	1	7	9.5	8.3	12.7	14.5	9.6	8.6	3

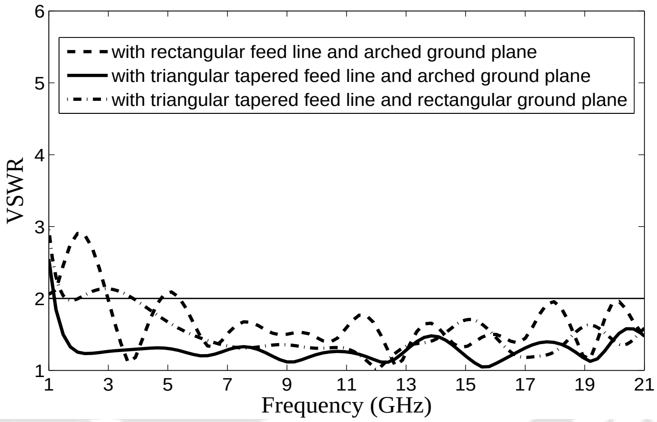

Figure 6.2: Full band VSWR curve vs frequency for different feed line and ground plane.

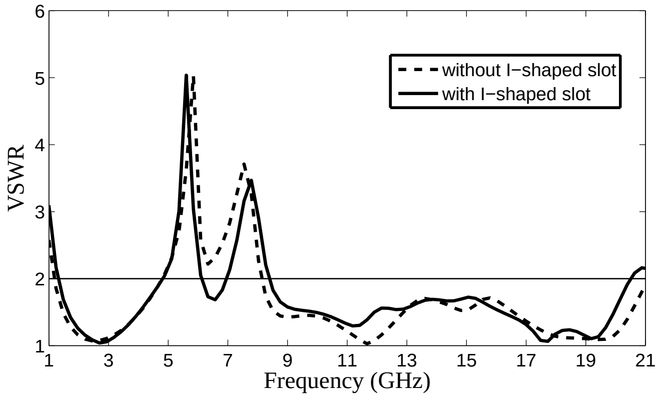

Figure 6.3: Simulated VSWR curve vs frequency for with and without I-shaped slot.

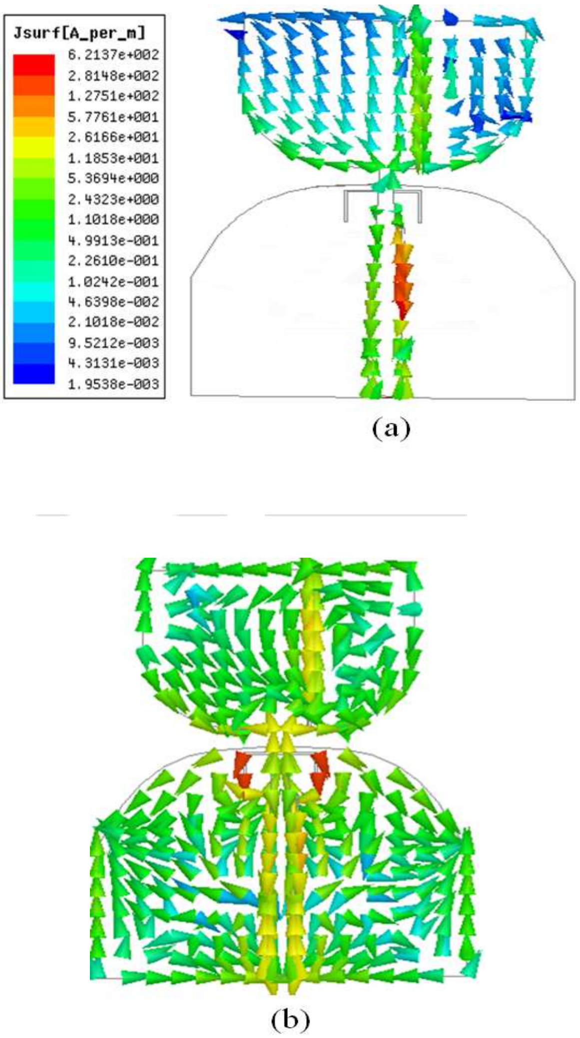

Figure 6.4: Simulated current distribution of the proposed dual band-notched SWB antenna at frequencies (a) 5.5 GHz (b) 7.7 GHz.

6.2 Dual band-notched SWB antenna using FR4 substrate

The proposed SWB band-notch monopole antenna is shown in Fig. 6.1. The proposed antenna composed of a triangular tapered feed line, an arched monopole patch etched with an I-shaped slot, an open circuited stub and an inverted U-shaped slot etched on the arched ground plane. The antenna is fabricated on FR4 substrate with dielectric constant of 4.4, loss tangent of .0018 and thickness of 1.6 mm. The overall size of the proposed antenna is about 30×30×1.6 mm^3. In the presented configuration, a triangular tapered feed line is precisely connected to arched shape patch, which provides extremely large impedance bandwidth greater than ultrawideband (UWB) bandwidth. Arched ground

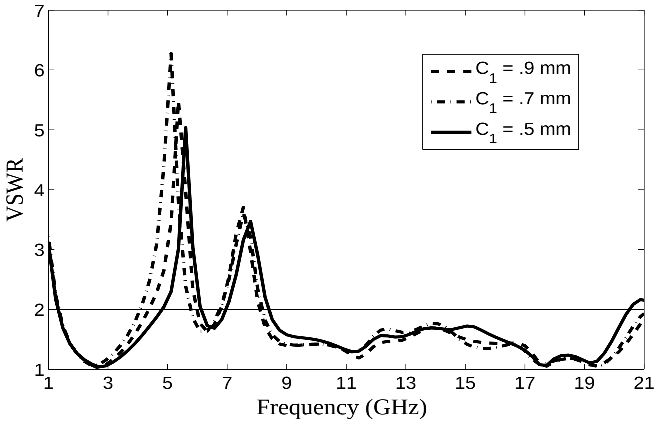

Figure 6.5: Simulated VSWR behavior with respect to frequency for different values of C_1.

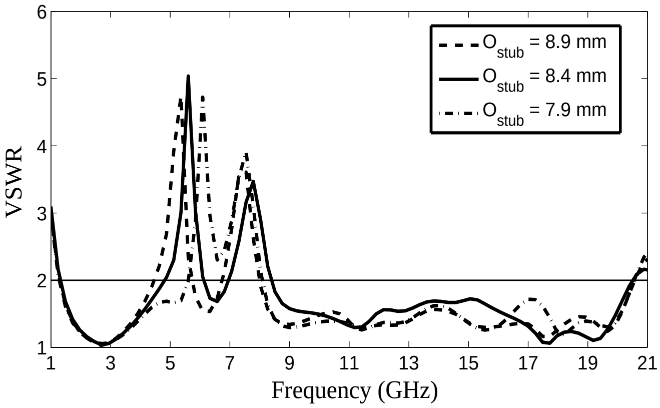

Figure 6.6: Simulated VSWR vs frequency curves with different values of O_{stub}.

plane also play an important role for improving the impedance bandwidth, because antenna can adjust the electromagnetic coupling effects between the patch and the arched ground plane and hence impedance bandwidth is considerably enhanced. The dual notch performance in the proposed antenna can be easily realized by introducing an open-circuited stub on the right side of the triangular tapered feed line and an inverted U-shaped slot in the arched ground plane. Suitable resonant frequency band-notch (i.e. 5.5 GHz) performance can be achieved by adjusting the length of open-circuited stub. In addition by adjusting the parameter W_S, L_S and T of an inverted U-shaped slot another band-notch (i.e. 7.7 GHz center frequency) performance can be created.

6.2.1 Results and discussions

6.2.1.1 SWB monopole antenna with full-band

In this section, parameter of the proposed antenna was optimized in such a way that antenna gives an extremely wide bandwidth with two reasonable band-notch performance. The proposed antenna

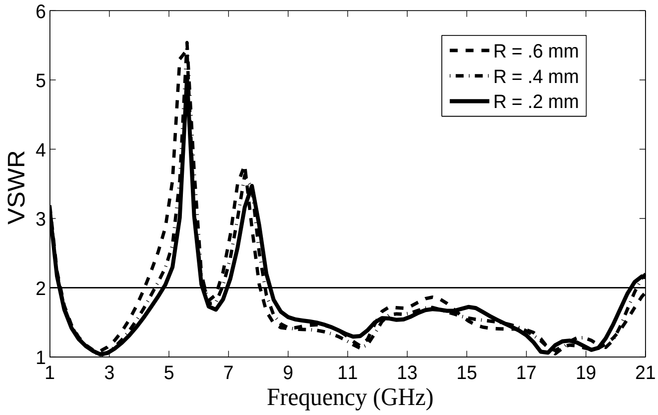

Figure 6.7: Simulated VSWR vs frequency curves with different values of R of the open circuited-stub.

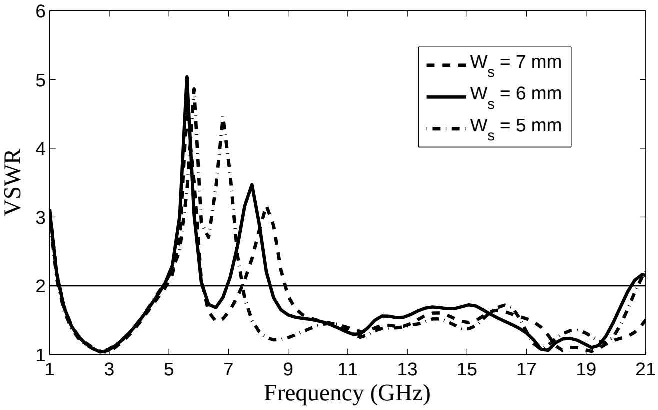

Figure 6.8: Simulated VSWR vs frequency curves with different values of W_s.

has been designed and simulated using High Frequency Simulation Software (HFSS) version 14. The optimized dimensions of the proposed antenna are given in Table 6.1. Fig. 6.2 shows that full band VSWR curve for different feed line and ground plane for the proposed SWB antenna. Here we can see that antenna starts resonating from 1.3 GHz. It can be observed that by applying rectangular feed line with arched ground plane instead of triangular tapered feed line with an arched ground plane, there is impedance mismatch at frequencies 2 GHz and 5 GHz. When triangular tapered feed line with rectangular ground plane was applied, it can be observed that wide impedance bandwidth can be obtained at higher frequencies but the bandwidth is slightly affected between the frequency band of 2−4 GHz. Hence triangular tapered feedline with arched ground plane gives the best impedance matching.

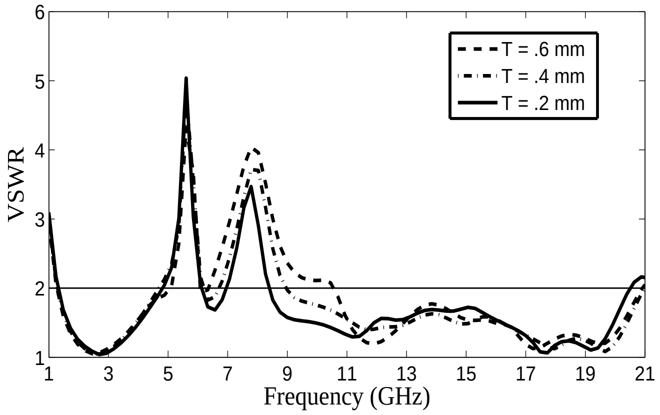

Figure 6.9: Simulated VSWR vs frequency curves with different values of T.

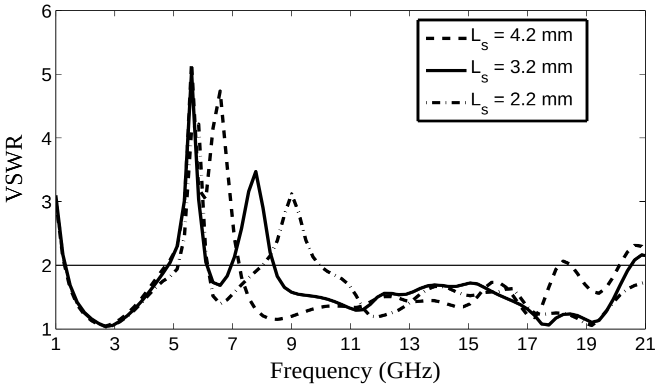

Figure 6.10: Simulated VSWR vs frequency curves with different values of L_s.

6.2.1.2 SWB monopole antenna with dual band-notches

By adding an open-circuited stub on the right side of triangular tapered feed line, a single band-notch (5−6 GHz /WLAN band) characteristic is achieved. The open-circuited stub acts as an one quarter-wave resonant structure and can perturbs the current distribution at certain frequency band (5−6 GHz), where the band-notched performance of the proposed antenna is expected. Here the optimized electrical length G of an open-circuited stub is set to approximately $0.25\lambda_g$. Dimension of the open-circuited stub is selected according to the following formula

$$\mathrm{G} \simeq .25\lambda_g \simeq O_{stub} + {}^{R}\!/_{2} + C_1 \tag{6.1}$$

The guided wavelength ($\lambda_g = {}^{\lambda_0}\!/\!\sqrt{\varepsilon_{eff}}$) is the corresponding band-notch frequency at 5.5 GHz and is equal to 33.19 mm. To create a second band-notch (7−8.4 GHz / for down link: 7.25−7.745 GHz

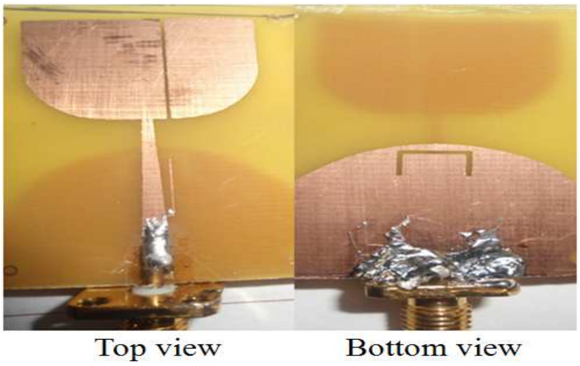

Figure 6.11: Photograph of the proposed dual band-notched SWB antenna.

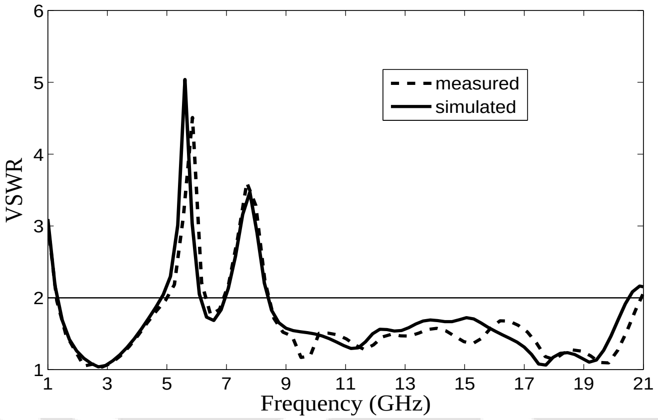

Figure 6.12: Measured and simulated VSWR vs frequency curve of the proposed antenna.

and uplink: 7.9−8.395 GHz of X-band satellite communication systems) performance, an inverted U-shaped slot is etched on the arched ground plane. An inverted U-shaped slot acts as one half wavelength resonant structure and can perturb the current distribution at frequency band (7−8.2 GHz). An inverted U-shaped slot dimension is selected according to the following formula

$$\mathrm{G}_1 \simeq .5\lambda_g \simeq W_s + 2L_s - 2T \tag{6.2}$$

In similar way, here λ_g was found to be 23.7 mm at 7.7 GHz. Further improve the notching performance, an I-shaped slot is etched on the arched radiating patch as shown in fig. 6.3. Fig. 6.3 shows that simulated VSWR curve for with and without I-shaped slot and it is to be noted that, by placing an I-shape slot on the radiating patch, enhanced resonance was observed between the frequency from 6−7 GHz.

For further investigation of these notch frequencies, the simulated current distribution of the pro-

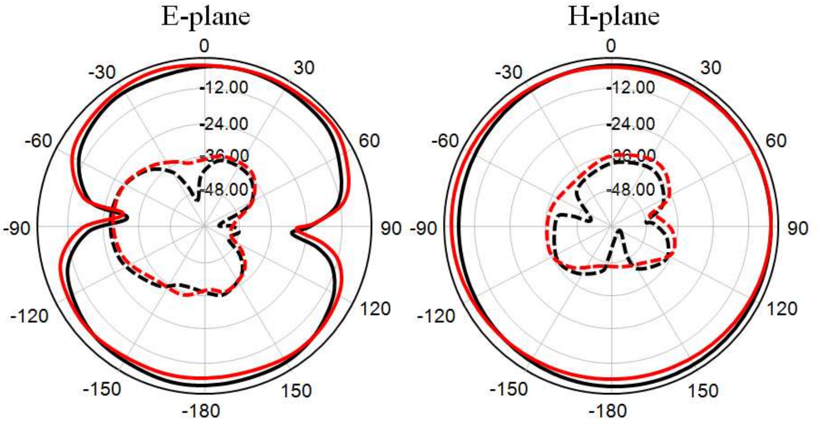

Figure 6.13: Simulated (red lines) and measured (black lines) radiation pattern for the proposed dual band-notched SWB monopole antenna at 3.1 GHz. Solid line is co-polarization and dashed line is cross-polarization.

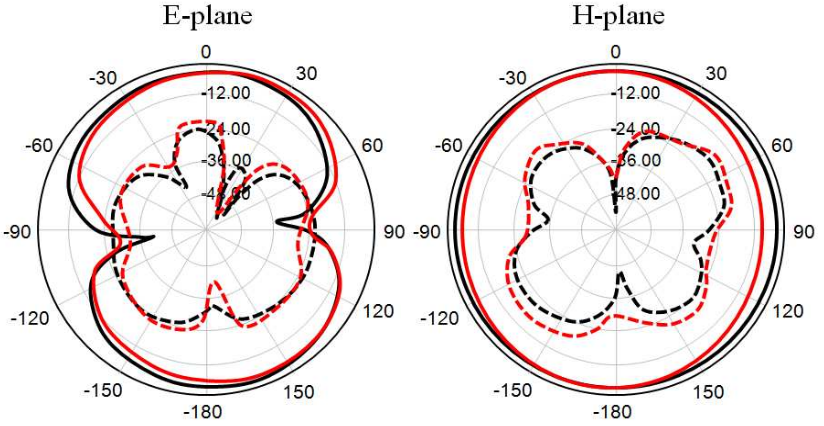

Figure 6.14: Simulated (red lines) and measured (black lines) radiation pattern for the proposed dual band-notched SWB monopole antenna at 6.5 GHz. Solid line is co-polarization and dashed line is cross-polarization.

posed dual band-notch SWB antenna at frequencies 5.5 GHz and 7.7 GHz are shown in Fig. 6.4 (a) and 6.4 (b). It can be observed in Fig. 6.4 (a) and 6.4 (b) that the majority of current is concentrated on an open circuited-stub at 5.5 GHz and an inverted U-shaped slot at 7.7 GHz, while minimum current is concentrated on the rest part of the antenna at frequencies 5.5 and 7.7 GHz. It implies that at notch frequencies antenna creates strong resonance. And also it can be seen that considerable amount of current flowing in I-shaped slot as shown in Fig. 6.4 (b), which plays a role to excite enhanced resonance between the frequency range of 6−7 GHz.

To fully comprehend, the parametric study of the proposed antenna is carried out for further

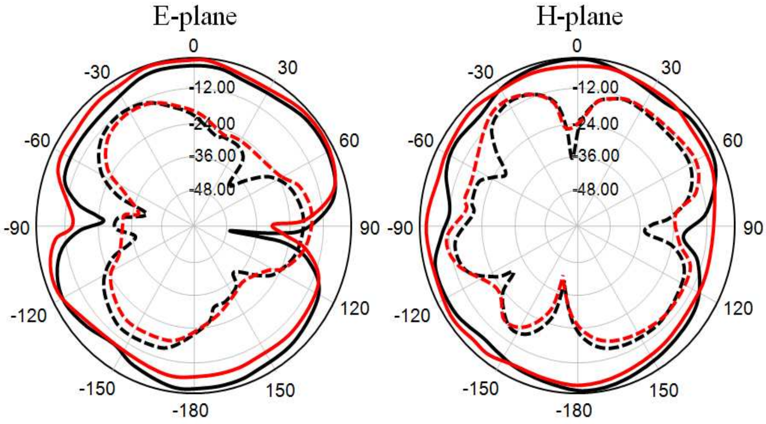

Figure 6.15: Simulated (red lines) and measured (black lines) radiation pattern for the proposed dual band-notched SWB monopole antenna at 10 GHz. Solid line is co-polarization and dashed line is cross-polarization.

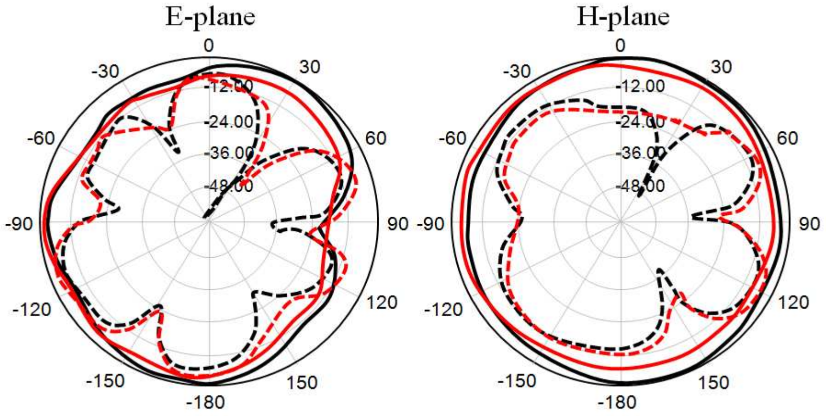

Figure 6.16: Simulated (red lines) and measured (black lines) radiation pattern for the proposed dual band-notched SWB monopole antenna at 15 GHz. Solid line is co-polarization and dashed line is cross-polarization.

analysis. By properly changing the parameters of the proposed monopole antenna, dual notched band can be generated. The dual notch performances are decided by the following parameters C_1, O_{stub}, R, W_s, T and L_s. The first notched band is basically determined by the parameters of C_1, O_{stub} and R. Fig. 6.5 depicts the simulated VSWR behavior with respect to frequency for different values of C_1. From the simulation results of VSWR, it can be observed that as C_1 increases from 0.5 mm to 0.9 mm with other parameters constant, the centre frequency of the first notch shifted towards left, while centre frequency of the second band-notch is slightly affected. So the optimized value of C_1 is taken as to be 0.5 mm. Fig. 6.6 plots the simulated VSWR curves with different values of O_{stub}. As clearly

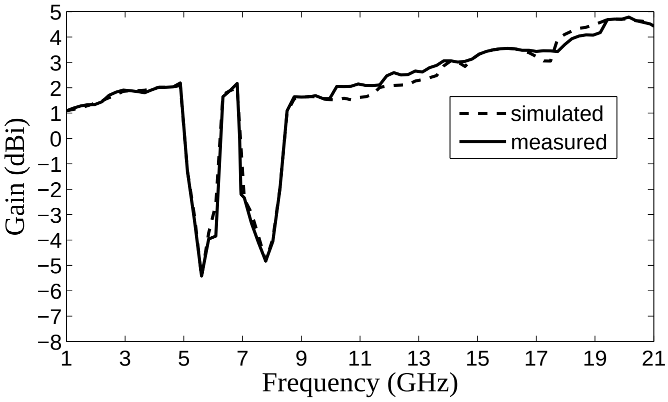

Figure 6.17: Measured and simulated gain vs frequency of the proposed antenna.

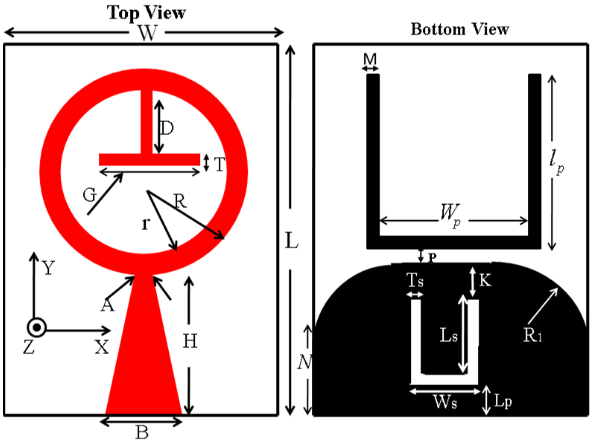

Figure 6.18: Geometry of the proposed band-notched monopole antenna.

shown in Fig. 6 when the length (O_{stub}) of the open circuited stub increases from 8.4 to 8.9 mm, the centre frequency of the first notch band is varied from 5.5 GHz to 5.28 GHz. However, as the value of O_{stub} decreases from 8.4 to 7.9 mm, the centre frequency of the first notch band is much varied. As it is seen in Fig. 6.7, when the thickness R of the open circuited stub increased from 0.2 to 0.6 mm, the lower frequency of first notch band decreases from 5 GHz to 4 GHz.

In similar way, the parameters W_s, T and L_s of an inverted U-shaped slot are also varied to see the influences on the second notched band performance. Fig. 6.8 illustrates the simulated VSWR curves for different values of W_s. As the value of W_s increases from 6 to 7 mm, the center frequency of the second band notched is varied from 7.7 to 8.6 GHz, while center frequency of the first band notched is fixed. However, decreasing the value of W_s from 6 to 5 mm, the center frequency of the second band notched shifted from 7.7 GHz to 6.8 GHz and also impedance matching becomes worse between the frequency ranges of 6−7 GHz. Similarly we can control the second band notched frequency by changing the other parameters of T and L_s as shown in Fig. 6.9 and 6.10. The photograph of the fabricated SWB dual band-notch monopole antenna is shown in Fig. 6.11. The proposed antenna was successfully measured by Rohde and Schwarz ZVA24 network analyzer. Fig. 6.12 shows measured and simulated VSWR curve of the proposed antenna. Fig. 6.13 to Fig. 6.16 shows simulated and measured radiation pattern E-plane and H-plane of the proposed SWB antenna at (a) 3.1 GHz (b) 6.5 GHz (c) 10 GHz (d) 15 GHz. It can be observed that the pattern is almost omnidirectional throughout UWB frequency band, while more cross polar component has been observed at frequency 15 GHz. Fig. 6.17 shows simulated and measured peak gain in dBi for the SWB dual band-notched antenna. It can be observed that the gain variation of the proposed antenna within SWB frequency band is from 1.4 to 4.8 dBi, except the two notch bands.

6.3 Compact dual band-notched SWB antenna using RT/Duroid 5870 substrate

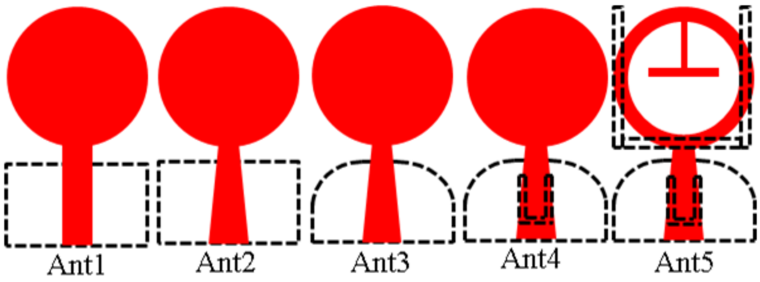

Figure 6.19: Design evolution of the proposed SWB dual band-notched antenna.

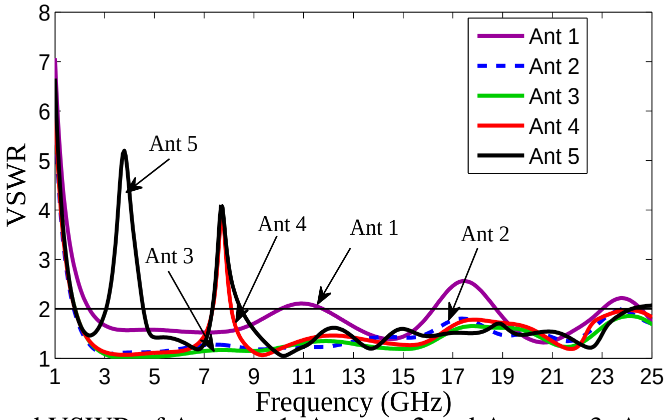

Figure 6.20: Simulated VSWR of Antenna 1, Antenna 2 and Antenna 3, Antenna 4 and Antenna 5.

The configuration of the proposed SWB circular ring monopole antenna with dual band-notched

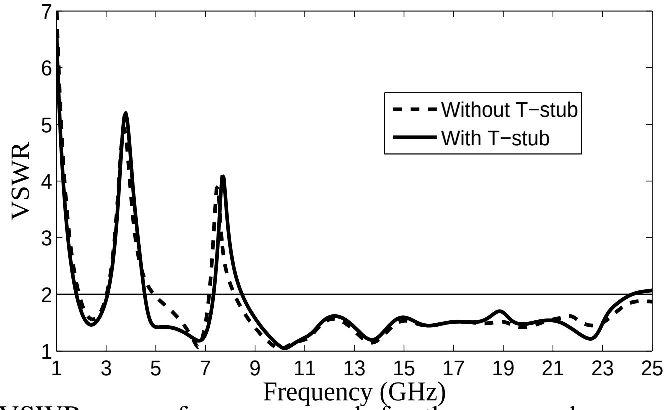

Figure 6.21: Simulated VSWR versus frequency graph for the proposed compact SWB dual band-notched antenna with and without inverted T-shaped stub.

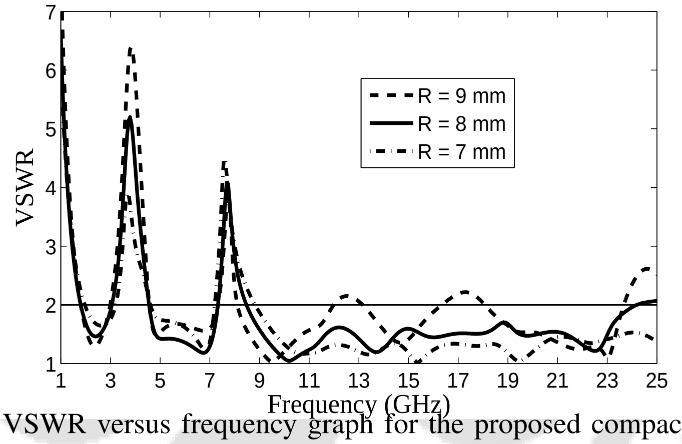

Figure 6.22: Simulated VSWR versus frequency graph for the proposed compact SWB dual band-notched antenna with different value of R.

characteristics is illustrated in Fig. 6.18. The designed circular ring patch antenna is printed on the RT/Duroid 5870 substrate of thickness 0.787 mm and dielectric constant 2.32, which is excited by a 50 Ω triangular tapered microstrip feed line. The proposed antenna (overall dimension of about 24×30×0.787 mm^3) consists of a circular ring radiating patch with T-shaped stub that are protruded inside radiating ring. The rear side of the RT/Duroid substrate composed of a round-corner finite ground plane (RCFGP) with embedded U-shaped slot and a U-shaped parasitic element, which is placed under the circular ring patch. The microstrip feed line has been tapered near the circular ring antenna feeding point in order to improve the impedance matching at higher frequencies. Because of tapering involves gradual changes in impedance function (i.e., a multi-section transformer), it increases the bandwidth of the impedance transformer and antenna load impedance becomes closer to characteristic impedance of the microstrip feed line. RCFGP is also responsible for impedance

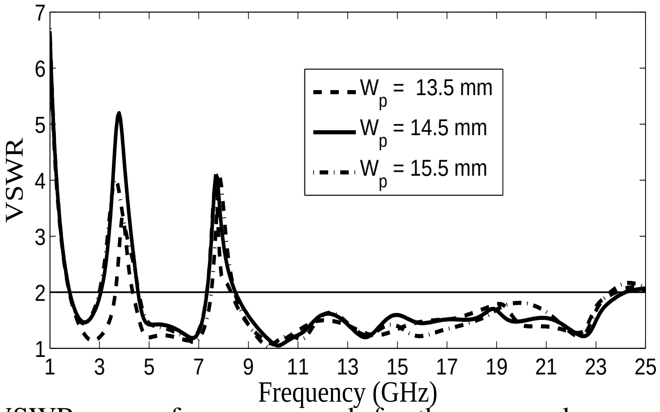

Figure 6.23: Simulated VSWR versus frequency graph for the proposed compact SWB dual band-notched antenna with different value of W_p.

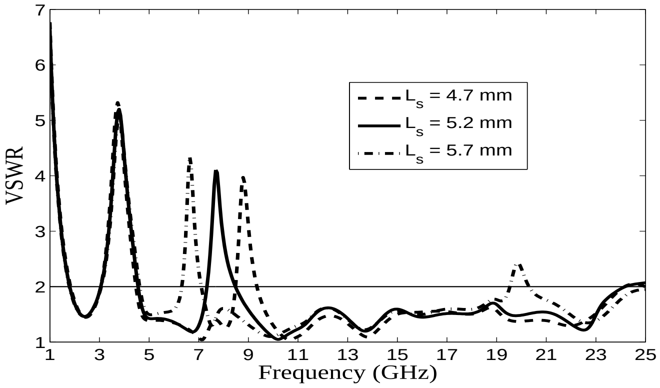

Figure 6.24: Simulated VSWR versus frequency graph for the proposed compact SWB dual band-notched antenna with different value of L_s.

matching, especially at higher frequencies because it provide smooth current path and hence improve the impedance bandwidth between the frequency band of 23.5−24 GHz. The optimal dimensions of the proposed antennas are as follows: $L = 30$ mm, $W = 24$ mm, $H = 13$ mm, $A = 1$ mm, $B = 1$ mm, $G = 5.5$ mm, $D = 4.5$ mm, $T = 0.5$ mm, $R = 8$ mm, $r = 6$ mm, $N = 6.2$ mm, $W_p = 14.5$ mm, $l_p = 16.5$ mm, $M = 0.5$ mm, $p = 1$ mm, $T_s = 0.2$ mm, $L_s = 5.2$ mm, $W_s = 1.5$ mm, $L_p = 4.5$ mm, $K = 1.6$ mm and $R_1 = 4.9$ mm. Here the optimized electrical length of U-shaped parasitic element U_1 and U-shaped slot U_2 are set to approximately $0.5\lambda_g$ and $0.25\lambda_g$, where $U_1 = W_p + 2l_p + 2M$, $U_2 = W_s + 2L_s + 2T_s$ and λ_g is the guided wavelength corresponding to band notch frequencies at 3.8 and 7.8 GHz. Fig. 6.19 presents design evolution of the proposed SWB dual band-notched printed monopole antenna and illustrates the steps for enhancing the impedance bandwidth as well as formation of dual band-notched characteristics. The corresponding simulated VSWR characteristics comparison of Antenna

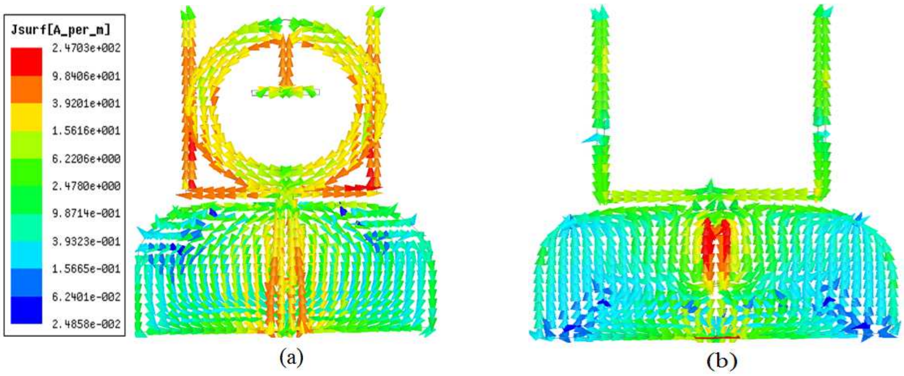

Figure 6.25: Simulated surface current distributions at frequencies (a) 3.8 and (b) 7.8 GHz.

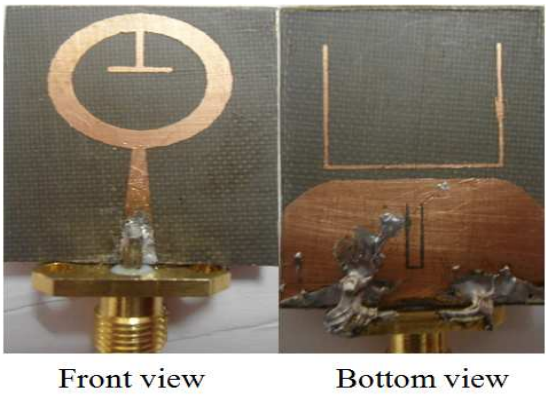

Figure 6.26: Image of the fabricated proposed SWB dual band-notched antenna.

1, Antenna 2 and Antenna 3, Antenna 4 and Antenna 5 are shown in Fig. 6.20. As shown in Fig. 6.19 Antenna 1 consists of simple monopole disc connected with a rectangular feed line and rectangular finite ground plane that provides bandwidth with frequency band of 2.8−9.9 GHz as depicted in Fig. 6.20. To improve the impedance bandwidth of the Antenna 1, rectangular feed line has been replaced by a triangular tapered feed line (Antenna 2) and offers wide bandwidth of 1.6−23.5 GHz without increasing the dimensions of Antenna 1 as depicted in Fig. 6.20. To further increase the bandwidth of the Antenna 2, we modified the rectangular ground plane of the Antenna 2 into round-cornered ground plane (Antenna 3). It is worth nothing that, the Antenna 3 excites additional resonance especially at the higher frequencies and hence the impedance matching characteristics tend to improve over the entire band, resulting in an extremely large bandwidth of 1.6−25 GHz (shown by Fig. 6.20) or above. It is capable of supporting super wideband (SWB) radios without increasing the dimensions of Antenna 2. Now to generate the first band-stop characteristics for X-band satellite communication

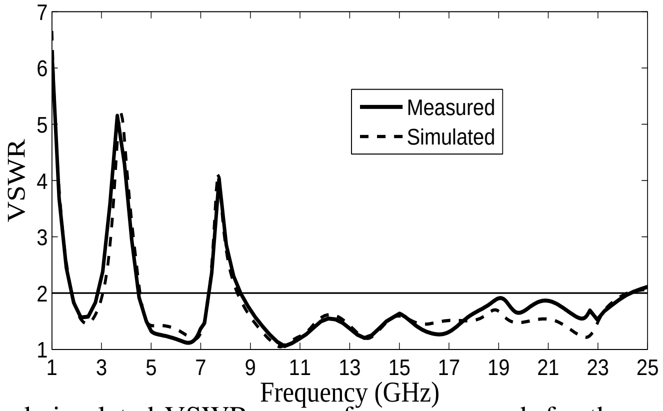

Figure 6.27: Measured and simulated VSWR versus frequency graph for the proposed compact SWB dual band-notched antenna.

systems (7.2−8.4 GHz), a U-shaped slot is inserted in the RCFGP (Antenna 4). By employing U-shaped parasitic element on the rear side of the substrate and an inverted T-shaped stub within the ring shaped radiation patch we can generate the second band-stop characteristics for WiMAX/C-band (3.2−4.4 GHz) application as illustrated in Fig. 6.20 (Antenna 5). The effect of inverted T-shaped stub on the WiMAX/C-band (3.2−4.4 GHz) X-band satellite communication systems (7.2−8.4 GHz) is shown in Fig. 6.21. From the Fig. 6.21 it is found that without inverted T-shaped stub, the upper edge frequency of WiMAX/C-band increases from 4.4 GHz to 4.9 GHz, while upper edge frequency of the X-band satellite communication systems decreases from 8.4 to 8.1 GHz, which do not cover the uplink frequency (7.9−8.395 GHz) of X-band satellite communication systems. The wide frequency bandwidth of WiMAX/ C band notched characteristics (3.2−4.9 GHz) unnecessarily blocks useful frequencies from 4.4 to 4.9 GHz.

Table 6.2: Comparison of the size and bandwidth of the proposed circular ring monopole antenna to traditional antennas

Antenna Structures	Dimensions (W×L×h)	Ratio BW
Quasi-CSRR shaped [50]	46.4×38.5×1 mm^3	6.2:5
Square-shaped [51]	26×32×0.8 mm^3	3.9:2
Circular ring-shaped [52]	30×30×1.6 mm^3	5.0:3
Fork-shape [53]	24×36×1.524 mm^3	4.0:1
Proposed ring-shaped	24×30×0.787 mm^3	15.6:2

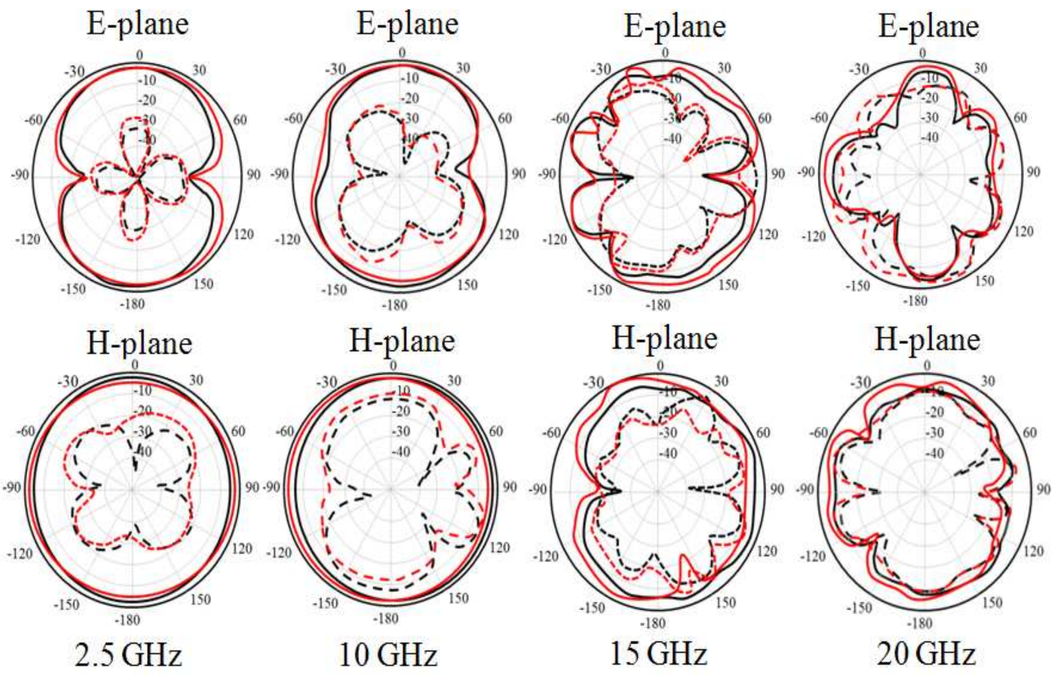

Figure 6.28: Simulated (red lines) and measured (black lines) radiation pattern proposed compact SWB dual band-notched antenna. Solid line is co-polarization and dashed line is cross-polarization.

6.3.1 Parametric study and experimental Results

To know more details about dual-notch functionality of the proposed SWB antenna, parametric study has been carried out. Dual band-notched characteristics of the SWB antenna can be controlled mainly by the following parameters: R, W_p and L_s for the radiating ring patch, U-shaped parasitic element and U-shaped slot respectively. Fig. 6.22 depicts the simulated VSWR curves for different values of outer radius R of circular ring patch. It can be observed that by increasing the value of R from 8 to 9 mm, the first notch band blocks deeper (amplitude of VSWR is about 6.5) within WiMAX/C-band, however center frequency of the second notch band (X-band) is shifted from 7.8 to 7.4 GHz and also there is an impedance mismatch at higher frequencies (12−13 GHz and 16.5−18 GHz). When the value of R = 7 mm, the impedance matching within SWB region is excellent, the center frequency of the first (WiMAX/C-band) and second (X-band) notched band is also appropriate. So the optimum value of R is 7 mm. The simulated VSWR for different values of W_p (width U-shaped parasitic element) is plotted in Fig. 6.23. In this arrangement by varying the value of W_p from 18.1

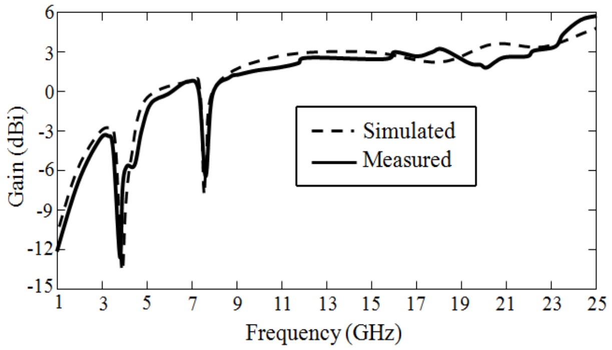

Figure 6.29: Simulated and measured gain versus frequency graph for the proposed compact SWB dual band-notched antenna.

to 20.1 mm, center frequency of the second (X-band) notched band characteristics is in sensitive; however bandwidth of the first notch band (WiMAX/C-band) is decreased significantly. Therefore, the optimum value of W_p is decided to be 19.1 mm. Fig. 6.24 shows the effect of the length L_s of U-shaped slot on the simulated VSWR curves. From the Fig. 6.24 it can be found that, when length L_s of U-shaped slot changes from 4.7 to 5.7 mm, the center frequency of the second notched band is varied from 9 GHz to 6.5 GHz, however there is no variation within the first notched band region. Therefore the value of L_s has been selected to be 5.2 mm, which controls the variable notched band with center frequency of 3.8 GHz. Fig. 6.25 (a) and (b) illustrates the simulated surface current distribution for the proposed SWB monopole antenna at band-notch center frequencies of 3.8 and 7.8 GHz. From the Fig. 6.25 (a) it is clearly seen that high current is gathered on the U-shaped parasitic element around the 3.8 GHz notched frequency and they are opposite in direction (out-of-phase) to the current flowing on the ring shaped patch as well as inverted T shaped stub, which cancel out the effective radiation. Hence, at 3.8 GHz impedance matching was very poor due to band-notch characteristics. Similarly, at frequency 7.8 GHz it can be observed that strong current is crowded on U-shaped slot and very small current concentrated on the ground plane and offered strong attenuation near the notch frequency (7.8 GHz) than the other resonance frequency. Image of the fabricated antenna is shown in Fig. 6.26. The measurement result is carried out with a Rohde and Schwarz ZVA24 vector network analyzer. Simulated and measured VSWR versus frequency graph for the proposed SWB dual band-notched antenna is depicted in Fig. 6.27. Good agreement has been obtained between simulation and experimental of VSWR results. Fig. 6.28 shows the simulated and measured radiation pattern of the proposed SWB monopole antenna. It indicates that at low frequencies (2.5 and 10 GHz), antenna has a nearly omni-directional radiation pattern in the H-plane and bidirectional (eight shaped) patterns in the E-plane with negligible cross polarization. However at the higher frequencies 15 and 20 GHz, the cross-polarization level rises in the E and H-planes, which is probably due to almost horizontal surface current component flow on the radiating patch at higher frequencies. The simulated and measured gain versus frequency graph for the proposed dual band-notch SWB monopole antenna is shown in Fig. 6.29. From the graph, it can be observed that the peak gain of the proposed antenna is 5.8 dBi, while gain sharply drops in the vicinity of 3.8 and 7.8 GHz stop bands.

6.4 Summary

This chapter provides a super-wideband antenna along with dual band notched functionality. To avoid the interference problem from the existing narrow band system, it is necessary for SWB antennas to have dual band-notched characteristics. Here also like previous chapter two different antenna structures have been realized using two different substrates, one with FR4 substrate and another with RT/Duroid 5870 substrate. All simulated and measured results of the both antennas are well matched.

7

Conclusions and future work

Contents

7.1 Summary of the present work

UWB antennas are highly desirable for short range communication system with high data transmission. But the current users of WPAN are also hungry to increase more and more bandwidth and demanding like a SWB antenna to cover both short range and long-range communication system. Due to extremely large bandwidth (ratio bandwidth of more than 10:1) which is a requirement for very high data rate SWB antenna has come into the picture. Therefore, the main objective of the thesis is to design, fabricate and test of compact printed monopole antenna for SWB applications. It has been found that printed monopole antennas as superior from the existing planar monopole antennas in terms of size compactness, suitable for integration with MMIC, effective radiation characteristics and appropriate gain profile. Single and dual band-notch printed monopole antennas with compact size and large bandwidth have been designed, fabricated and tested successfully for SWB application.

A triangular printed monopole antenna has been designed for UWB applications, which stems from an original printed triangular monopole by introducing a round-corner partial ground plane and a microstrip transition (single section transformer) between the microstrip feed line and the printed triangular patch that provides a wide impedance bandwidth from 1.8 GHz to 15 GHz. Parametric studies show that the length of the microstrip transition significantly improve performance of the printed triangular monopole antenna. It has been also observed that by changing the shape of the partially etched rectangular ground plane to round-cornered ground plane the impedance bandwidth can be improved without increasing the size of the proposed antenna. The proposed UWB triangular printed monopole antenna has approximately omnidirectional radiation patterns within the entire frequency band and small size compared to conventional antenna. In the frequency domain, the simulated and measured return losses of the antenna agrees well. In addition a time domain characteristics of the proposed antenna has been also carried out successfully

The design aspects of SWB printed monopole antenna has illustrated briefly. A triangular tapering and Raicus optimal taper have been employed to enhance the bandwidth. Length and width of the feed line and feed region of the proposed SWB antenna have been calculated theoretically. Although, lower frequency end of the proposed trapezoidal patch antenna have been calculated theoretically. Each part of the antenna has been optimized in such a way that it gives best performance over the entire frequency band. The proposed SWB antenna was designed, simulated, fabricated and experimental results are obtained using Rohde and Schwarz ZVA24 network analyzer. Stable radiation pattern and constant gain in the SWB frequency regions are obtained.

A full band SWB printed monopole antenna has been successfully designed, optimized, fabricated and tested. A triangular tapered feed line is used for feeding the exponentially tapered feed region and patch of the proposed antenna. It has been found experimentally that the antenna is well matched for a very broad frequency range from 2.5−80 GHz. Due to large bandwidth, this SWB printed monopole antenna may be used for spectrum sensing in cognitive radio. The designed antenna has constant group delay and acceptable gain characteristics within the operating frequency band. Time domain characteristics of the proposed antenna have been measured and validated that the proposed antenna is suitable candidate for UWB/SWB applications. In the time domain, it has been observed that the overall ringing is better than the existing UWB antennas in the literature.

A single band-notched SWB printed monopole antenna has been designed, optimized, fabricated and tested. The designed single band-notched SWB antenna is evolved from a full band SWB monopole antenna. The proposed single band-notch SWB antenna offers impedance bandwidth from 1.1−100 GHz (ratio bandwidth of 90.9:1), except in the band of 4.75−6 GHz. Two different band-notched SWB monopole antennas structure have been designed and fabricated with two different substrates, one with FR4 substrate (1.1−100) and another with RT/Duroid 5870 substrate (.9−100). With proper and simple U-shaped and C-shaped parasitic element integrated with ground plane, a band-notched performance from 4.75 to 6.0 GHz can be achieved. It has been observed that the RT/Duroid substrate is more versatile than FR4 substrate, especially when compared to return loss and gain performance of the both antennas.

A Compact dual band-notched Printed monopole SWB antenna has been proposed and extensively investigated. To avoid the interference problem from the existing narrow band system, it is necessary for SWB antennas to have dual band-notched characteristics. Here also like previous chapter two different antenna structures have been realized using two different substrates, one with FR4 substrate and another with RT/Duroid 5870 substrate. All simulated and measured results of the both antennas are well matched.

7.2 Conclusions

It has been concluded that by employing tapers in the printed monopole antennas, SWB antenna impedance matching can be enhanced. To get the best antenna performance each part of antenna such as feed line, feed region and radiating patch have been optimized. Lower bandwidth edge frequency and design of the antenna have been calculated theoretically. To get the band-notch characteristics U-shaped parasitic elements and U-shaped slots have been employed. Another way of obtaining the band-notched characteristics is employing an open ended stub and it has been erected from the triangular tapered microstrip feed-line. Some of the contributions of this thesis are:

(a) A new compact printed triangular monopole antenna has been proposed for UWB application. This compact antenna uses a triangular radiating patch, a microstrip transition (near the front end of the radiating patch), a 50 Ω microstrip feed line and a round-cornered ground plane that provides a measured bandwidth from 1.8 GHz to 15.0 GHz. The proposed antenna structure has wide bandwidth and small size compared to the conventional antenna [38–43].

(b) Proposed a design methodology for SWB printed monopole antenna. This SWB monopole antenna has been composed of three parts: feed region, feed line and radiating patch. Each part of the antenna has been optimized to get best antenna performance and extremely large bandwidth (2.8−100 GHz) has been obtained.

(c) Proposed a new printed monopole antenna for super wideband applications. The simulated result shows that it is a super wideband antenna applicable for frequencies from 2.5 GHz to 80 GHz, while measured results have been shown upto 25 GHz (due to limitation of the available vector network analyzer) and can cover most of the communication systems as compared to [44–46].

(d) Proposed a new structure for realization of super-wideband radiation characteristics (.9−100 GHz) along with notch capability. By introducing U-shaped and C-shaped parasitic element single band-notch functionality has been introduced in the frequency band of 5−6 GHz for WLAN. Proposed antenna has been designed to notch within SWB region, however till date most of the antennas have been designed to notch within UWB [47–49] region.

(e) In this section a compact dual band-notched monopole antenna is proposed for super wideband (SWB) applications. Here two different antennas have been examined using two different substrates. First antenna has been designed using FR4 substrate and second antenna has been designed using RT/Duroid substrate. Dual band-notched functionality has been realized using inverted U-shaped slot, open-circuited stub (for WLAN) and U-shaped parasitic element. Proposed antenna has small size and large bandwidth with dual band-notched characteristic as compared to conventional antenna [50–53].

7.3 Suggestions for future work

- **Equivalent circuit analysis for the SWB printed monopole antenna**:- This SWB printed monopole antenna can be analyzed by equivalent circuit analysis. As the antennas are the resonant devices, all the components such as feed-lines, ground plane and the radiating element can be demonstrated in the form of the equivalent circuit containing either series or parallel RLC circuits. If the circuit parameters such as R, L and C can be extracted correctly, then all the antenna parameters such as scattering parameters and input impedance characteristics can be validated properly along with the simulated and measured antenna characteristics. Hence the accurate equivalent circuit analysis and mathematical or analytical extraction of circuit parameters of the printed monopole antennas are needed to have another confirmation test along with the simulated and measured parameters.

- **Measurement of SWB antenna upto 100 GHz**:- It has been observed that proposed SWB antenna would work well up to 100 GHz but experimental results studied up to 25 GHz since this is the upper measurement frequency of our vector network analyzer. Therefore, in future this printed monopole SWB antenna will be measured upto 100 GHz.

- **Cross-polarization at higher frequencies**:- It has been noticed that SWB printed monopole antenna exhibit high cross-polarization at higher frequencies (above 15 GHz). High cross-polarization occurs probably due to increased horizontal current component. To overcome this problem further research may focus on some new techniques to reduce this.

- **Miniaturization of SWB printed monopole antenna**:- The radiation element of the printed monopole antenna can be designed in the form of fractals instead of traditional tapered patch to achieve the size reduction of the printed monopole antennas. Hence the effect of applying fractals, in reducing the size of printed monopole antennas can be further investigated.

- **Finite Difference Time Domain analysis for the SWB printed monopole antenna**:- This SWB printed monopole antenna can also be analyzed by Finite Difference Time Domain (FDTD) methods.

Bibliography

[1] Federal Communications Commission, "First report and order in the matter of revision of part 15 of the commission's rules regarding ultra-wideband transmission systems," *ET-Docket*, pp. 98–153, Apr. 22 2002.

[2] V. Rumsey, *Frequency Independent Antennas*, New York: Academic Press 1966.

[3] C. E. Shannon, "A mathematical theory of communication," *Bell Syst. Tech. J.*, vol. 27, pp. 379–656, October 1948.

[4] J. Liu, K. P. Esselle, S. G. Hay, and S. S. Zhong, "Compact super-wideband asymmetric monopole antenna with dual-branch feed for bandwidth enhancement," *Electron. Lett.*, vol. 49, no. 8, pp. 515–516, April 2013.

[5] E. Grayaver, "Implementing software defined radio," *Springer*, 2013.

[6] J. Liu, K. P. Esselle, S. G. Hay, Z. Sun, and S. Zhong, "A compact super-wideband antenna pair with polarization diversity," *IEEE Antennas and Wireless Propagation Letters*, vol. 12, pp. 1472–1475, 2013.

[7] C. A. Balanis, "Antenna theory analysis and design," *John Wiley & Sons*, Inc, 2005.

[8] http://www.ahsystems.com/.

[9] http://www.iet.ntnu.no/.

[10] http://www.clampco.it/.

[11] Q. Ju, "RF system design of transceivers for wireless communications," *Springer Science+Business Media*, Inc, 2005.

[12] "IEEE standard definitions of terms for antennas," *IEEE Std 145-1993*, pp. 1–32, April 2013.

[13] C. A. Balanis, "Antenna theory. analysis and design," *Third ed. Wiley-Inter science*, 2005.

[14] L. J. Chu, "Physical limitations of omnidirectional antennas," *J. Appl. Phys.*, vol. 19, pp. 1163–1175, December 1948.

[15] R. F. Harrington, "Effect of antenna size on gain, bandwidth and efficiency," *J. Res. Nat. Bur. Stand.*, vol. 64D, pp. 1–12, January-February 1960.

[16] J. S. Mclean, "A re-examination of the fundamental limits on the radiation q of electrically small antennas," *IEEE Transactions on Antennas and Propagation*, vol. 44, pp. 672–676, May 1996.

[17] R. C. Hansen, "Fundamental limitations in antennas," *Proceedings of the IEEE*, vol. 69, no. 2, pp. 170–182, February 1981.

[18] R. Garg, P. Bahartia, and A. Ittipiboon, "Microstrip antenna design handbook," *Artech House, Boston, London*, 2001.

[19] H. Kawakami and G. Sato, “Broadband characteristics of rotationally symmetric antennas and thin wire constructs,” *IEEE Transactions on Antennas and Propagation*, no. 1, 1987.

[20] H. Nakano, N. Ikeda, Y. Wu, R. Suzuki, H. Mimaki, and J. Yamauchi, “Realization of dual-frequency and wide-band VSWR performances using normal-mode helical and inverted-F antennas,” *IEEE Transactions on Antennas and Propagation*, no. 6, 1998.

[21] S. D. Rogers and C. M. Butler, “Cage antennas optimized for bandwidth,” *Electronics Letters*, no. 11, 2000.

[22] W. Cho, M. Kanda, H. Hwang, and M. Howard, “A disk-loaded thick cylindrical dipole antenna for validation of an EMC test site from 30 to 300 MHz,” *IEEE Transactions on Electromagnetic Compatibility*, no. 2, 2000.

[23] G. Dubost and S. Zisler, “Antennas a large bande,” 1976.

[24] G. H. Brown and O. M., “Experimentally determined radiation characteristics of conical and triangular antennas,” *RCA Review*, no. 4, 1952.

[25] N. P. Agrawall, G. Kumar, and K. P. Ray, “Wide-band planar monopole antenna,” *IEEE Transactions on Antennas and Propagation*, no. 2, 1998.

[26] M. J. Ammann, “Square planar monopole antenna,” *IEE National Conference on Antennas and Propagation*, no. 2, 1999.

[27] M. J. Ammann and Z. N. Chen, “Wideband monopole antennas for multi-band wireless systems,” *IEEE Antennas and Propagation Magazine*, no. 2, 2003.

[28] C. Puente and R. Pous, “Fractal design of multiband and low side-lobe arrays,” *IEEE Transactions on Antennas and Propagation*, no. 5, 1996.

[29] Z. N. Chen and M. Y. W. Chia, “Broadband planar antennas design and applications,” *West Sussex, England: John Wiley Sons, Ltd.*, 2006.

[30] J. Liang, C. Chiau, X. Chen, and C. Parini, “Printed circular disc monopole antenna for ultra-wideband applications,” *Electron. Lett.*, vol. 40, no. 20, pp. 1246 – 1247, Sept. 2004.

[31] J. Liang, C. C. Chiau, X. Chen, and C. G. Parini, “Study of a printed circular disc monopole antenna for UWB systems,” *IEEE Transactions on Antennas and Propagation*, vol. 53, no. 11, pp. 3500–3504, Nov 2005.

[32] K. H. Kim and S. O. Park, “Analysis of the small band-rejected antenna with the parasitic strip for UWB,” *IEEE Transactions on Antennas and Propagation*, vol. 54, no. 6, pp. 1688–1692, June 2006.

[33] Y. J. Cho, K. H. Kim, D. H. Choi, S. S. Lee, and S. O. Park, “A miniature UWB planar monopole antenna with 5-GHz band-rejection filter and the time-domain characteristics,” *IEEE Transactions on Antennas and Propagation*, vol. 54, no. 5, pp. 1453–1460, May 2006.

[34] H. D. Chen and H. T. Chen, “CPW-Fed Dual-Frequency Monopole Aantenna,” *IEEE Transactions on Antennas and Propagation*, vol. 52, no. 4, pp. 978–982, April 2004.

[35] S. S. Zhong, X. L. Liang, and W. Wang, “Compact elliptical monopole antenna with impedance bandwidth in excess of 21:1,” *IEEE Transactions on Antennas and Propagation*, vol. 55, no. 11, pp. 3082–3085, Nov 2007.

[36] N. Fortino, J. Dauvignac, G. Kossiavas, and R. Staraj, “Design optimization of UWB printed antenna for omnidirectional pulse radiation,” *IEEE Transactions on Antennas and Propagation*, vol. 56, no. 7, pp. 1875–1881, July 2008.

[37] Q. X. Chu and Y. Y. Yang, “A compact ultrawideband antenna with 3.4/5.5 ghz dual band-notched characteristics,” *IEEE Transactions on Antennas and Propagation*, vol. 56, no. 12, pp. 3637–3644, Dec 2008.

[38] S. Y. Suh, W. Stutzman, and W. Davis, “A new ultrawideband printed monopole antenna: The planar inverted cone antenna (PICA),” *IEEE Transactions on Antennas and Propagation*, vol. 52, no. 5, pp. 1361 – 1364, May 2004.

[39] C. C. Lin, Y. C. Kan, L. C. Kuo, and H. R. Chuang, “A planar triangular monopole antenna for UWB communication,” *IEEE Antenna and Wireless Propag. Letters*, vol. 15, no. 10, pp. 624–626, Oct. 2005.

[40] J. Liang, C. Chiau, X. Chen, and C. Parini, “Printed circular disc monopole antenna for ultra-wideband applications,” *Electron. Lett.*, vol. 40, no. 20, pp. 1246 – 1247, Sept. 2004.

[41] S. K. Mishra, R. K. Gupta, A. Vaidya, and J. Mukherjee, “A compact dual-band fork-shaped monopole antenna for bluetooth and UWB applications,” *IEEE Antenna and Wireless Propag. Letters*, vol. 10, no. 20, pp. 627–630, July 2011.

[42] A. Elboushi, O. M. Ahmed, and A. R. Sebak, “Study of ellpitical slot UWB antennas with a 5.0 - 6.0 GHz band-notch capability,” *Progress In Electromagnetics Research*, vol. 16, no. 20, pp. 207–222, Sept. 2010.

[43] M. Y. Man, R. Yang, Z. Y. Lei, Y. J. Xie, and J. Fan, “Ultra-wideband planar inverted-F antennas with cut-etched ground plane,” *Electron. Lett.*, vol. 48, no. 14, pp. 817–818, July 2012.

[44] N. P. Agrawall, G. Kumar, and K. P. Ray, “Wide-band planar monopole antenna,” *IEEE Transactions on Antennas and Propagation*, no. 2, 1998.

[45] M. J. Ammann and Z. N. Chen, “Wideband monopole antennas for multi-band wireless systems,” *IEEE Antennas and Propagation Magazine*, no. 2, 2003.

[46] L. Jianxin, C. C. Chiau, X. Chen, and C. G. Parini, “Study of a printed circular disc monopole antenna for uwb systems,” *IEEE Transactions on Antennas and Propagation*, vol. 53, no. 11, pp. 3500–3504, Nov 2005.

[47] R. Zaker, C. Ghobadi, and J. Nourinia, “Novel modified UWB planar monopole antenna with variable frequency band-notch function,” *IEEE Antennas and Wireless Propagation Letters*, vol. 7, pp. 112–114, 2008.

[48] N. Choi, C. Jung, J. Byun, F. J. Harackiewicz, M. J. Park, Y. S. Chung, T. Kim, and B. Lee, “Compact UWB antenna with I-shaped band-notch parasitic element for laptop applications,” *IEEE Antennas and Wireless Propagation Letters*, vol. 8, pp. 580–582, 2009.

[49] M. Rostamzadeh, S. Mohamadi, J. Nourinia, C. Ghobadi, and M. Ojaroudi, “Square monopole antenna for UWB applications with novel rod-shaped parasitic structures and novel V-shaped slots in the ground plane,” *IEEE Antennas and Wireless Propagation Letters*, vol. 11, pp. 446–449, 2012.

[50] W. T. Li, Y. Q. Hei, W. Feng, and X. W. Shi, “Planar antenna for 3G/Bluetooth/WiMAX and UWB applications with dual band-notched characteristics,” *IEEE Antennas and Wireless Propagation Letters*, vol. 11, pp. 61–64, 2012.

[51] W. Jiang and W. Che, “A novel UWB antenna with dual notched bands for WiMAX and WLAN applications,” *IEEE Antennas and Wireless Propagation Letters*, vol. 11, pp. 293–296, 2012.

[52] M. Shokri, H. Shirzad, S. Movagharnia, B. Virdee, Z. Amiri, and S. Asiaban, “Planar monopole antenna with dual interference suppression functionality,” *IEEE Antennas and Wireless Propagation Letters*, vol. 12, pp. 1554–1557, 2013.

[53] K. Ryu and A. Kishk, “UWB antenna with single or dual band-notches for lower WLAN band and upper WLAN band,” *IEEE Transactions on Antennas and Propagation*, vol. 57, no. 12, pp. 3942–3950, Dec 2009.

[54] H. Schantz, *The Art and Science of Ultra wideband Antennas*, Artech House Inc. 2005.

[55] F. Report and Order, “Revision of part 15 of the commission’s rule regarding ultra-wideband transmission systems FCC 02-48,” Federal Communication Commission 2002.

[56] http://en.wikipedia.org/wiki/Ultra-wideband.

[57] N. Daniele, M. Pezzin, K. J. Derivaz, S., and P. Rouzet, “Principle and motivation of uwb technology for high data rate wpan application,” *Smart Object Conference*, 2003.

[58] F. Nekoogar, “Ultra-wideband communications,” *Fundamentals and Applications*, Prentice Hall 2005.

[59] M. Z. Win and R. A. Scholtz, “On the robustness of ultra -wide bandwidth signals in dense multipath environments,” *IEEE Commun. Lett.*, vol. 2, no. 2, pp. 51–53, Feb 1998.

[60] J. D. Taylor, “Introduction to ultra-wideband radar systems,” Boca Raton, FL: CRC Press 1995.

[61] I. Oppermann, M. Hamalainen, and J. Iinatti, “Uwb theory and applications,” John Wiley & Sons Ltd. 2004.

[62] R. J. Fontana, “Recent system applications of short-pulse ultra- wideband (UWB) technology,” *IEEE Transactions on Microwave Theory and Tech.*, vol. 52, no. 9, pp. 2087–2104, Sept. 2004.

[63] S. Licul, J. A. N. Noronha, W. A. Davis, D. G. Sweeney, C. R. Anderson, and T. M. Bielawa, “A parametric study of time-domain characteristics of possible UWB antenna architectures,” *IEEE 58th Vehicular Technology Conference*, vol. 6-9, no. 9, pp. 3110–3114, Oct. 2003.

[64] “WPAN high rate alternative phy taskgroup 3a (tg3a),” *IEEE 802.15 [Online]. Available: http://ieee802.org/15/pub/TG3a.html.*

[65] D. W. Winters, J. D. Shea, E. L. Madsen, G. R. Frank, B. D. V. Veen, and S. C. Hagness, “Estimating the breast surface using UWB microwave monostatic backscatter measurements,” *IEEE Trans. Biomed. Eng.*, vol. 55, no. 1, pp. 247–256, Jun. 2008.

[66] X. N. Low, Z. N. Chen, and W. K. Toh, “Ultrawideband suspended plate antenna with enhance impedance and radiation performance,” *IEEE Transactions on Antennas and Propagation*, vol. 56, no. 8, pp. 2490–2495, Aug. 2008.

[67] M. Ammann, “Control of the impedance bandwidth of wideband planar monopole antennas using a beveling technique,” *Microw. Opt. Technol. Lett.*, vol. 30, no. 10, pp. 229–232, Aug. 2004.

[68] J. Jung, W. Choi, and J. Choi, “Compact broadband antenna with an L-shaped notch,” *IEICE Trans. Commun.*, vol. E89-B, no. 6, pp. 1968–1971, Aug. 2006.

[69] S. H. Wi, Y. S. Lee, and J. G. Yook, “Wideband microstrip patch antenna with U-shaped parasitic elements,” *IEEE Transactions on Antennas and Propagation*, vol. 55, no. 4, pp. 1196–1199, Apr. 2007.

[70] H. Oraizi and S. Hedayati, “Miniaturized uwb monopole microstrip antenna design by the combination of giusepe peano and sierpinski carpet fractals,” *IEEE Antenna and Wireless Propag. Letters*, vol. 10, no. 4, pp. 67–70, Mar. 2011.

[71] M. N. Moghadasi and B. S. Virdee, “Compact UWB planar monopole antenna,” *IEEE Antenna and Wireless Propag. Letters*, vol. 8, no. 14, pp. 1382–1385, Jan. 2009.

[72] H. Kim, D. Park, and Y. Joo, “All-digital low-power CMOS pulse generator for UWB system,” *Electron. Lett.*, vol. 4, no. 24, pp. 1534–1535, Nov. 2004.

[73] Y. Chen, W. T. Joines, Z. Xie, G. Shi, Q. H. Liu, and L. Carin, “Double-sided exponentially tapered gpr antenna and its transmission line feed structure,” *Antennas and Propagation, IEEE Transactions on*, vol. 54, no. 9, pp. 2615–2623, Sept 2006.

[74] S. P. Mathur and A. K. Sinha, “Design of microstrip exponentially tapered lines to match helical antennas to standard coaxial transmission lines,” *IEE Proc. Microw. Antennas and Propag.*, vol. 135, no. 4, pp. 272–274, Mar. 1988.

[75] D. Raicu, “Universal taper for compensation of step discontinuities in microstrip lines,” *IEEE Trans. Antennas Propagat.*, vol. 1, no. 9, pp. 249–251, Sept. 1991.

[76] R. W. Klopfenstein, “A Transmission Line of Improved Design,” *Proceedings of the I. R. E.*, pp. 31–35, 1956.

[77] D. M. Pozar, “Microwave engineering,” *John Wiley & Sons*, 2005.

[78] R. S. Kshetrimayum and R. Pillalamarri, “Novel uwb printed monopole antenna with triangular tapered feed lines,” *IEICE Electronics Express (ELEX)*, vol. 5, no. 8, pp. 242–247, April 2008.

[79] M. Manohar, R. S. Kshetrimayum, and A. K. Gogoi, “Printed monopole antenna with tapered feed line, feed region and patch for super wideband applications,” *IET Microwaves, Antennas and Propagation*, vol. 8, pp. 39–45, Jan. 2014.

[80] Q. Wu, R. Jin, J. Geng, and M. Ding, “Printed omni-directional UWB monopole antenna with very compact size,” *IEEE Trans. Antennas Propagat.*, vol. 56, no. 3, pp. 896–899, Mar. 2008.

[81] D. M. Pozar, “Microwave engineering,” *John Wiley & Sons*, New York 2007.

[82] *Ansoft High Frequency Structure Simulation (HFSS)*, Online, Ansoft Corporation 2012, Ver. 14.

[83] C. A. Balanis, “Antenna theory analysis and design,” *John Wiley & Sons*, 2005.

[84] R. E. Collin, “Foundations for microwave engineering,” McGraw Hill 1966.

[85] J. Y. Deng, Y. Z. Yin, S. G. Zhou, and Q. Z. Liu, “Compact ultra-wideband antenna with tri-band notched characteristic,” *Electronics Letters*, vol. 44, no. 21, pp. 1231–1232, Oct. 2008.

[86] J. R. Panda and R. S. Kshetrimayum, “A 3.4/5.5 ghz dual-band notched UWB printed monopole antenna with two open-circuited stubs in the microstrip feedline,” *Microwave Optical Technology Letters*, vol. 53, no. 53, pp. 2973–2978, Dec. 2011.

[87] M. Mehranpour, J. Nourinia, C. Ghobadi, and M. Ojaroudi, "Dual band-notched square monopole antenna for ultrawideband applications," *IEEE Antennas and Wireless Propagation Letters*, vol. 11, pp. 172–175, 2012.

[88] K. Chung, J. Kim, and J. Choi, "Wideband microstrip-fed monopole antenna having frequency band-notch function," *IEEE Microwave Wireless Component Letters*, vol. 15, no. 11, pp. 766–768, Nov. 2005.

[89] Y. Zhu, F. S. Zhang, C. Lin, Q. Zhang, and J. X. Huang, "A novel dual band-notched monopole antenna for ultra-wideband application," *IEEE Microwave Wireless Component Letters*, vol. 15, no. 11, pp. 766–768, Nov. 2005.

[90] Y. J. Cho, K. H. Kim, D. H. Choi, S. S. Lee, and S. O. Park, "A miniature UWB planar monopole antenna with 5-GHz band-rejection filter and the time-domain characteristics," *IEEE Transactions on Antennas and Propagation*, vol. 54, no. 5, pp. 1453–1460, May 2006.

[91] M. N. Sarifi, S. K. Podilchak, M. Essaaidi, and Y. M. M. Antar, "Compact disc monopole antennas for current and future ultrawideband (UWB) applications," *IEEE Trans. Antennas Propagat.*, vol. 59, no. 12, pp. 4470– 4480, Dec. 2011.

[92] J. Liu, S. Zhong, and K. P. Esselle, "A printed elliptical monopole antenna with modified feeding structure for bandwidth enhancement," *IEEE Trans. Antennas Propagat.*, vol. 59, no. 2, pp. 667–670, Feb. 2011.

[93] K. S. Yngvesson, D. H. Schaubert, T. L. Korzeniowski, E. L. Kollberg, T. Thungren, and J. F. Johansson, "Endfire tapered slot antennas on dielectric substrates," *IEEE Trans. Antennas Propagat.*, vol. 35, pp. 1392–1400, Dec. 1985.

[94] J. C. Liang, C. Chiau, X. Chen, and C. G. Parini, "Study of a printed circular disc monopole antenna for UWB systems," *IEEE Trans. Antennas Propagat.*, vol. 53, no. 11, pp. 3500–3504, Nov. 2005.

[95] K. G. Thomas, N. Lenin, and R. Sivaramakrishnan, "Ultrawideband planar disc monopole," *IEEE Trans. Antennas Propagat.*, vol. 54, no. 4, pp. 1339–1341, April 2006.

[96] M. Gopikrishna, D. D. Krishna, C. K. Anandan, P. Mohanan, and K. Vasudevan, "Design of a compact semi-elliptic monopole slot antenna for UWB systems," *IEEE Trans. Antennas Propagat.*, vol. 57, no. 6, pp. 1834–1837, June 2009.

[97] Y. Chen, W. T. Joines, Z. Xie, G. Shi, Q. H. Liu, and L. Carin, "Double-sided exponentially tapered GPR antenna and Its transmission line feed structure," *IEEE Trans. Antennas Propagat.*, vol. 54, no. 9, pp. 2615–2623, Sept. 2006.

[98] S. Nikolaou, G. E. Ponchak, J. Papapolymerou, and M. M. Tentzeris, "Conformal double exponentially tapered slot antenna (DETSA) on LCP for UWB applications," *IEEE Trans. Antennas Propagat.*, vol. 54, no. 6, pp. 1663–1669, June 2006.

[99] R. S. Kshetrimayum and R. Pillalamarri, "Novel uwb printed monopole antenna with triangular tapered feed lines," *IEICE Electronics Express (ELEX)*, vol. 5, no. 8, pp. 242–247, April 2008.

[100] Q. Wu, R. Jin, J. Geng, and M. Ding, "Printed omni-directional UWB monopole antenna with very compact size," *IEEE Trans. Antennas Propagat.*, vol. 56, no. 3, pp. 896–899, Mar. 2008.

[101] ——, "Printed omni-directional UWB monopole antenna with very compact size," *IEEE Trans. Antennas Propagat.*, vol. 56, no. 3, pp. 896–899, Mar. 2008.

[102] M. John and M. J. Ammann, “Optimization of impedance bandwidth for the printed rectangular monopole antenna,” *Microw. Opt. Tech. Lett.*, vol. 47, no. 2, pp. 153–154, Oct. 2005.

[103] T. G. Ma and S. K. Jeng, “Planar miniature tapered-slot-fed annular slot antennas for ultrawideband radios,” *IEEE Trans. Antennas Propagat.*, vol. 53, no. 3, pp. 1194–1202, Mar. 2005.

[104] Y. Ranga and K. P. Ray, “Ultrawideband printed elliptical monopole antennas,” *IEEE Trans. Antennas Propagat.*, vol. 55, no. 4, pp. 1189–1192, April 2007.

[105] *Ansoft High Frequency Structure Simulation (HFSS)*, Online, Ansoft Corporation 2012, Ver. 14.

[106] W. Wiesbeck, G. Adamiuk, and C. Sturm, “Basic properties and design principles of uwb antennas,” *Proc. IEEE*, vol. 97, no. 2, pp. 372–385, Feb. 2009.

[107] W. Sorgel and W. Wiesbeck, “Influence of the design antennas on the ultra-wideband transmission,” *EURASIP Journal on Applied, Signal Processing*, no. 3, pp. 296–305, Feb. 2005.

[108] H. Kim, D. Park, and Y. Joo, “All-digital low-power CMOS pulse generator for UWB system,” *Electron. Lett.*, vol. 40, no. 24, pp. 1534–1535, Nov. 2004.

[109] N. Telzhensky and Y. Leviatan, “Novel method of UWB antenna optimization for specified input signal forms by means of genetic algorithm,” *IEEE Trans. Antennas Propagat.*, vol. 54, no. 8, pp. 2216–2225, Aug. 2006.

[110] E. Grayaver, “Implementing software defined radio,” *IEEE Trans. Antennas Propagat.*, (Springer, 2013) 2013.

[111] V. Waladi, N. Mohammadi, Y. Zehforoosh, A. Habashi, and J. Nourinia, “A novel modified star-triangular fractal (MSTF) monopole antenna for super-wideband applications,” *Antennas and Wireless Propagation Letters, IEEE*, vol. 12, pp. 651–654, 2013.

[112] K. R. Chen, C. Sim, and J.-S. Row, “A compact monopole antenna for super wideband applications,” *Antennas and Wireless Propagation Letters, IEEE*, vol. 10, pp. 488–491, 2011.

[113] Y. Dong, W. Hong, L. Liu, Y. Zhang, and Z. Kuai, “Performance analysis of a printed super-wideband antenna,” *Microwave and Optical Technology Letters*, vol. 51, no. 4, pp. 949–956, April 2009.

[114] Y. Zhu, F. S. Zhang, C. Lin, Q. Zhang, and J. X. Huang, “A novel dual band-notched monopole antenna for ultra-wideband application,” *Progress In Electromagnetics Research Letters*, vol. 16, pp. 109–117, Aug. 2010.

[115] Y. J. Cho, K. H. Kim, D. H. Choi, S. S. Lee, and S. O. Park, “A miniature UWB planar monopole antenna with 5-GHz band-rejection filter and the time-domain characteristics,” *IEEE Trans. Antennas Propag.*, vol. 54, no. 5, pp. 1453–1460, May 2006.

[116] B. Ahmadi and R. Faraji Dana, “A miniaturised monopole antenna for ultra-wide band applications with band-notch filter,” *IET Microwaves, Antennas Propagation*, vol. 3, no. 8, pp. 1224–1231, 2009.

[117] C. Y. Huang and P. Y. Chiu, “Dual-band monopole antenna with shorted parasitic element,” *Electronics Letters*, vol. 41, no. 21, pp. 1154–1155, Oct. 2005.

[118] C. Y. Pan, T. S. Horng, W. S. Chen, and C. H. Huang, “Dual wideband printed monopole antenna for WLAN/WiMAX applications,” *IEEE Antennas and Wireless Propagation Letters*, vol. 6, pp. 149–151, 2007.

[119] Q. Wu, R. Jin, J. Geng, and J. Lao, "Ultra-wideband rectangular disk monopole antenna with notched ground," *Electronics Letters*, vol. 43, no. 11, pp. 605–606, May 2007.

[120] M. Abdollahvand, G. Dadashzadeh, and D. Mostafa, "Compact dual band-notched printed monopole antenna for UWB application," *IEEE Antennas and Wireless Propagation Letters*, vol. 9, pp. 1148–1151, 2010.

[121] M. Srifi, S. Podilchak, M. Essaaidi, and Y. M. M. Antar, "Compact disc monopole antennas for current and future ultrawideband (UWB) applications," *IEEE Trans. Antennas Propag.*, vol. 59, no. 12, pp. 4470–4480, Dec. 2011.

[122] R. A. Sainati, "CAD of microstrip antennas for wireless applications," Artech House Boston 1996.

[123] I. Oppermann, M. Hamalainen, and J. Iinatti, "UWB theory and applications," *New York: Wiley*, pp. 3–4, 2004.

[124] C. Deng, Y. J. Xie, and p. Li, "CPW-fed planar printed monopole antenna with impedance bandwidth enhanced," *IEEE Antennas Wireless Propag. Lett.*, vol. 8, pp. 1394–1397, 2009.

[125] S. S. Zhong, X. L. Liang, and W. Wang, "Compact elliptical monopole antenna with impedance bandwidth in excess of 21:1," *IEEE Trans. Antennas Propag.*, vol. 55, no. 11, pp. 3082–3085, Nov. 2007.

[126] K. R. Chen, C. Sim, and J. S. Row, "A compact monopole antenna for super wideband applications," *IEEE Antennas and Wireless Propagation Letters*, vol. 10, pp. 488–491, 2011.

[127] M. Mehranpour, J. Nourinia, C. Ghobadi, and M. Ojaroudi, "Dual band-notched square monopole antenna for ultrawideband applications," *IEEE Antennas and Wireless Propagation Letters*, vol. 11, pp. 172–175, 2012.

[128] W. Jiang and C. Wenquan, "A novel UWB antenna with dual notched bands for WiMAX and WLAN applications," *IEEE Antennas and Wireless Propagation Letters*, vol. 11, pp. 172–175, 2012.

[129] T. D. Nguyen, D. H. Lee, and H. C. Park, "Design and analysis of compact printed triple band-notched UWB antenna," *IEEE Antennas and Wireless Propagation Letters*, vol. 10, pp. 403–406, 2011.

[130] J. Y. Deng, Y. Z. Yin, S. G. Zhou, and Q. Z. Liu, "Compact ultra-wideband antenna with tri-band notched characteristic," *Electronics Letters*, vol. 44, no. 21, pp. 1231–1232, Oct. 2008.

List of Publications

Journal Publications

1. **Murli Manohar**, Rakhesh Singh Kshetrimayum and Anup Kumar Gogoi, ”**Printed monopole antenna with tapered feed line, feed region and patch for super wideband applications**,” *IET Microwaves, Antennas and Propagation*, Vol. 8, Issue 1, pp. 39-45, Jan. 2014.
2. **Murli Manohar**, Rakhesh Singh Kshetrimayum and Anup Kumar Gogoi, ”**A compact printed triangular monopole antenna for ultra-wideband application**,” *Microwave and Optical Technology Letters (MOTL)*, Vol. 56, Issue 5, May 2014, pp. 1155-1159.

Conference Publications

1. **Murli Manohar**, U. K. Nemani, Kshterimayum Rakhesh Singh and Anup Kumar Gogoi, ”**A novel super wideband notched printed trapezoidal monopole antenna with triangular tapered feedline**,” In proc. International Conference on Signal Processing and Communications (SPCOM), Bangalore, India, July 2014.

Under Review:

1. **Murli Manohar**, Rakhesh Singh Kshetrimayum and Anup Kumar Gogoi, ”**Design of Dual Band-Notched Printed Monopole Antenna for Super-wideband (SWB) Applications**,” *under review for International Journal of Electronics*.
2. **Murli Manohar**, Rakhesh Singh Kshetrimayum and Anup Kumar Gogoi, ”**A Compact Dual Band-Notched Circular Ring Printed Monopole antenna for Super wideband Applications**,” *under review for IET Electronics Letters*.
3. **Murli Manohar**, Rakhesh Singh Kshetrimayum and Anup Kumar Gogoi, ”**Compact Printed Monopole Antenna with Single Band Suppression Characteristics for Super-Wideband Applications**,” *under review for International Journal of Microwave and Wireless Technologies*.

Bio-Data

1	Name:	Murli Manohar
2	Date of Birth:	02-December-84
3	Educational Qualifications:	June-2008 B.E. in electronics and telecommunication engg. from AMIETE, New Delhi. June-2010 M.TECH in electrical engg. from NIT Rourkela. September-2014 Thesis submitted for Ph.D degree at IIT Guwahati.
4	Work Experience:	Faculty member, Dept. of electronics and communication NIT Goa, July 2014 -
5	Permanent Address:	S/O Late Surendra Prasad Pandit Warsaliganj, Mirjanhat (Post) Bhagalpur (District) Bihar (State), India Pincode-812005
6	Contact Address:	Room No. 25 Married Hostel Indian Institute of Technology Guwahati North Guwahati 781039 Assam, India
7	Contact Number	(+91)-8876736904